

**Study of stand-alone and grid-connected setups of renewable
energy systems for Newfoundland**

By

©Seyedali Meghdadi

A thesis submitted to the

School of Graduate Studies

in partial fulfillment of the requirements for the degree of

MASTER OF ENGINEERING

Faculty of Engineering and Applied Science

Memorial University of Newfoundland

St. John's

Newfoundland and Labrador

Abstract

Decreases in the cost of renewable energy systems such as solar panels and wind turbines, increasing demand for renewable energy sources to provide a sustainable future, and worldwide regulations to reduce greenhouse gas emissions have made renewable energy sources (RES) the strongest candidate to substitute for oil/gas power plants. Rich natural resources in Newfoundland and Labrador have established the province as a resource-based powerhouse. Hence, study of renewable energy setups for this region is of prominent importance.

Renewable energy systems are chiefly categorized into the small-scale stand-alone and large-scale grid-connected systems. Generally, the term “large-scale renewable energy” refers to any large renewable energy projects (e.g. 100 KW or greater) which can make a significant contribution to energy needs. However, in this thesis it refers to wind farms due to the small amount of annual solar radiation in the Newfoundland region. The term “small-scale or local scale renewable energy” refers to personal and communal renewable energy harnessing systems mainly located in rural areas far from the grid. The largest differences between local scale and large scale systems are installation and maintenance costs, the magnitude of the energy harnessing systems, resilience ability (the capacity of a system to absorb disturbance and still retain its basic function), and energy storage capabilities. These differences mean that system design and analysis will be different for each category.

This thesis aims to model, simulate and analyze the stand-alone and grid-connected setups of renewable energy systems customized for Newfoundland in order to meet current and

future electricity needs with environmentally friendly, stable, and competitively priced power. It details potential design improvements as follows:

(1) Small-scale renewable energy systems can be combined with conventional generators and energy storage devices in Hybrid Power Systems (HPS) to overcome the intermittency and uncontrollability issues of renewable power generators. Proper design of such a system is crucial for reliable, economic, and eco-friendly operation. In this thesis, a unique methodology for optimally sizing the combination of wind turbine, solar panel, and a battery bank in a Wind-PV Hybrid system is introduced. This method allows 2% lack of power supply in a year. Two off-grid systems are detailed and modeled in Matlab code and the sizing results of both systems are then compared to the results of the Homer software. Proposed method of sizing results in 30% of reduction to the initial cost of the system.

(2) Solar panels are often installed in climates with a considerable amount of snowfall and freezing rain in winter. For instance, St. John's on the Avalon Peninsula received more than three meters of snow in 2014. The optimal sizing objective of the solar panel in all renewable energy systems is to harness the maximum energy from solar insolation. Since snow accumulation poses an obstacle to the performance of solar panels, reducing their efficiency, it is essential to remove snow from panels as soon as possible. The design of a system that can accurately detect snow on panels and sends alerts in case of snow cover can play a significant role in the improvement of solar panel efficiency. This system was designed, built, and then tested for three months during the winter of 2014 in the engineering building at Memorial University of Newfoundland (47°34'28.9"N 52°44'07.8"W) using solar panels, a battery, a load, a microcontroller, a voltage and a

current sensor, and a light dependent resistor. This system proves capable of precisely identifying more than 5 cm of snow accumulation on solar panels and sending alerts.

(3) In large-scale renewable energy systems, proper investigation of the grid connection impact of wind farms is essential for the following reasons: Firstly, in wind turbines, generating systems are different from conventional grid coupled synchronous generators and interact differently with the power system. Secondly, the specific type of applied wind turbine has some aspects of interaction with the grid, particularly for wind turbines with and without power electronic converters.

Analyzing connection of large-scale wind farms, simulating 500MW of wind capacity to the isolated grid of Newfoundland with the purpose of probing stability and reliability of the grid is conducted in “phasor simulation type” using Matlab/ Simulink. As a case study, the impact of the Fermeuse wind farm (46°58'42"N 52°57'18"W) on the isolated grid of Newfoundland is explored in “discrete simulation type” for three permissible scenarios, which are constant wind speed, variable wind speed, and reconnection of the wind farm to the grid. Results indicate that variable wind speeds cause very small fluctuations in the frequency and the current injected into the grid, meaning the grid is quite stiff. Also, system trip and reconnection will result in a frequency variation of 0.35 Hz, where some harmonics coming from the converter can be noticed, and voltage variation of less than 5%.

Acknowledgements

I would like to express my sincere gratitude and appreciation to Dr. Tariq M. Iqbal for his priceless guidance, advice and financial support through the course of this work. I also would like to thank Greg O’Leary and Glenn St. Croix for their support.

Financial support for this project has been provided by National Science and Engineering Research Council of Canada (NSERC).

Table of Contents

Abstract.....	i
Acknowledgements	iv
List of tables.....	viii
List of figures.....	viii
List of Symbols	xi
Acronyms	xiv
1. Introduction	1
1.1 Background and objectives	1
1.2 Thesis outline	4
2. Literature review	5
2.1 Hybrid small-scale renewable systems	5
2.2 Snow detection on solar panels	9
2.3 Large-scale grid connected renewable systems	12
3. System sizing of small-scale stand-alone system for Newfoundland.....	14
3.1 Introduction	14
3.2 Hybrid system components	14
3.2.1 Wind turbines	15
3.2.2 Photovoltaic panels	17
3.2.3 Battery energy storage	18
3.3 System sizing using Matlab	19
3.3.1 Demand power estimation	20
3.3.2 Size and type of components	22
3.3.2.1 Typical solar panel modules	22
3.3.2.2 Typical Wind Turbines	23
3.3.2.3 Battery	25
3.3.3 Model of components	25
3.3.3.1 Wind turbine	25
3.3.3.2 Solar panel.....	27
3.3.3.3 Battery	29
3.3.4 Available energy and NLPS.....	30

3.4 System sizing in Homer.....	32
3.4.1 Introduction to Homer software	32
3.4.2 System sizing procedure.....	33
3.4.3 Homer results	34
3.5 Conclusion.....	36
3.6 Case study: Compare HOMER example with the developed code.....	38
3.6.1 Homer results	42
3.6.2 Mathematical model	44
3.6.2.1 Wind turbine model.....	44
3.6.3 Conclusion	46
4. Improving off-grid systems: Snow detection on PVs	47
4.1 Introduction	47
4.2 Design of snow detection system	48
4.3 Alert algorithm	50
4.4 Arduino code.....	54
4.5 Experimental Results	55
4.6 Conclusion.....	57
5. Connection of large-scale wind power to the isolated grid of Newfoundland.....	59
5.1 Introduction	59
5.2 Study Parameters	60
5.2.1 Load Forecast.....	60
5.2.2 Wind plants	61
5.3 Power system planning and operating criteria.....	62
5.3.1 Voltage Criteria	63
5.3.2 Stability Criteria	63
5.4 Study assumptions.....	64
5.5 NLH's PSS/E model	64
5.6 Simulink model	66
5.7 Simulation and Analysis	73
5.7.1 Voltage regulation results	74
5.7.2 Transient stability.....	74

5.8 Conclusion.....	76
5.9 Case study: The impact of Fermeuse wind farm on the Newfoundland grid ...	78
5.9.1 Introduction	78
5.9.2 Location of the wind farm.....	79
5.9.3 Power system planning and operating criteria	80
5.9.4 Single line diagram of the system	80
5.9.5 System Components.....	82
5.9.5.1 Wind power generation system	82
5.9.5.2 Wind Turbine.....	83
5.9.5.3 Two-mass model of drivetrain.....	83
5.9.5.4 Generator.....	85
5.9.5.5 Converter.....	88
5.9.6 Simulink system model.....	89
5.9.7 Simulation Results	94
5.9.8 Conclusion	99
6. Conclusion	101
6.1 Introduction	101
6.3 Recommendations for improvement	103
References	105
Appendices.....	111
A.1. Annual energy output of wind turbines	111
A.2. Matlab code:	111
A.3. Fitting polynomial	114
A.4. Wind turbine function.....	115
A.5. Output power.....	116
B. Snow detection code on Arduino:.....	117
C. Wind farm simulation blocks	124

List of tables

Table 2-1: Summary of merits and demerits of different optimization techniques	8
Table 3-1: Demand load estimation of a cabin	20
Table 3-2: Typical solar panel modules	23
Table 3-3: Typical wind turbines	24
Table 3-4: Power and wind speed	24
Table 3-5: system architecture	34
Table 3-6: Cost summary of the HPS	34
Table 3-7: Net percent costs of hybrid power system.....	35
Table 3-8: Annualized costs of hybrid power system.....	35
Table 3-9: Generators annual power production.....	35
Table 3-10: Comparison of results between Homer and the developed code.....	36
Table 3-11: System architecture	42
Table 3-12: Cost summary	43
Table 3-13: Net percent cost	43
Table 3-14: Comparison of results between Homer and the developed code.....	46
Table 5-1: List of distributed wind plants for the base year 2020	61
Table 5-2: Results of base case year 2020 analyses.....	66
Table 5-3: Protection system parameters	72
Table 5-4: Fermeuse wind farm buses	81
Table 5-5: Fermeuse wind farm transmission lines and transformers data.....	81
Table 5-6: Wind turbine specifications	93
Table 5-7: Induction generator parameters	93

List of figures

Figure 2-1: Data processing flowchart.....	10
Figure 2-2: Software algorithm flowcharts: (a) End device and (b) Coordinator.....	11
Figure 3-1: Hybrid renewable wind-PV-battery system	15
Figure 3-2: horizontal-axis (HAWT) versus vertical-axis (VAWT) wind turbine	16
Figure 3-3: Equivalent circuit of a PV module	17
Figure 3-4: Load matching for a photovoltaic panel with a given insolation	18
Figure 3-5: Chemical reaction when battery is charged or discharged.....	18
Figure 3-6: Monthly average data of AC load	21
Figure 3-7: Monthly average data of DC load	22
Figure 3-8: Monthly average data of wind speed	27
Figure 3-9: Monthly average data of solar insolation	28
Figure 3-10: Algorithm for optimal sizing of the system	32
Figure 3-11: System schematics in Homer	34
Figure 3-12: Monthly average electric production	36

Figure 3-13: Monthly average of solar insolation data	38
Figure 3-14: Monthly average of wind speed data	39
Figure 3-15: Monthly average of load data.....	39
Figure 3-16: System overview in Homer.....	40
Figure 3-17-(a) to (c): System components in Homer	41
Figure 3-18: Primary load inputs in Homer	42
Figure 3-19: Optimal system type graph	44
Figure 3-20: Turbine power curve and polynomial equation fitting the output power	45
Figure 4-1: (a) snow melting; (b) sheet sliding.....	48
Figure 4-2: System circuit diagram.....	49
Figure 4-3: Average of sensors readings during three months (12pm-2pm)	51
Figure 4-4: Algorithm for snow detection	53
Figure 4-5: System setup	55
Figure 4-6: Clean panels	56
Figure 4-7: Snow on panels	56
Figure 4-8: Tweeted message	57
Figure 4-9: Twitter messages.....	57
Figure 5-1: 2008-2011 NLH annual average system generation load shape	60
Figure 5-2: Wind turbine power characteristics.....	62
Figure 5-4-(a) to (d): Simulink model	71
Figure 5-5-(a) and (b): Protection algorithm.....	73
Figure 5-6: Current, voltage, P and Q scopes at constant wind speed.....	75
Figure 5-7: Current, voltage, P and Q scope at variable wind speed.....	76
Figure 5-8: Bird-eye view of a part of the wind farm.....	79
Figure 5-9: View of the wind farm from its transformer station	79
Figure 5-10: Fermeuse wind farm grid connection single line diagram	80
Figure 5-11: Control of a variable speed DFIG generator based wind energy conversion.....	82
Figure 5-12: Equivalent diagram of the wind turbine drive train	84
Figure 5-13: Equivalent circuit representation of an induction machine in synchronously rotating reference frame: (a) d-axis; (b) q-axis	88
Figure 5-14: Electrical control model of wind turbine	89
Figure 5-15: Simulink model of wind farm	92
Figure 5-16- (a) to (d): Simulink model results for variable wind speeds.....	95
Figure 5-17-(a) to (c): Simulink model results for constant wind speed	97
Figure 5-18-(a) to (c): Simulink results when fault occurs.....	98
Figure C-1: Wind generation block	124
Figure C-2: Wind turbine block.....	125
Figure C-3: Drivetrain block.....	125
Figure C-4: Wind turbine and drivetrain.....	126
Figure C-5: A 27MW DFIG wind turbine	126

Figure C-6: Electrical model of wound rotor using abc to d-q transformation and state space model of asynchronous machine	127
Figure C-7: Mechanical model of machine.....	128
Figure C-8: Calculate V_{ab-gc}	128
Figure C-9: Calculate V_{ab-rc}	129
Figure C-10: Calculate V_{dc}	129

List of Symbols

$C_p(\lambda, \beta)$	Power coefficient
A	Sweep area
v	Wind speed
β	Pitch angle
T_m	Mechanical torque
C_F	Capacity factor of wind turbine
P_m	Power developed by the wind turbine
Z	Height above ground level
Z_{ref}	Reference height (10m)
Z_0	Roughness length
G_{ref}	Irradiance of $1000\text{w}/\text{m}^2$
\dot{G}	Average irradiance
$T_{c,ref}$	Reference temperature (25 degrees)
V_{mp}	PV voltage at maximum power point
$V_{mp,ref}$	V_{mp} at reference operating condition
μ_{VOC}	Open circuit temperature coefficient
μ_{ISC}	Short circuit temperature coefficient
I_{mp}	PV current at maximum power
$I_{mp,ref}$	I_{mp} at reference operating condition

$I_{SC,ref}$	Short circuit current at reference operating condition
P_{mp}	PV power at maximum power point
T_c	PV operating temperature
Y_{pv}	Rated capacity of the PV panel
f_{pv}	PV derating factor
β	Tilt angle
$\hat{G}_t(\beta)$	Solar radiation incident on the PV array at angle β
$\hat{G}_{t,STC}$	Incident radiation at standard test conditions
$B(\beta)$	Beam radiation
$D(\beta)$	Diffuse radiation
DOD	Depth of discharge
E_{bmin}	Battery minimum allowable energy
E_{bmax}	Battery maximum allowable energy
E_{WT}	Energy generated by WT
E_{PV}	Energy generated by PVs
N_{WT}	Number of WTs
N_{PV}	Number of PV panels in the PV array
$E_{b,t}$	Energy stored in batteries in hour t
$E_{b,t-1}$	Energy stored in batteries in previous hour
$E_{L,t}$	Load demand
$\eta_{inv.}$	Inverter efficiency

$\eta_{bat.}$	Battery efficiency
δ	Self discharge rate of the battery
T'_{wtr}	Wind turbine torque
J'_{wtr}	Wind turbine moment of inertia
Ω'_{wtr}	Wind turbine mechanical speed
D'_e	Damping constant
K'_{se}	The equivalent stiffness
d-axis	Direct component
q-axis	Quadrature component
0-axis	Zero component
S	Stator variable
R	Rotor variable
Φ	Flux variable
λ	Flux linkage variable
r_s	Stator winding resistance of induction machine
r'_r	Rotor winding resistance of induction machine
L_{ls}	Leakage inductance of stator winding
L'_{lr}	Leakage inductance of rotor winding
L_m	Magnetizing inductance

Acronyms

AEO	Annual Average Output
DFIG	Doubly Fed Induction Generator
HPS	Hybrid Power System
LCOE	Levelized Cost Of Electricity
LDR	Light Dependent Resistor
LPSP	Loss Of Power Supply Probability
LVRT	Low Voltage Ride Through
MPPT	Maximum Power Point Tracker
NLH	Newfoundland Hydro
NP	Newfoundland Power
NUG	Non-Utility Generator
PLL	Phase Locked Loop
PWM	Pulse Width Modulation
RES	Renewable Energy Sources
SOC	State Of Charge
WECS	Wind Energy Conversion System

1. Introduction

1.1 Background and objectives

This thesis aims to model and analyze the stand-alone and grid-connected renewable energy systems for Newfoundland in order to meet current and future electricity needs with environmentally friendly, stable, and competitively priced power.

In small-scale, off-grid renewable energy systems, a single renewable energy generator which relies on either wind speed or solar insolation is not predictable due to its periodic and seasonal variations. To allow these systems to meet the requirements of a variable load, some form of energy storage must be integrated. Loss of power supply probability (LPSP) is defined as the probability that an insufficient power supply results when the hybrid system is unable to satisfy the load demand. An LPSP 0 means the load will always be satisfied whereas an LPSP 1 means that the load will never be satisfied [1]. To guarantee low LPSP and low initial cost of the system, which are optimization objectives, a system sizing algorithm is designed, calculating the exact number of required components while ensuring the desired reliability of the generation system is reached. Desirable reliability is a trade-off: a balance achieved between two desirable but incompatible features, cost and LPSP. For instance, the bigger the size of the energy storage system, the better the system copes with the fluctuations in energy production. However, to minimize the initial cost of the system, the number of batteries in the battery bank should be minimized as they are the most expensive components of the system. Due to the fact that the power supply from the central grid using long transmission lines has a very high maintenance and protection cost

and high transmission loss, this study investigates design of a hybrid wind-PV-battery renewable energy system for an off-grid cabin with the unique meteorological data of Newfoundland.

In order to improve the efficiency of solar panels in any renewable energy system, snow must be cleared immediately from the face of the panels due to the fact that snow accumulation affects the performance of PVs and drastically decreases the output power. This leads to overestimation in the size of solar panels needed. To address this issue, a system setup using a 100W solar panel, an Arduino Uno microcontroller, a current and a voltage sensor, a Light Dependent Resistor (LDR), a 12V lamp working as load, and a 12V battery was installed in Faculty of Engineering building of MUN, St. John's, Newfoundland and run for three months in the winter of 2014. During the experiment it was noted that five centimeters of snow on panels could be a distinguishable feature affecting the PVs performance and this amount is used as a check point in the algorithm. In the end, a novel algorithm for snow detection based on field tests and a low cost system as described above have been developed and validated.

In large-scale systems, to ensure a low levelized cost of electricity (LCOE), that is the price at which electricity must be generated from a specific source to break even over the lifetime of the project, annual meteorological data of the region play a significant role. In order to design a large-scale renewable source system for Newfoundland, regarding the low annual average of solar insolation versus the high annual average of wind speed in this region, it is economical to use wind farms rather than solar farms. Connection of wind farms to the power grid presents challenges to power systems. Technical constraints of power generation integration in a power system are associated with the thermal limit, frequency

and voltage control, and stability. Grid codes are designed to specify the relevant requirements to be met in order to integrate wind turbines into the grid [2]. Relying on wind turbines to generate power in large-scale grid connected plants introduces some barriers due to uncontrollability and unpredictability of the resources, resulting in fluctuations in the output power. However, it is theorized that geographic diversity of large-scale wind farms results in smoothing of overall power output. This implies the importance of investigating wind farms' aggregated power to clarify aforementioned barriers. Considering the precise specifications of wind farms and the characteristics of Newfoundland's utility grid, to demonstrate the impact of change in wind speed on a utility grid, the Matlab/Simulink model used is a dynamic system with 500MW of wind power capacity. This model exhibits wind power integrated into the Newfoundland grid. Wind capacity extends to approximately 100% of Newfoundland Hydro (NLH) power generation for an extreme light load in the year 2020. The load is about 26% of Newfoundland power and NLH rural peak loading. Industrial customers' loading is judged to be 78% of the forecasted peak. The simulation is implemented in phasors simulation type as running a huge simulink file could take a few days. This impeded measuring frequency fluctuates during the simulation. Results of the analysis provide an estimate of voltage fluctuation expected in the system. Moreover, as a case study, the impact of the Fermeuse wind farm, located on the southern shore of the Avalon Peninsula in Newfoundland, is investigated. Modeling it in Matlab/Simulink discrete simulation type enabled estimating voltage and frequency fluctuations.

1.2 Thesis outline

Chapter 2 gives a brief outline of various energy system configurations, reviews the literature on renewable energy systems models, small-scale remote and large-scale grid-connected, and methods of snow detection on solar panels. Chapter 3 presents a novel algorithm for optimal sizing of a hybrid wind-PV-battery system for a cabin located in Newfoundland. This chapter details the steps of designing the algorithm and its implementation. Also, a built-in example of Homer software is explained and results are compared with the explained sizing algorithm. Chapter 4 discusses improvements in optimization of small-scale renewable energy systems. Snow accumulation on solar panels decreases the efficiency of panels and leads to over sizing solar panels required for the system. This chapter introduces a low cost method of snow detection on solar panels found in field tests and details the design of the system setup. Chapter 5 investigates the grid connection of large-scale wind capacity to the isolated grid of Newfoundland and provides a Simulink model, considering all electrical and mechanical aspects of wind farms. Also, in this chapter the impact of the Fermeuse wind farm on the grid of Newfoundland is described for three possible scenarios.

Overall, this thesis aims to investigate small-scale remote and large-scale grid-connected renewable energy systems for Newfoundland.

2. Literature review

2.1 Hybrid small-scale renewable systems

Hybrid Renewable Energy Systems are popular and convenient for stand-alone power generation in isolated sites due to renewable energy technologies advances and power electronic converters [3]. Environmental factors are advantage of the hybrid system due to the lower consumption of oil/gas [4]. From the financial point of view, the costs of renewable generators are predictable since they are not influenced by fuel price fluctuations [5]. However, solar or wind resources have an unpredictable nature as they are dependent on weather. Therefore, as a common disadvantage of both generation sources, they have to be oversized to make their stand-alone systems entirely reliable for the times when there is not enough solar radiation or wind resources available [6]. This problem can be partially overcome by integrating these two energy resource, using the strengths of one source to overcome the weakness of the other [7].

Because of intermittent solar radiation and wind speed characteristics, resulting in the fluctuation of energy production from the hybrid system, power reliability analyses are considered a major step in system design process. There are a number of methods to investigate the reliability of hybrid systems. The most popular method is loss of power supply probability (LPSP), the probability that the hybrid system is not able to satisfy the load demand resulting in an insufficient power supply [8], [9]. The design of a reliable stand-alone hybrid PV–wind –battery system can be conducted using the LPSP as the key design parameter.

An optimum sizing method is necessary to efficiently and economically utilize the renewable energy resources and to obtain the minimum initial capital investment while maintaining system reliability. To reach these goals, choosing the right sizing of all components is crucial [10], [11]. Simulation programs such as HOMER and HOGA are the most common tools to find optimum configuration. HOMER has a user friendly and straightforward environment. However, calculations and algorithms are not visible, which does not let the user simply select proper components of the system. In HOGA, optimization is conducted by Genetic Algorithms with the purpose of minimizing total system costs. Therefore, optimization is mono-objective [12].

Zhou, Wei, et al. (2010) indicated five main techniques of optimization for a solar-wind hybrid system [7]:

A. Probabilistic approach

This approach treats generators, storage and costs independently, knowing the probability density of renewable resources (wind and solar insolation) [13].

B. Graphic construction technique

To find the optimum combination of components, this method uses long-term data of solar radiation and wind speed to satisfy a given load and desired LPSP [14].

C. Iterative technique

This method utilizes the iterative optimization technique following the LPSP model and Levelized Cost of Energy model for power reliability and system cost respectively [15].

D. Artificial intelligence methods

Artificial intelligence methods, such as the Genetic Algorithm (GA) and Fuzzy Logic, are used to maximize economic benefits of a hybrid system as they are not restricted by local

optimal [16]. However, these methods are harder to implement in a code. During this research some issues due to the convergence of results were observed.

E. Multi-objective design

This technique searches for the configuration that has the lowest total cost through the lifetime of installation. This method has at least two objectives: cost and pollutant emissions which are in contrast since reduction of pollution implies a rise in components' costs (and vice versa) [17].

The table below indicates a simple summary of the relative merits and demerits of different optimization methodologies [7].

This thesis will discuss a method for sizing of hybrid solar-wind systems based on the NLPSP (Number of times that Loss of Power Supply happens) optimization approach allowing 2% lack of power supply resulting in 30-40% reduction of the initial cost of the solar-wind hybrid renewable energy system.

		Advantages	Disadvantages
Software tools	HOMER	User friendly.	Does not let user intuitively select appropriate system components.
	HOGA	Carried out by genetic algorithms.	Simulation is carried out using 1h intervals.
Optimization techniques	Graphic construction method	Eliminate the need of time-series data.	Only two parameters can be included in the optimization process.
	Probabilistic approach		Cannot represent the dynamic changing performance of a system.
	Iterative technique		Usually results in increased computational efforts and suboptimal solutions.
	Artificial intelligence		Finds the global optimum with relative computational simplicity.
	Multi objective design	Can optimize simultaneously at least two contrasting objectives.	

Table 2-1: Summary of merits and demerits of different optimization techniques

2.2 Snow detection on solar panels

To optimize a hybrid wind-PV system it is inevitable to exploit components to perform at their maximum efficiency. To increase efficiency of a solar panel, understanding the effect of snow is vital. There are many variables to determine the effect of snowfall on PV performance such as ambient temperature, precipitation characteristics, humidity, etc. [18], [19], [20]. A new image data method for determining the probability distribution of snow accumulation on a module was developed by Becker et al. (2006) [21]. They found that snowfall losses are dependent on the angle and technology of the panel being considered. Moreover, they noticed that the effects of increased Albedo in the surroundings of a PV system can increase output power of the system [19]. To have a reference, or to compare actual system output to a modelled system output over a specific time period, recent studies have relied on continuous clearing of a set of control modules [20]. Wirth, Georg, et al (2010) used satellite imaging to identify times when a photovoltaic plant is covered with snow [22].

Andrews et al (2013), commissioned and monitored a multi-angle, multi-technology PV system over two winters. In their implemented data processing flowchart (Figure 2-1), G_t and D_t represent the time series of measured global and diffuse irradiation respectively. Module performance in this case is defined as a time series of short circuit current, I_{sc} . They introduced and validated a new methodology with this system, which allows the determination of snowfall losses from time-series performance [19].

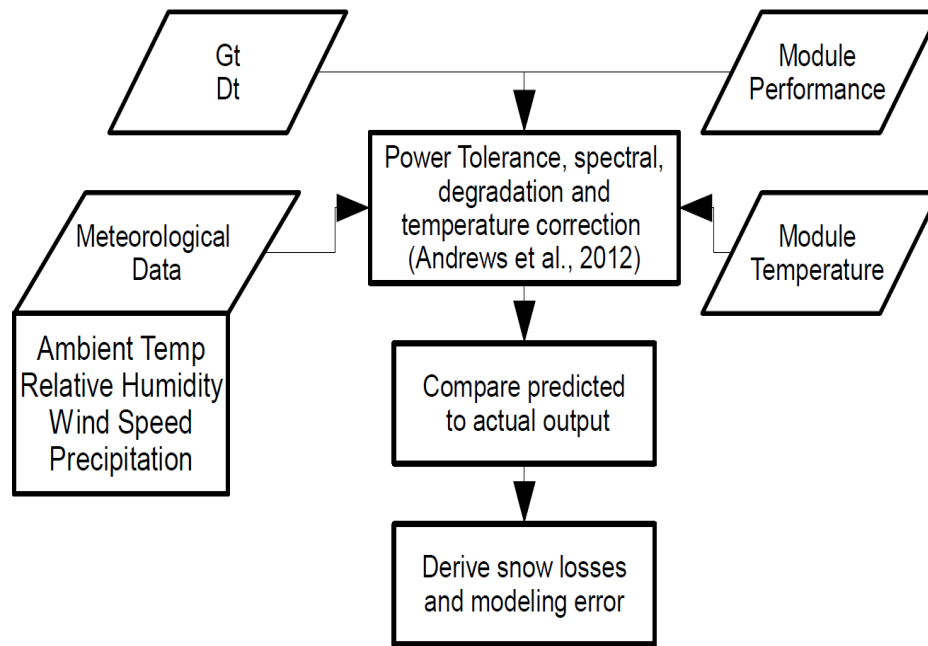


Figure 2-1: Data processing flowchart [19]

Rashidi-Moallem et al. (2011) introduced a solar photovoltaic performance monitoring system utilizing a wireless Zigbee microcontroller [18]. They proposed a system to detect non-ideal operating conditions observing the performance of an array of PV panels. Figure 2-2 indicates how this algorithm works.

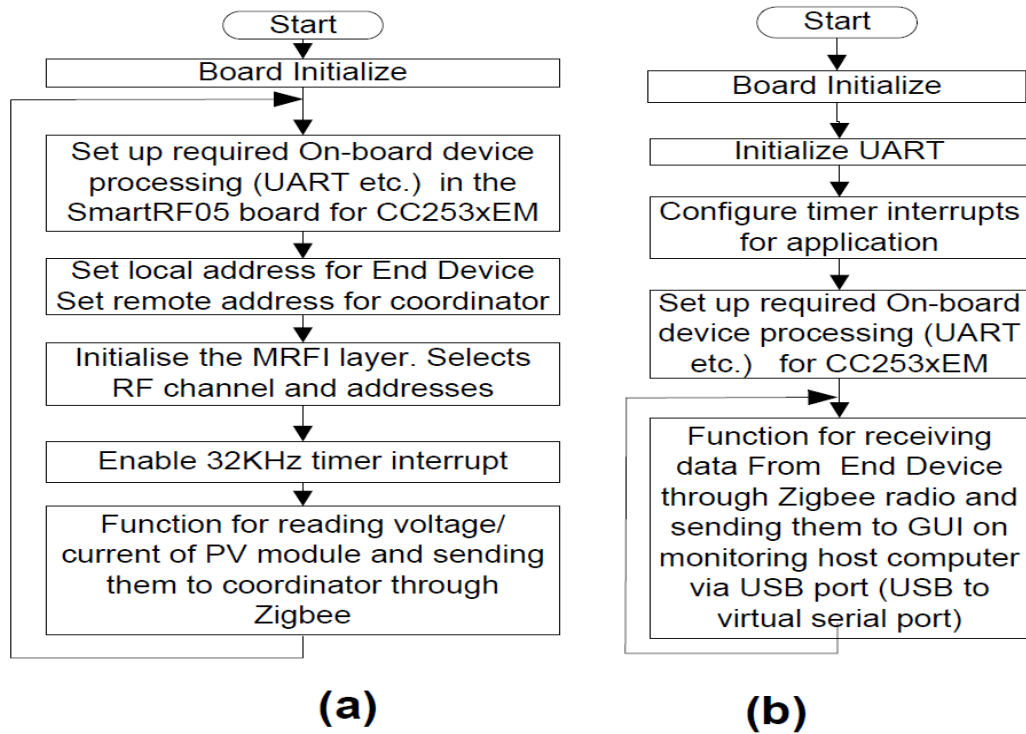


Figure 2-2: Software algorithm flowcharts: (a) End device and (b) Coordinator [18]

Aforementioned works and solutions are not only expensive to implement but also may not be accurate enough. Moreover, some data logging systems are commercially available capable of detecting snow on solar panels by comparing outputs of two panels next to each other. Such detection systems consume significant power, are not capable of sending alerts and are expensive. This thesis presents a novel low cost system algorithm established with field tests, thus resulting in accurately detecting snow on panels and notifying the owner to clean the panels by means of twitter messages. No dedicated host PC or data logging system is required since it exploits a low cost and low power Arduino Uno board along with a Wi-Fi shield. Results provided in this thesis confirm accurate detection of more than five centimeters of snow using the method introduced in this thesis.

2.3 Large-scale grid connected renewable systems

As of May 2014, the wind power generating capacity of Canada was 8,517 megawatts (MW), providing about 3% of Canada's electricity demand [23]. The Canadian Wind Energy Association has outlined a future strategy for meeting 20% of the country's energy needs for wind energy to reach a capacity of 55,000 MW by 2025. Wind farms are the fastest growing large-scale grid-connected form of renewable energy plants around the world. Large scale wind farms of hundreds of MW level are being developed and are connected to the power utility grid in many countries around the world [24].

Wind power penetration level is the percentage of demand covered by wind energy in a certain region. This can be high, considering the growth of the number of wind farms in utility grids. For example, the average wind power penetration levels are normally 20-30 % on an annual basis with peak penetration level up to 100%. This will effectively reduce the requirement for fossil fuel based conventional power generation, resulting in fewer pollutant emissions. However, increase of wind penetration level presents many challenges to power systems. These challenges are power system operation, control, system stability, and power quality [24], [25]. Moreover, Chen Z. [24] found that the impact of connecting a wind farm on the grid voltage is directly related to the short circuit level. If the short circuit impedance of the network is small, then the voltage variations will be small which indicates that the grid is strong. For large value of short circuit impedance, the variation of voltage will be large indicating a weak grid.

Chuong T.T [26] addresses the impact of wind power on voltage at distribution level. He presented a method to observe the relationship between active power and voltage at the

load bus to identify voltage stability limit. He found the main factor causing unacceptable voltage profiles is the instability of the distribution system to meet the demand for reactive power. Under normal operating conditions, the bus voltage magnitude increases as reactive power injected at the same bus is increased. Although voltage stability is a localized issue, its impact can spread as it is a function of transmitted real power, injected reactive power and receiving voltage. To overcome the bus bar constraints, generator, excitation system, protection settings and timing are required to be carefully applied to ensure accepted network voltage.

Technical constraints of power generation integration in a power system are specified by grid codes. These specifications have to be met in order to safely integrate wind power to grid. Generally, these issues are investigated by modeling wind farms in software, such as Matlab/Simulink, Etap, PSS/E, PowerWorld, etc. Then, potential operation and control methods to meet challenges are discussed [27], [28].

This thesis will investigate the important issues related to the large scale wind power integration into modern power systems as follows:

Firstly, wind power generation and transmission will be described. Then, the impacts of wind farms on power quality issues are to be analyzed. The technical requirements for a wind farm grid connection will be introduced. Additionally, the effect of geographically diversified wind farms on the grid stability will also be discussed. A simulation model illustrates a stability problem and a possible method of improving the stability.

3. System sizing of small-scale stand-alone system for Newfoundland

3.1 Introduction

A small hybrid electric system that combines wind and solar (photovoltaic or PV) power technologies offers several complementary advantages over either single source system. In North American countries, wind speeds are low in the summer when the sun shines brightest and longest. Wind is strong in the winter when less sunlight is available. Since peak operating times for wind and solar systems occur at different times of the day and year, hybrid systems supplement each other to produce power when it is needed. When neither the wind nor the sun is producing enough power, hybrid systems provide power using storage, such as a battery bank.

3.2 Hybrid system components

A hybrid system includes renewable generators, controllable loads, and an energy storage device. To make all of the subsystems work together for the cases where the system has a DC and an AC bus, hybrid systems include power converters.

Figure 3-1 depicts an example of a hybrid system [29]. DC loads, a battery bank, solar panel and a wind turbine are connected to the DC bus of the system. AC loads are connected to the AC bus supplied through a converter, transferring power from the DC bus to the AC bus.

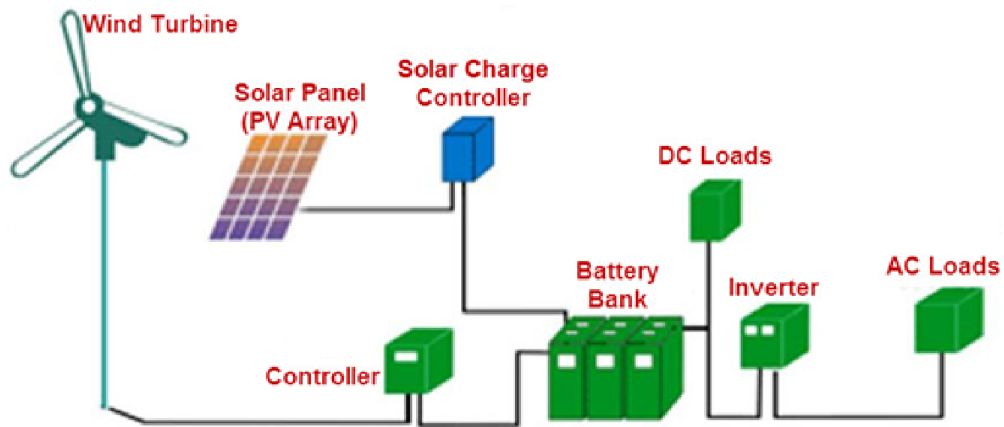


Figure 3-1: Hybrid renewable wind-PV-battery system [29]

3.2.1 Wind turbines

A wind turbine converts energy in wind to electricity. Wind turbines can be categorized as explained below:

1. Based on rotor axis orientation
 - a) Horizontal axis
 - b) Vertical axis

Horizontal axis turbines are the most common design of modern turbines since they have higher efficiency and a lower cost-to-power ratio compared to vertical axis turbines. A noticeable disadvantage of horizontal axis turbines is that most system components, such as the generator, breaks, converter, and gearbox in a nacelle, are mounted on a tower which requires a complex design and restricts servicing.

Figure 3-2 depicts the schematics of both turbines [30].

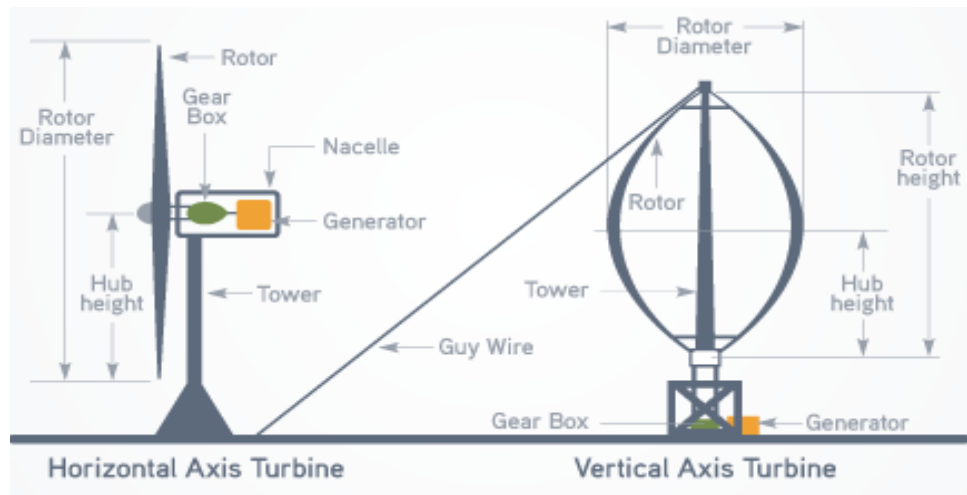


Figure 3-2: horizontal-axis (HAWT) versus vertical-axis (VAWT) wind turbine [30]

2. Based on the size and energy production capacity

a) Small wind turbine ($\leq 300\text{kW}$)

b) Large wind turbine ($> 300\text{kW}$)

3. Based on rotor speed

a) Fixed speed

b) Variable speed

A fixed speed wind turbine normally uses a Squirrel Cage Induction Generator to convert mechanical energy to electricity. This type of generation system needs an external source of reactive power to create a magnetic field. A variable speed wind turbine mostly employs a Doubly-Fed Induction Generator which has the ability to control the power factor by consuming or producing reactive power. Moreover, variable speed turbines will produce more energy than constant speed turbines.

In addition to the generators mentioned above, some wind turbines use synchronous or permanent magnet generators. Also, there are a number of wind turbines that supply DC

power as their principal output. These machines are typically in a smaller size range, 5 kW or less. With proper control, they can operate in conjunction with AC or DC loads. These small turbines are commonly used to supply power to small houses and cabins.

3.2.2 Photovoltaic panels

Photovoltaic panels, also known as PV panels, provide a useful complement to wind turbines. Panels generate electricity from incident solar radiation. A photovoltaic panel is inherently a DC power source.

The equivalent circuit of a PV module is shown below.

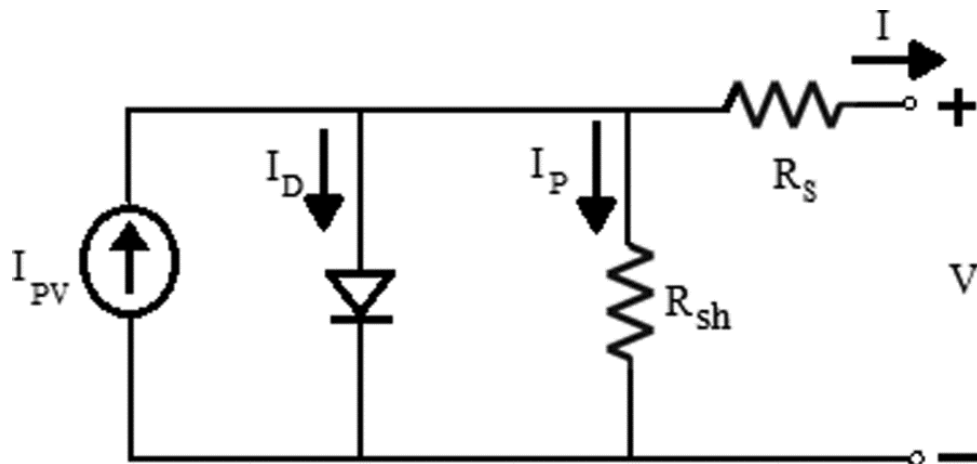


Figure 3-3: Equivalent circuit of a PV module

The variations of solar radiation result in fluctuations in the power output of solar panels. Figure 3-4 depicts current-voltage characteristics of a typical solar panel at a given temperature and solar insolation. The output power of a PV panel is dependent on the load to which it is connected and at any given operating condition there is normally only one operating point. This is where both the panel and load have the same voltage and current, and is shown in Figure 3-4, where load and PV I-V curves cross. It is important to use

power conditioning equipment, Maximum Power Point Tracker (MPPT), to increase the efficiency of solar panels by matching the load with the characteristics of the PV cell.

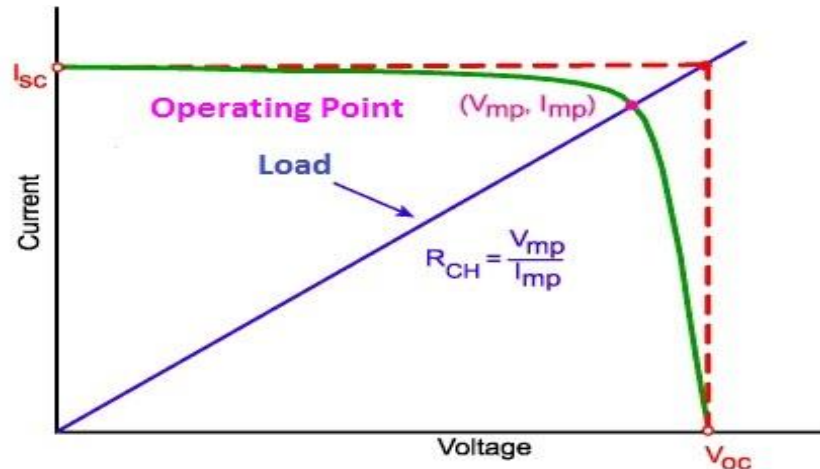


Figure 3-4: Load matching for a photovoltaic panel with a given insolation

3.2.3 Battery energy storage

Storage is very common with small hybrid power systems and the lead-acid battery is the most popular option as it is inexpensive compared to newer technologies. The chemical reaction of the production of voltage in a lead-acid battery is as follows [31]:

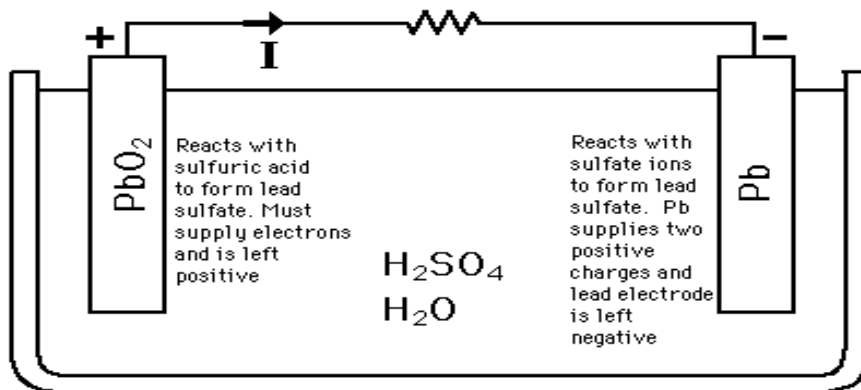
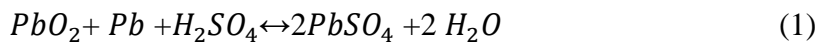


Figure 3-5: Chemical reaction when battery is charged or discharged

A number of battery behavior affect their use in hybrid power systems. For example, battery capacity, expressed in ampere-hours (Ah) which is the product of discharged current and the duration time of discharge, is a function of current level. Terminal voltage of Battery is a function of state of charge and current level. Moreover, temperature affects battery capacity and battery life.

Battery storage systems are modular and multiple batteries can store a large amount of energy. These storage systems are inherently DC devices.

3.3 System sizing using Matlab

The novel optimization algorithm presented in this chapter is based on two constraints: Loss of Power Supply (LPS) and initial cost of the system. To calculate these values the following steps are taken:

First, the demand power is estimated. Then, to meet technical aspects of the design, the size and type of each component is determined. Third, generators are modeled to calculate output power of the system. Afterwards, available energy to the system at each time step, which is the summation of battery energy and the generators' output power, is calculated and number of times that loss of power supply happens (NLPS) is counted. The uniqueness of this algorithm is that it allows blackouts which occur for a small number of hours in a year (2 percent). This saves a great deal of money (in this case around 30%) for the investment. In the end, the optimum number of components, minimizing NLPS and cost, is found.

3.3.1 Demand power estimation

Here, an estimation of demand power for a cabin located in Newfoundland is to be conducted. The average household in this region will use electricity more for lighting and fridge, and then to supply basic equipment such as coffee maker, radio, and TV respectively. Moreover, it is assumed that heating is done with propane. In order to calculate refrigerator power consumption, it is assumed that the motor is off half of the day.

Appliance Load	AC	DC	(A) Rated Wattage	(B) Hours Used Per Day	(C) Watt Hours Per Day (A)*(B)	
					AC	DC
Kitchen lights(2)	Y		15	3h*2 lights	90	
Living room Lights(2)	Y		15	5(*2)	150	
Bedroom lights(2)	Y		11	2(*2)	44	
Basement, Bathroom, Hall lights(4)	Y		15	1(*4)	60	
Small Fridge	Y		150	3.4	510	
Water pump		Y	90	2		180
OutdoorLights(2)	Y		15	8(*2)	240	
Washer	Y		160	1	160	
MicrowaveOven	Y		1000	0.5	500	
Radio	Y		5	7	35	
TV		Y	60	3		180
Vacuum cleaner	Y		800	0.25	200	
Intermittent loads (Coffee maker)	Y		1000	0.5	500	

Table 3-1: Demand load estimation of a cabin

Subtotal:

AC: 2489wh/d

DC: 360wh/d

Also, it is assumed that the cabin is only used on the weekends (roughly about 120 days a year) so the fridge is off at other times of the week, so its estimated use is 3.4 hours a day.

Table 3-1 lists appliance load and the amount of energy consumed per day.

DC to AC inverter efficiency ranges from 80-95 percent. If we consider the efficiency of DC-AC inverter equal to 0.9, AC loads have to be adjusted for inverter losses:

$$\text{Adjusted AC load} = 2489/0.9 = 2760 \text{ Wh/d}$$

$$\text{Total daily load} = \text{DC loads} + \text{Adjusted AC load} = 3120 \text{ Wh/d}$$

$$\text{Estimated Annual Load} = 3120 * 120 = 374 \text{ kWh}$$

The figures below shows monthly average value of AC and DC load (kW) estimated for the cabin, synthesized randomly for each day of a month to be used in the Matlab code and the Homer software.

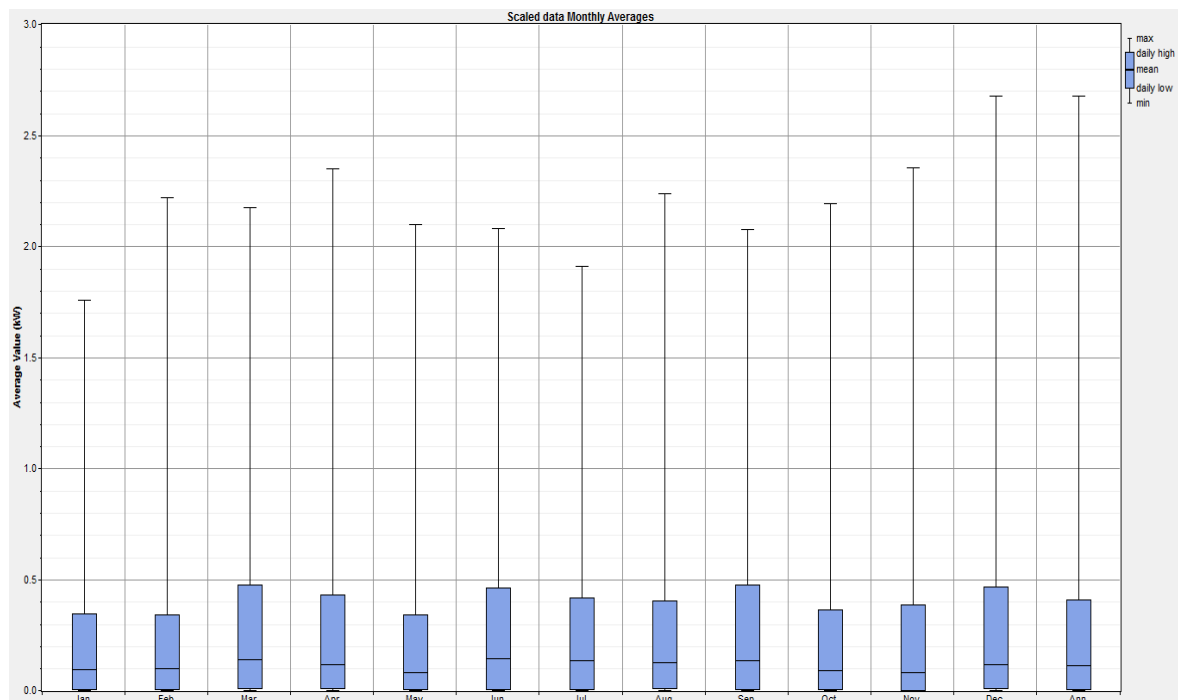


Figure 3-6: Monthly average data of AC load

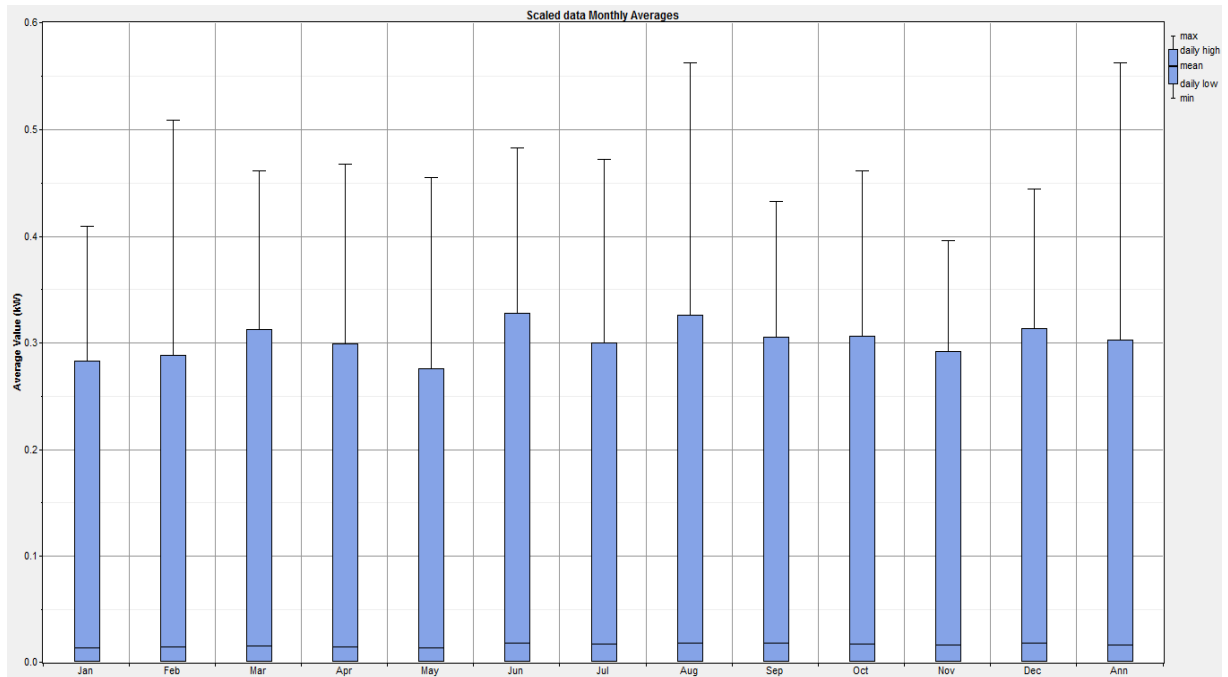


Figure 3-7: Monthly average data of DC load

3.3.2 Size and type of components

Assuming the annual available sunlight in St. John's is equal to $3.25\text{kWh}/\text{m}^2$ and wind speed 6m/s (or 13.5mph), which has to be converted based on the hub height of the turbine, sizing of the components is approximately conducted.

Below, some information about solar panel modules, wind turbines and batteries available in the market along with their prices, nominal voltage and rated power are presented.

3.3.2.1 Typical solar panel modules

The performance of a PV module is affected by solar radiation, temperature and the characteristics of the PV module.

Table 3-2 Indicates typical solar panel modules' specification, power, nominal voltage, and nominal current, available in the market [32].

Module	Rated Power(W)	Nominal Voltage(V)	Nominal Current(A)
Kyocera KC 120	120	16.9	7.1
Siemens SM100	100	17.0/34.0	5.9/2.95
BP Solar BP-275	75	17	4.45
CANROM-65	65	16.5	4.2
Photowatt PWX500	50	17	2.8
Uni-Solar US-21	21	21	1.27

Table 3-2: Typical solar panel modules [32]

To determine size of module, array size can be determined as follows [32]:

$$\text{Array size} = \frac{\text{Total daily load}}{\text{Peak sunlight hours}} * 0.77 \quad (2)$$

In (2), the factor 0.77 assumes 90 percent batteries charge regulation efficiency and an 85 percent battery efficiency. From the technical point of view, to increase output voltage multiple panels are connected in series and to increase the current and the power at a given voltage, multiple panels are connected in parallel. Also, slope of the panels and their lifetime are assumed to be 47.55° and 20 years respectively.

3.3.2.2 Typical Wind Turbines

Table 3-3 shows specifications of typical wind turbines available in the market [33].

$$\text{Annual Energy Output (AEO)} = C_F * \text{Wind turbine rated power} * 8760 \quad (3)$$

C_F is the capacity factor of a wind turbine. Since power demand is below these turbines' output, a small wind turbine, Ampair HAWT –0.3 kW is used and the annual average output (AEO) of this small wind turbine is calculated step-by-step in MATLAB. These steps are as follows:

Turbine	Bergey	Ketrel	Proven 7	Whisper	Skystream
Specifications	XL.1	e.3000		200	3.7
Swept area (square feet)	53	76	103.6	63.5	113
Annual Energy Output at 13mph(KWh)	1,710	2,966	6,614	2,637	3,898
Price(\$)	2590	2950	9650	2995	5400
Warranty years	2	5	2	5	5

Table 3-3: Typical wind turbines [33]

Firstly, to find annual energy output, power output of the wind turbine corresponding to each wind speed is provided based on the manufacturer's data sheet. Secondly, available year round wind is loaded in the code. Thirdly, after plotting the histogram, annual energy output is calculated summing all the energy output, i.e. multiplication of histogram data and the power. The table below indicates power output of the Ampair HAWT –0.3 kW wind turbine based on the wind speed at the hub height [34].

m/s	1	2	3	4	5	6	7	8	9	10	11	12	13	14	15	16
W	0	0	4	10	20	34	51	76	110	144	192	248	293	300	300	300

Table 3-4: Power and wind speed [34]

In appendix A.1 a code is introduced to calculate annual energy output of wind turbines.

The annual energy output will be 176128 Wh (or 176 KWh).

This wind turbine costs around 600 USD and the Operation and Maintenance (O&M) costs for a wind turbine generally are in a range of 1.5% to 3% which, due to the low price of this turbine, can be considered as zero.

3.3.2.3 Battery

In order to determine the size of batteries, battery capacity can be determined as follows [32]:

$$\text{Battery capacity} = \frac{\text{Total daily load *days of storage}}{\text{Battery voltage}} *0.42 \quad (4)$$

The factor 0.42 in (3) assumes 85 percent battery efficiency and a 50 percent maximum depth of discharge. Technically, to increase output voltage, multiple batteries can be connected in series to increase the current, and power at a given voltage, multiple batteries can be connected in parallel. In order to have 12V terminals directly connect to the DC bus of the system, two 6V-1156Ah batteries are connected in series.

3.3.3 Model of components

Design of a hybrid solar–wind system is mainly dependent on the performance of individual components. As the first step of system sizing, individual components are mathematically modeled to predict the system’s performance. Then, their combination is evaluated to meet the demand reliability.

3.3.3.1 Wind turbine

The mathematical power developed by the wind turbine, P_m , can be expressed using Betz’s law [35]:

$$P_m = C_p(\lambda, \beta) \frac{\rho A}{2} v^3 \quad (5)$$

$$C_p(\lambda, \beta) = C_1 \left(\frac{C_2}{\lambda_i} - C_3 \beta - C_4 \right) e^{\frac{-C_5}{\lambda_i}} + C_6 \lambda \quad (6)$$

$$\frac{1}{\lambda_i} = \frac{1}{\lambda + C_7 \beta} \frac{C_8}{\beta^3 + 1} \quad (7)$$

$$\lambda = \frac{R\omega}{v} \quad (8)$$

Mechanical torque, T_m , is the ratio of mechanical power to turbine speed.

$$T_m = \frac{P_m}{\omega} \quad (9)$$

Average wind speed is a function of height. The ground produces friction forces that delay the winds in the lower layers. This effect is called wind shear and has important impacts on wind turbine operation. Different mathematical models have been proposed to describe wind shear. Prandtl's logarithmic law is one of the most popular methods used to convert wind speed considering to the hub height of turbine:

$$\frac{V_z}{V_{z_{ref}}} = \frac{\ln(Z/Z_0)}{\ln(Z_{ref}/Z_0)} \quad (10)$$

Wind turbine average output is calculated using the power curve of a wind turbine, available on the manufacturer's website, to represent the relation between average power from a wind turbine, average wind speed at hub height and average power. Figure 3-8 indicates monthly average wind speed data ($\frac{m}{s}$) for a year.

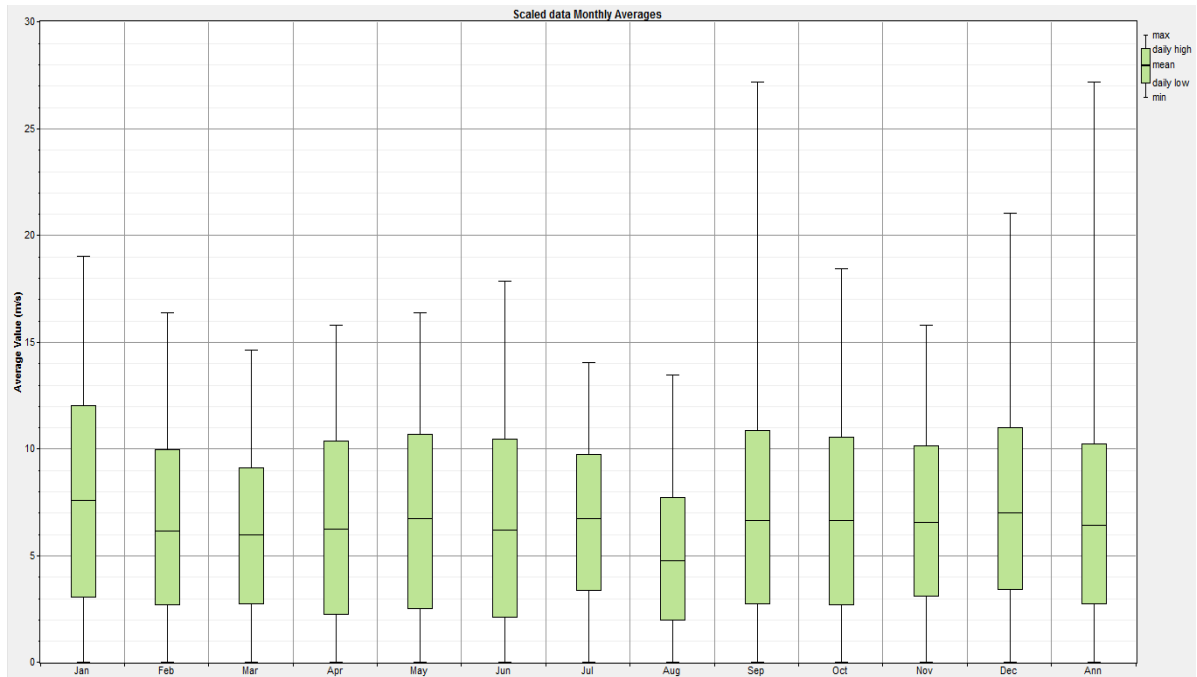


Figure 3-8: Monthly average data of wind speed

3.3.3.2 Solar panel

The output power from a PV panel is calculated by an analytical model which defines the current-voltage relationships based on the characteristics of the PV panel. Figure 3-9 indicates monthly average solar insolation data ($\frac{kW}{m^2}$) for a year.

Zhou, W. et al (2007) introduced a simplified simulation model with acceptable precision to estimate the accurate performance of PV modules [36]. This model includes the effects of radiation level and panel temperature on the output power.

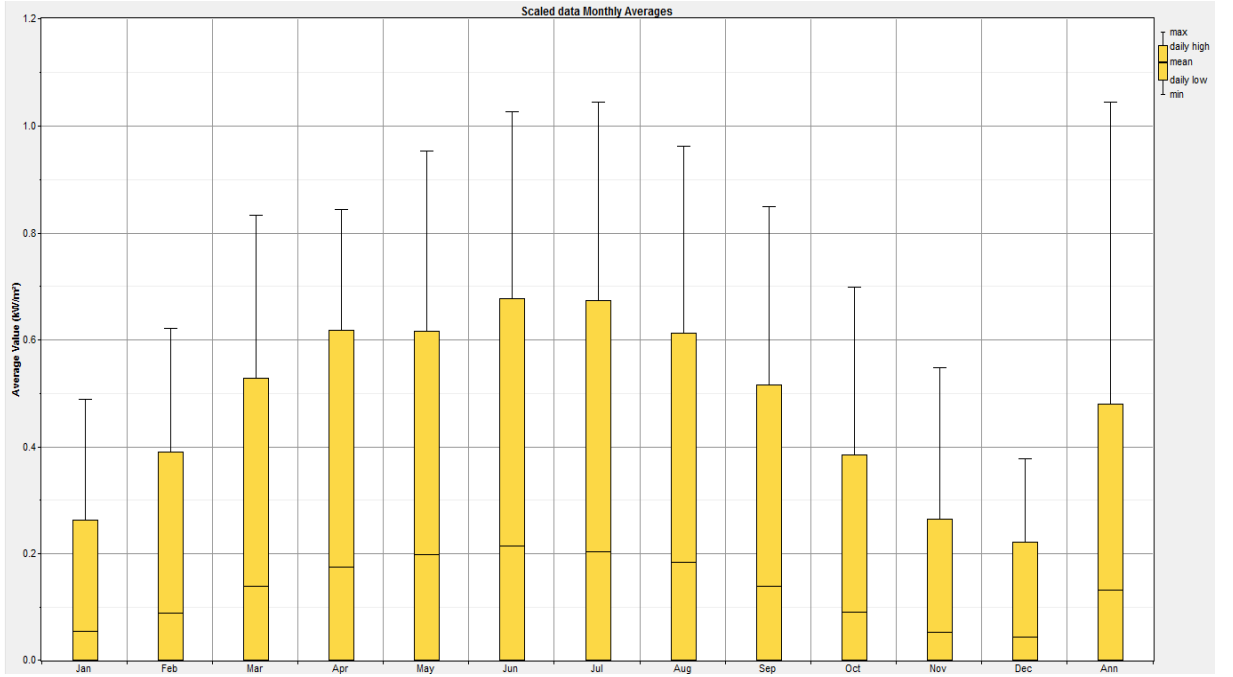


Figure 3-9: Monthly average data of solar insolation

The output power of a solar panel along with a Maximum Power Point Tracker (MPPT) is calculated as follows:

$$P_{mp} = V_{mp} * I_{mp} \quad (11)$$

$$V_{mp} = V_{mp,ref} + \mu_{VOC} * (T_c - T_{c,ref}) \quad (12)$$

$$I_{mp} = I_{mp,ref} + I_{SC,ref} * (\hat{G}/G_{ref}) + \mu_{ISC} (T_c - T_{c,ref}) \quad (13)$$

Since V_{mp} and I_{mp} are unknown, a method introduced by Messenger, Roger A. (2010) is used to calculate output energy of a solar panel at angle β , [37]:

$$P_{pv} = Y_{pv} f_{pv} \left(\frac{\hat{G}_T(\beta)}{\hat{G}_{T,STC}(0)} \right) \quad (14)$$

$$\hat{G}_T(\beta) = B(\beta) + D(\beta) \quad (15)$$

3.3.3.3 Battery

To design a hybrid system, understanding battery charge efficiency is important. Overestimating the loss results in a larger PV array size than required, whereas underestimating it results in unforeseen loss of load. It may also damage batteries due to its inability to provide a high state of charge (SOC). In this thesis, several factors affecting battery behavior have been taken into account, such as charging efficiency, the self-discharge rate and battery capacity, in order to model batteries.

In order to make a trade-off decision choosing battery size, battery depth of discharge (DOD: Indicates how deeply the battery is discharged), and PV array size, considering actual charge efficiency as a function of SOC is important [38]. Here, the battery charge efficiency is set equal to round-trip efficiency and discharge efficiency is set equal to one. Maximum battery life can be obtained if DOD is set equal to 30%-50%. Moreover, as batteries are installed inside the building, temperature effects on the performance of the batteries are neglected. The energy stored in a battery at any hour t , $E_{b,t}$, is subject to the following constraints [39]:

$$E_{bmin} \leq E_{b,t} \leq E_{bmax} \quad (16)$$

Let E_{bmax} as battery's nominal capacity value of SOC equal one.

$$E_{bmin} = (1-DOD) E_{bmax} \quad (17)$$

Here, it is assumed that the efficiencies of the MPPT, the battery controller and distribution lines are 1 and the inverter efficiency is 0.9.

3.3.4 Available energy and NLPS

The LPSP is defined as the ratio of all energy deficits to the total load demand during the considered period. An LPSP of zero means the load will be always satisfied and an LPSP of one means that the load will never be satisfied. NLPS means the number of times this power deficit happens in a year. From the SOC point of view, it basically means the long term average fraction of the load that is not supplied. This can be defined as follows [39]:

$$LPSP = \Pr \{ E_{b,t} < E_{bmax} ; \text{ for } t \leq T \} \quad (18)$$

The simulation period, T, is one year and the time steps are one hour.

The energy generated by wind turbines and PV arrays for each time step (or hour t), $E_{G,t}$, can be expressed as [39]:

$$E_{G,t} = N_{WT} * E_{WT} + N_{PV} * E_{PV} \quad (19)$$

If the generated energy from renewable sources exceeds that of the load demand, the batteries will be charged with the round trip efficiency ($\eta_{bat.}$) [39]:

$$E_{b,t} = E_{b,t-1} (1-\delta) + [E_{G,t} - E_{L,t} / \eta_{inv.}] \eta_{bat.} \quad (20)$$

When the load demand is greater than the available energy generated, the batteries will be discharged by the amount that is needed to cover the deficit as below [39]:

$$E_{b,t} = E_{b,t-1} (1-\delta) + [E_{L,t} / \eta_{inv.} - E_{G,t}] \eta_{bat.} \quad (21)$$

Summation of $E_{G,t}$ and $E_{b,t}$ is called available energy. If available energy does not satisfy the load demand for hour t, this deficit is called Loss of Power Supply (LPS) and can be expressed as follows [39]:

$$LPS_t = \Sigma LPS_t / \Sigma E_{L,t} \quad (22)$$

Finally, the algorithm minimizes NLPS allowing a minimum number of times for blackout occurrence, while minimizing the cost. This method finds the most optimum number of components regarding defined NLPSP and saves a great deal of money on the initial cost of the system. In the end, the array of optimum solutions displays the minimum components configuration. The flowchart below indicates the unique algorithm of optimal system sizing.

The results of the defined system implemented in Matalab code, shown in Appendix A.2, are as follows:

Five 100 watts solar panels, one 0.3 kW Ampair wind turbine and ten 1156 Ah batteries.

This system costs 15,520 USD.

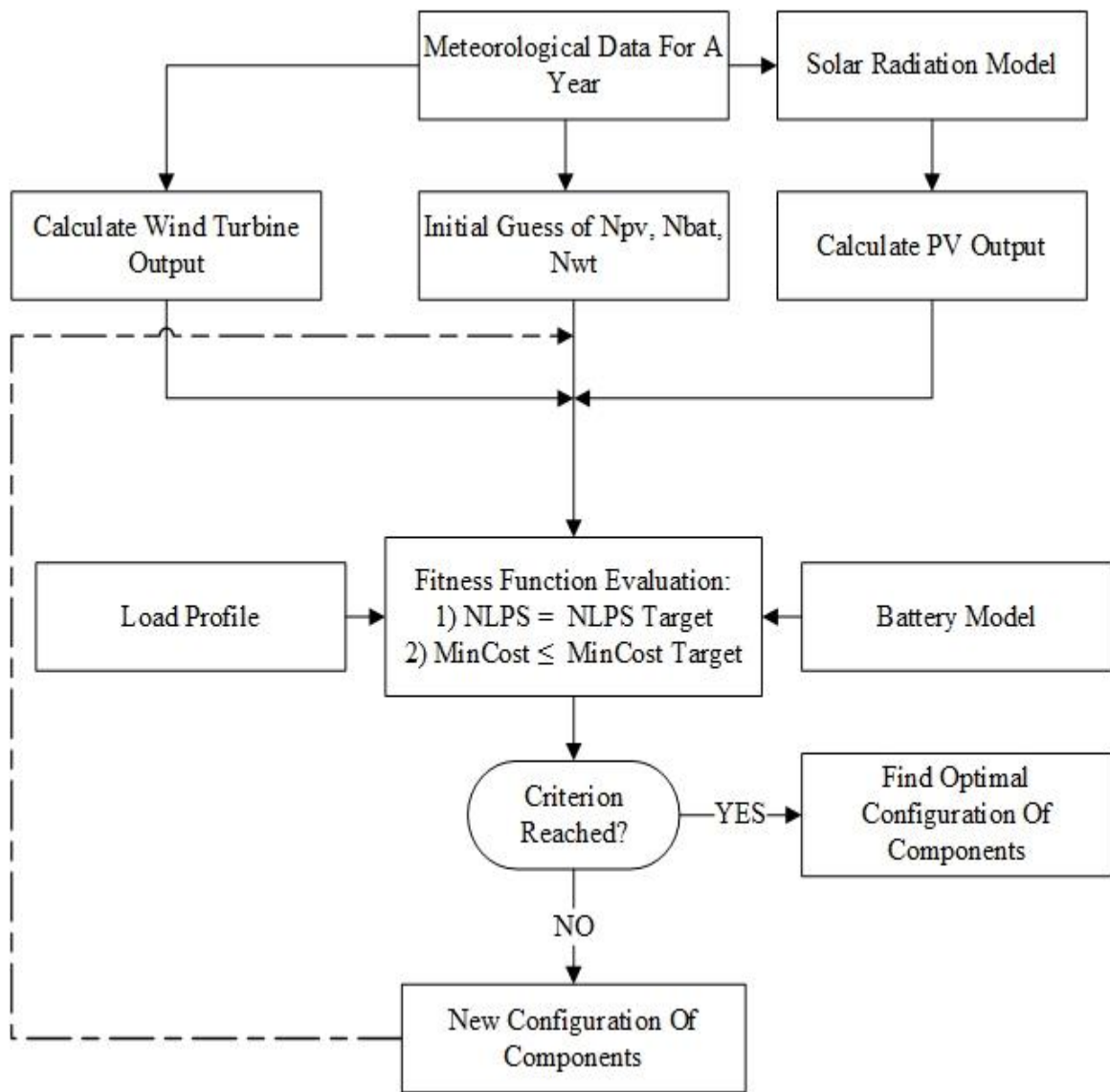


Figure 3-10: Algorithm for optimal sizing of the system

3.4 System sizing in Homer

3.4.1 Introduction to Homer software

HOMER (Hybrid Optimization Model for Electric Renewable) is a computer model that simplifies the task of designing hybrid renewable micro grids, whether remote or grid-connected. HOMER's optimization and sensitivity analysis algorithms enable evaluation of

the economic and technical feasibility of a large number of technologies. Moreover, it provides detailed simulation and optimization in a model that is simple in a user friendly environment [40].

3.4.2 System sizing procedure

In the system configuration, PV panels, wind turbines, and a battery bank are paralleled in order to supply power to the load demand. The excess energy generated from PV panels and wind turbines is stored in the battery banks until full capacity of the storage system is reached. Once the energy is deficit, the battery bank discharges to compensate for the shortfall in load demand. The difference in power generated between the renewable energy source and the electrical power demand decides whether the battery bank is in a charging or discharging state.

System design in the Homer software is conducted as follows:

First, year round insolation data, wind speed data, and load estimations are put into to the program. Second, system components are chosen and the decision on whether to have an AC coupled hybrid system, which is more efficient but has difficult dynamic control, or a DC one, which is less efficient but has easy dynamic control, is made. Moreover, we can either minimize the capital cost in spite of the large amount of excess electricity, or lower the amount of excess electricity by adding batteries which increases the capital cost. The excess electricity will go to the dump load. The system schematic in Homer software is as show below:

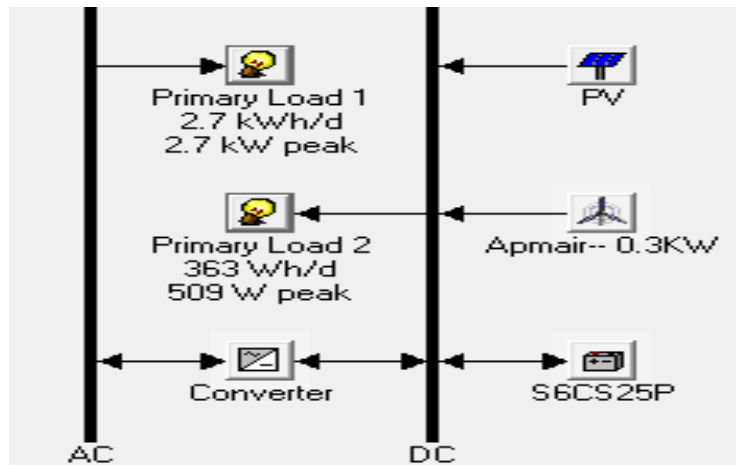


Figure 3-11: System schematics in Homer

3.4.3 Homer results

Here are the Homer software calculation results:

A. Sensitivity case

Wind Data Scaled Average: 6.43 m/s
 Apmair-- 0.3KW Hub Height: 10 m

B. System architecture

PV Array	0.6 kW
Wind turbine	2 Ampair-- 0.3KW
Battery	14 Surrerte 6CS25P
Inverter	3 kW
Rectifier	3 kW

Table 3-5: system architecture

C. Cost summary

Total net present cost	\$ 22,002
Levelized cost of energy	\$ 1.541/kWh
Operating cost	\$ 6.43/yr

Table 3-6: Cost summary of the HPS

D. Net Present Costs

Component	Capital	Replacement	O&M	Fuel	Salvage	Total
	(\$)	(\$)	(\$)	(\$)	(\$)	(\$)
PV	1,200	187	0	0	-105	1,282
Apmair-- 0.3KW	1,200	0	0	0	0	1,200
Surette 6CS25P	18,200	0	0	0	0	18,200
Converter	1,320	0	0	0	0	1,320
System	21,920	187	0	0	-105	22,002

Table 3-7: Net percent costs of hybrid power system

E. Annualized Costs

Component	Capital	Replacement	O&M	Fuel	Salvage	Total
	(\$/yr)	(\$/yr)	(\$/yr)	(\$/yr)	(\$/yr)	(\$/yr)
PV	94	15	0	0	-8	100
Apmair-- 0.3KW	94	0	0	0	0	94
Surette 6CS25P	1,424	0	0	0	0	1,424
Converter	103	0	0	0	0	103
System	1,715	15	0	0	-8	1,721

Table 3-8: Annualized costs of hybrid power system

F. Electrical

Component	Production	Fraction
	(kWh/yr)	
PV array	661	36%
Wind turbines	1,167	64%
Total	1,828	100%

Table 3-9: Generators annual power production

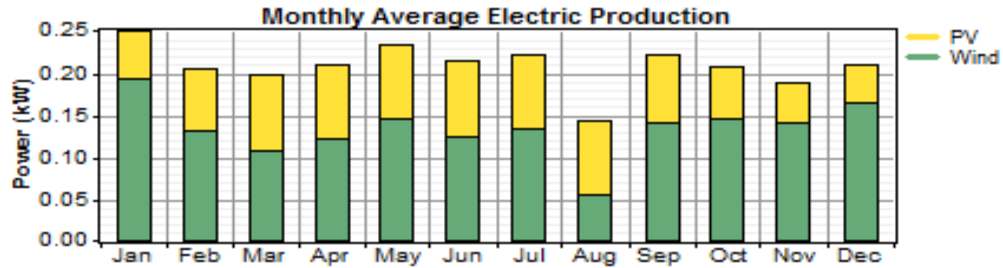


Figure 3-12: Monthly average electric production

3.5 Conclusion

The mathematical model is implemented in Matlab code, which is explained in Appendix A. After running the code, it is observed that the results from the developed code are logically in agreement with results of the Homer software. Table 3-10 indicates the comparison of results.

	Developed Code (for NLPS=200)	Homer Software
N_{PV}	5	6
N_{wt}	1	2
N_{bat}	10	14
Cost	15,520	22000

Table 3-10: Comparison of results between Homer and the developed code

Since there is no clear formulation to account for interest rate, replacement, and maintenance, these costs are neglected in estimating total cost of the developed code, which is a source of difference. More importantly, adjusting NLPS is not provided in the Homer software and so there is no option available to minimize the cost by allowing some hours of loss of power. In the developed code, by considering an acceptable number for the NLPS

(2%) about \$ 6480 USD are saved (30% of investment money), knowing that the bigger the size of the system the more initial cost saving happens.

3.6 Case study: Compare HOMER example with the developed code

The “Sample-OffGridHouseInDominicanRepublic.hmr” example analyzes PV and wind power systems for an off-grid house in tropical locales.

A range of load sizes, from 0.2 kWh/d to 1 kWh/day, and a range of wind speeds, from 4 m/s to 7 m/s are considered in this example.

Monthly average of solar, wind, and load data of Dominican example are shown below.

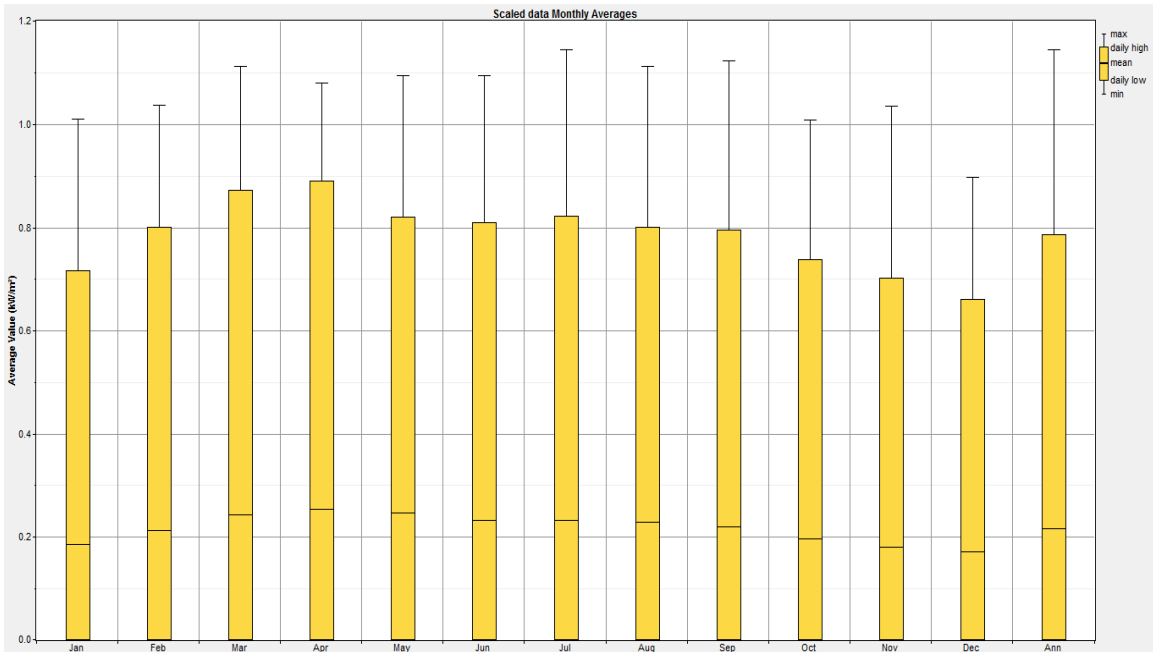


Figure 3-13: Monthly average of solar insolation data

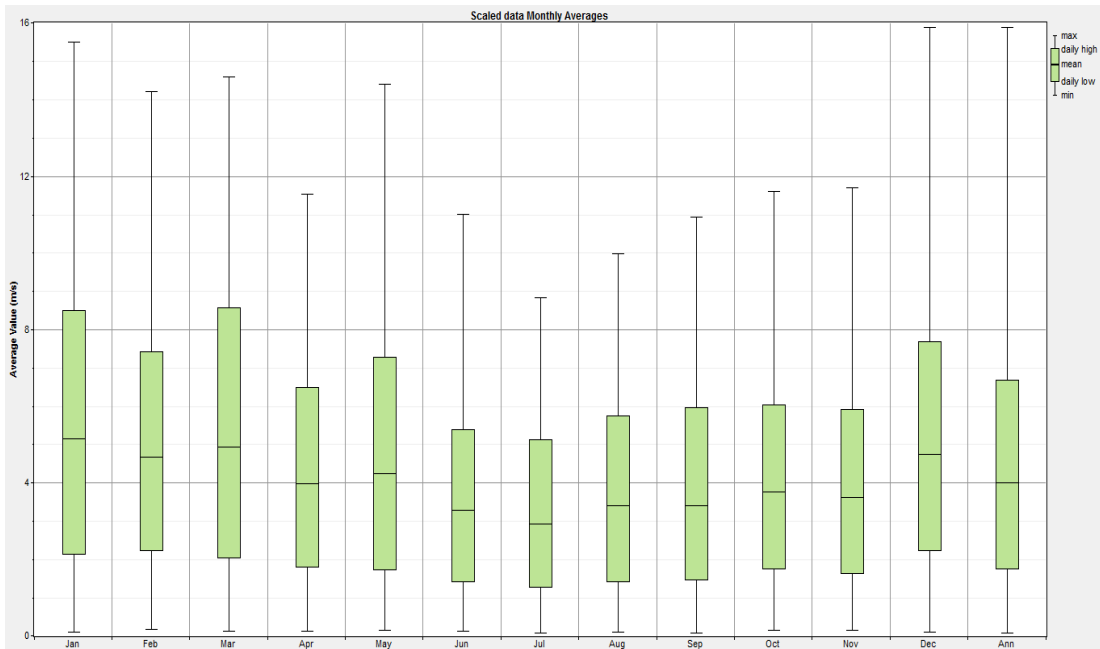


Figure 3-14: Monthly average of wind speed data

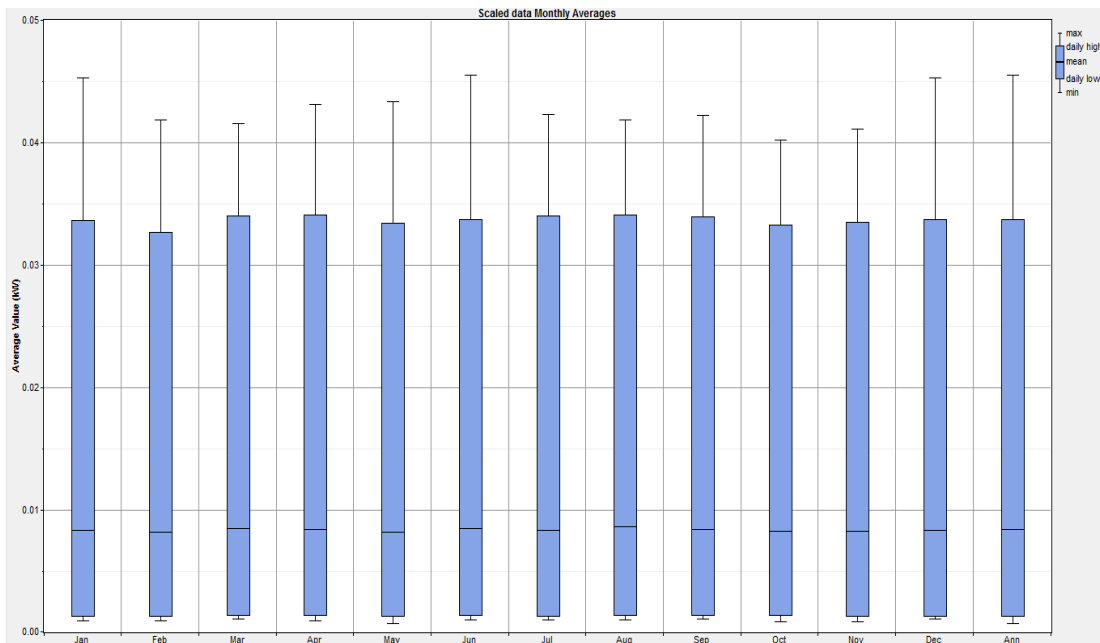


Figure 3-15: Monthly average of load data

Moreover, pictures below indicate a built in example system components and layouts available on the Homer website. Results are also reported from Off-Grid House in the Dominican Republic example in the Homer software.

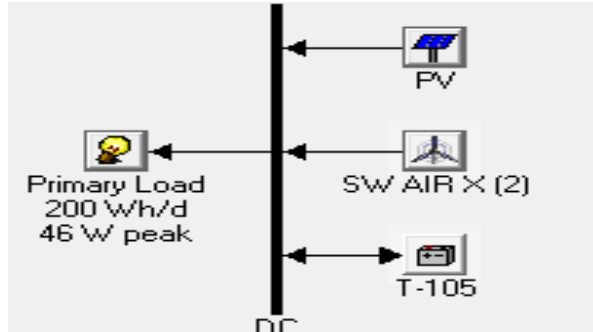


Figure 3-16: System overview in Homer

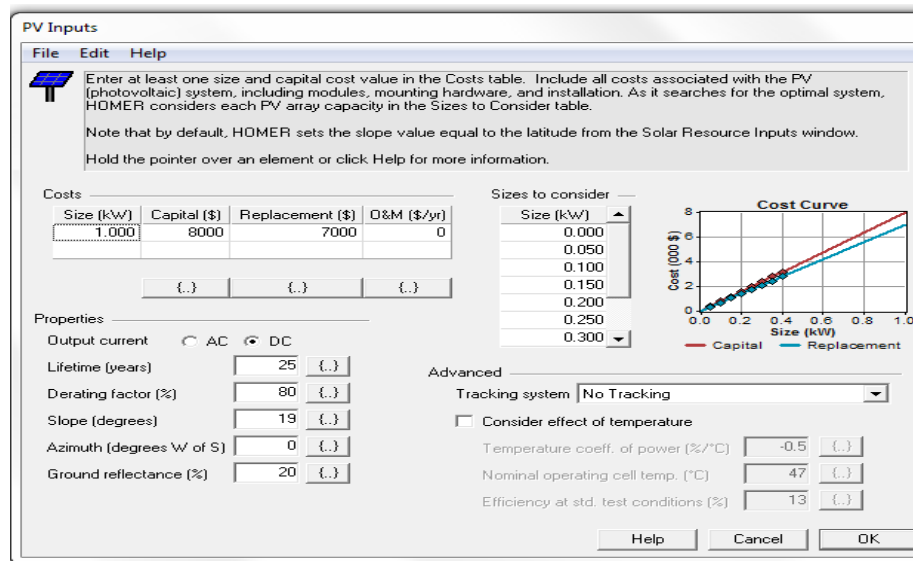


Figure 3-17-(a): PV inputs

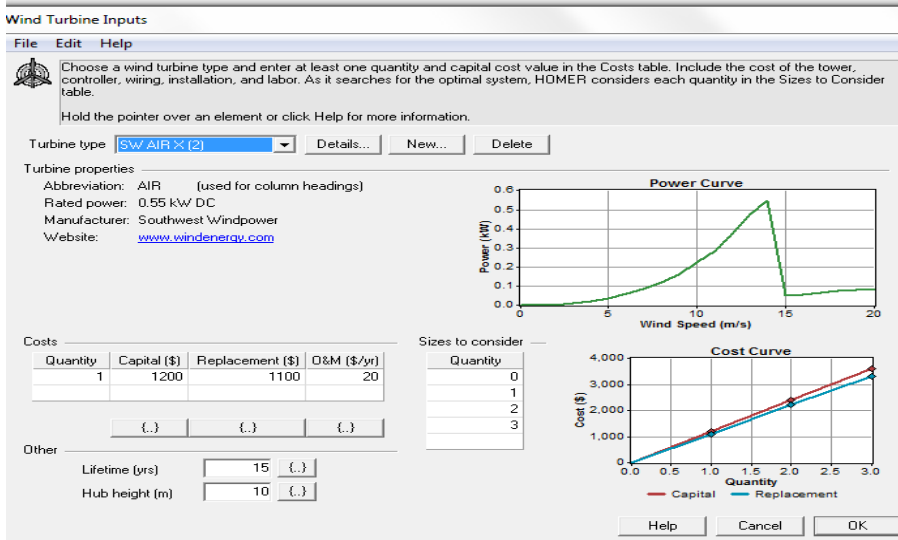


Figure 3-17-(b): Wind turbine inputs

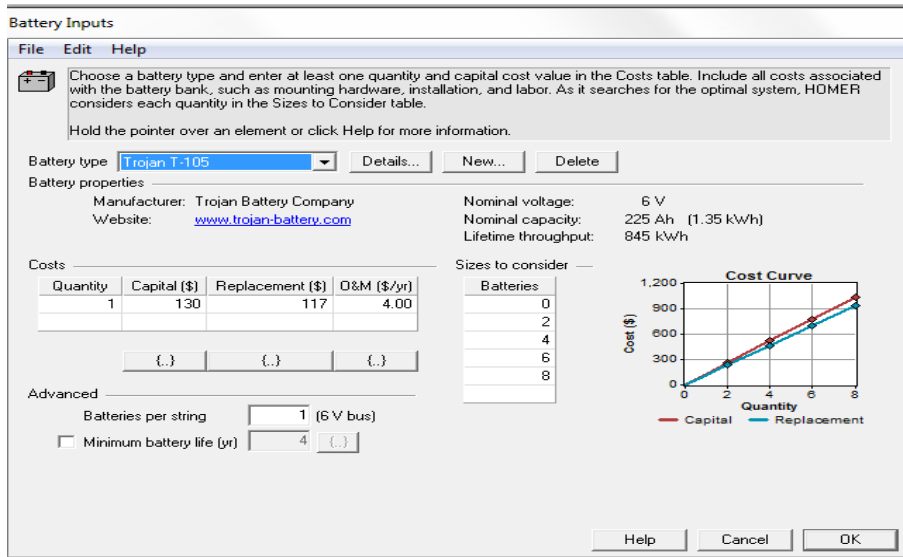


Figure 3-17-(c): Battery inputs

Figure 3-17-(a) to (c): System components in Homer

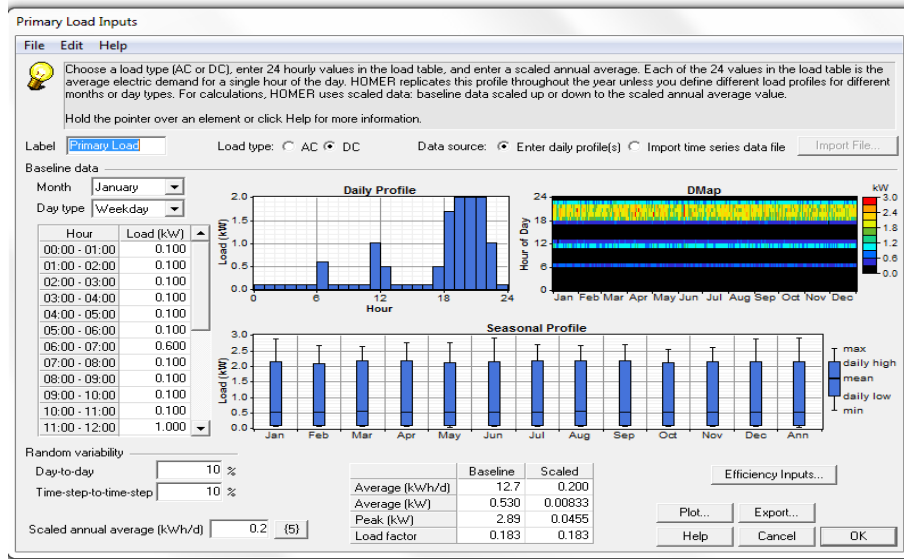


Figure 3-18: Primary load inputs in Homer

3.6.1 Homer results

A. Sensitivity case

Primary Load Scaled Average: 1 kWh/d

Wind Data Scaled Average: 7 m/s

B. System architecture

PV Array	0.05 kW
Wind turbine 1	SW AIR X (2)
Battery	2 Trojan T-105

Table 3-11: System architecture

C. Cost summary

Total net present cost	\$ 2,520
Levelized cost of energy	\$ 0.608/kWh
Operating cost	\$ 57.6/yr

Table 3-12: Cost summary

D. Net Present Costs

Component	Capital	Replacement	O&M	Fuel	Salvage	Total
	(\$)	(\$)	(\$)	(\$)	(\$)	(\$)
PV	400	0	0	0	-22	378
SW AIR X (2)	1,200	459	229	0	-229	1,660
Trojan T-105	260	131	92	0	0	482
System	1,860	590	321	0	-250	2,520

Table 3-13: Net percent cost

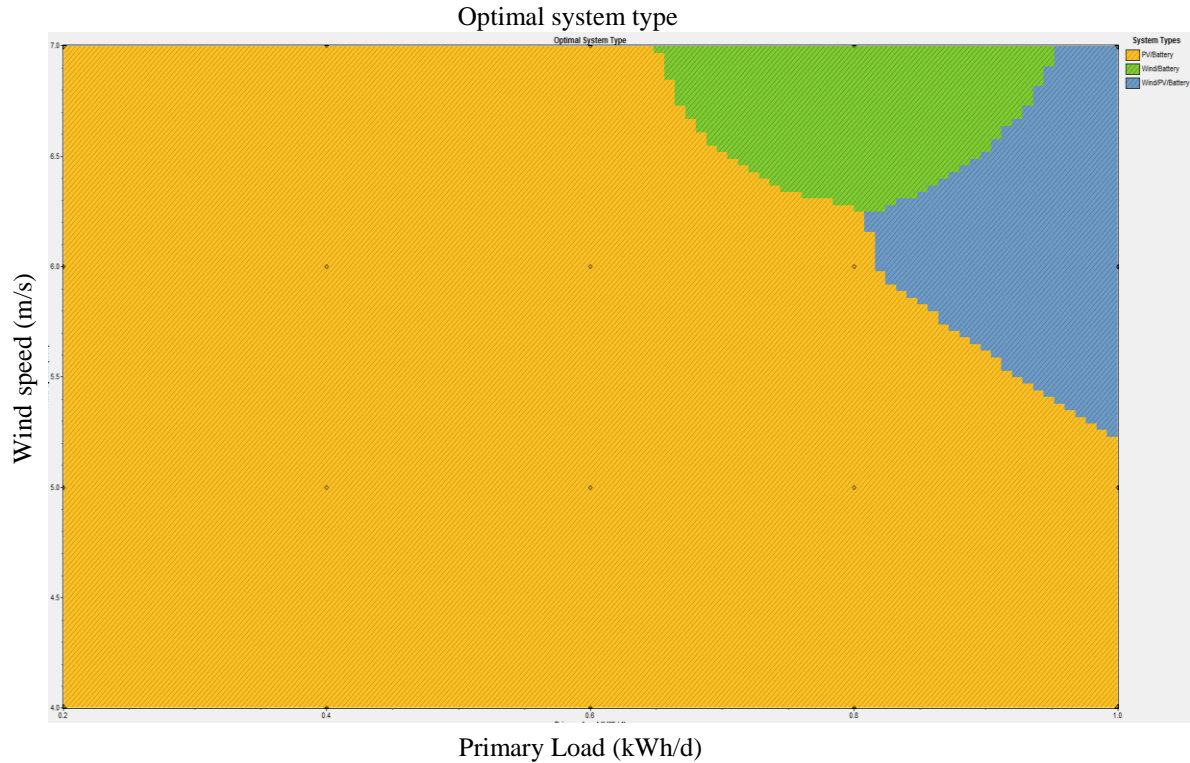


Figure 3-19: Optimal system type graph

The optimal system type graph (Figure 3-19) shows that PV/battery systems are optimal for most of the sensitivity space. Wind/battery and PV/wind/battery systems are optimal in one corner of the sensitivity space. Moreover, it shows that at the smaller sizes, the power is more expensive.

3.6.2 Mathematical model

Modeling components for this example are the same as in the previous code except for modeling the wind turbine. As we are using a different type of turbine, a new model is needed to account for it and to calculate generated power.

3.6.2.1 Wind turbine model

Compared to the last code, the only difference is defining an appropriate equation to represent SW AIR X (2) wind turbine output. In order to do that, we first need to input

corresponding generated power and wind speed data. Then, a polynomial equation is fitted, as shown in Figure 3-20, to make the output power function. The code to do so is available in Appendix A.3. The green line shows the first fit to the power curve with six degree of polynomial fit, explained in Appendix A.3, and the blue circles are the best fit to the turbine characteristics, explained in Appendix A.4.

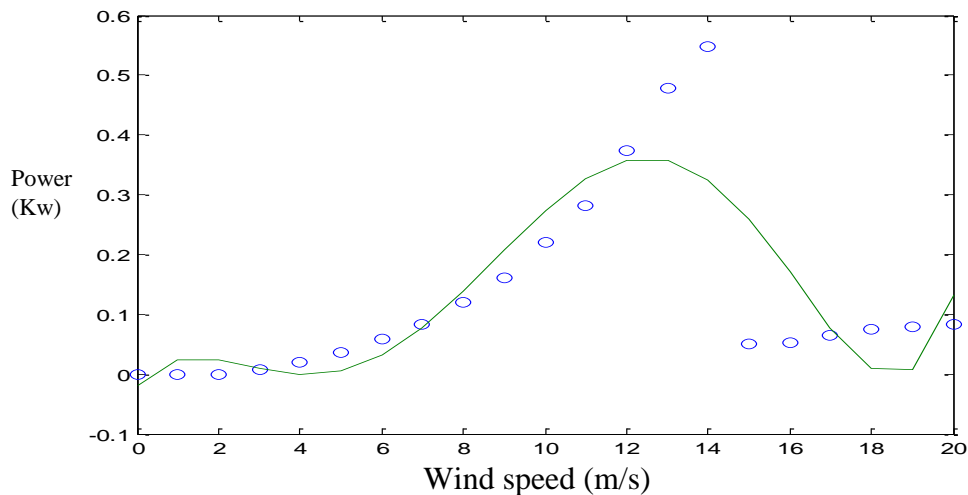


Figure 3-20: Turbine power curve and polynomial equation fitting the output power

The polynomial used to make the power generation function is explained in Appendix A.4. In order to provide the proper polynomial, it is considered that the output of the generator is equal to zero after reaching 14m/s, and the output power, represented with blue circles in Figure 3-20, is exactly the same as the Homer results. Appendix A.5 describes the code to calculate power output of the function. Using this method, the most accurate polynomial is extracted, and the generated power will be 954.42 kWh/yr, which is approximately the output power calculated by Homer software.

3.6.3 Conclusion

A methodology of calculation of the optimum size of a battery bank and the optimum size of a PV array in a hybrid wind-PV system for a given load and level of reliability was demonstrated. It is based on the use of long term data for both wind speed and irradiance for the site under consideration. For a given LPSP, a combination of the number of PV modules and the number of batteries was calculated. As we input models of components in the code detailed in Appendix A.2., we get a different number of components compared to what Homer suggests (Table 3-14). Considering an acceptable number for the NLPS (2%) about \$ 1460 USD are saved (42% of investment money). It is important to note that the optimum mix of PV modules and batteries depends on the particular site, load profile, and desired reliability of the hybrid system.

	Developed Code (for NLPS=200)	Homer Software
N_{PV}	0.1	0.05
N_{wt}	0	1
N_{bat}	2	2
Cost	1060	2520

Table 3-14: Comparison of results between Homer and the developed code

4. Improving off-grid systems: Snow detection on PVs

4.1 Introduction

The major problem with the optimal sizing of solar panels in a small-scale hybrid system is the effect of snow accumulation on the performance of PVs. Roughly 74% of PVs are installed in countries that experience some amount of snowfall [41], [42]. St. John's Newfoundland received more than three meters of snow during the winter of 2014. Generally, the lower the temperature of solar panels, the more output power would be generated due to reduced internal losses. However, snow presents an obstacle decreasing the efficiency of solar panels.

Energy inflow to a snow covered module can occur in three ways:

- a) Diffusion of short wave through snow
- b) Albedo reflection to the exposed rear of a module
- c) Conduction from parts of PV not covered with snow

Although some solar radiation can reach the surface of a snow covered panel, snow losses from a PV system can be as high as 20% for a low profile system to 0.3-2.7% for a highly exposed 28 degree roof mounted system, depending on orientation of PV modules and meteorological factors [43], [44]. This clearly indicates that solar panels should be cleared as soon as possible.

Snow removal can be done in several ways, such as snow shedding, which might occur in the form of either melt on the surface of the modules (see Figure 4-1-(a)), or sheet sliding (see Figure 4-1-(b)). Snow sliding happens due to sunlight or rise of temperature as some incidental radiation would penetrate the layer of snow and melt the snow-module layer to

produce a water layer. Moreover, increasing the tilt angle of panels using a stepper motor not only would lead the gathered layer of snow to slide, but also steeper tilt angles cause less snow to accumulate and therefore less power loss due to snowfall [42].

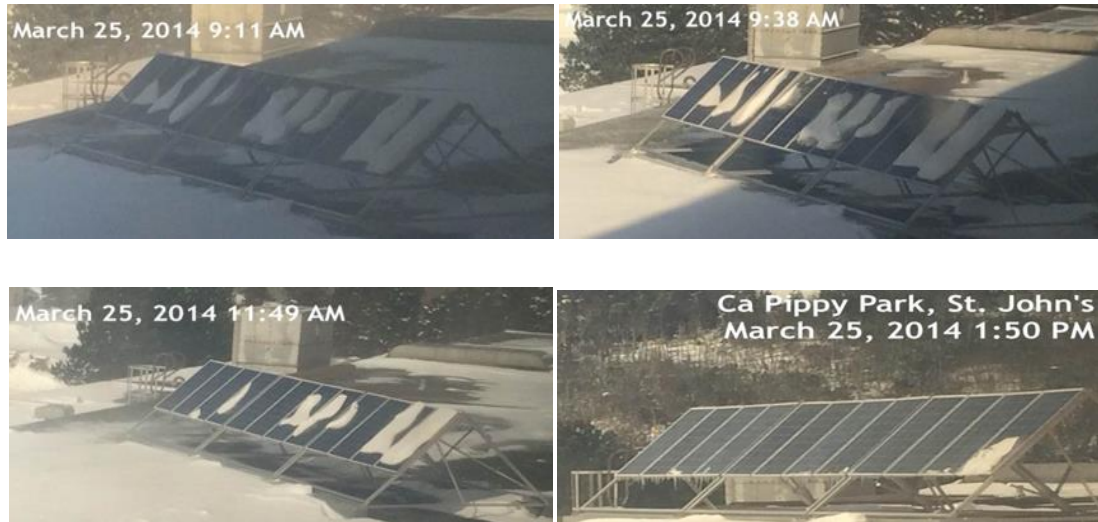


Figure 4-1-(a)



Figure 4-1- (b)

Figure 4-1: (a) snow melting; (b) sheet sliding

4.2 Design of snow detection system

As shown below, the designed system is comprised of a solar panel along with its Maximum Power Point Tracker (MPPT) to obtain maximum power by adjusting the current drawn. Moreover, a current sensor, a voltage sensor and a Light Dependent Resistor (LDR) are used to measure irradiance and the current status of the PV panel.

These three sensors provide enough data to enable the Arduino to determine if there is enough augmentation of snow on the panel.

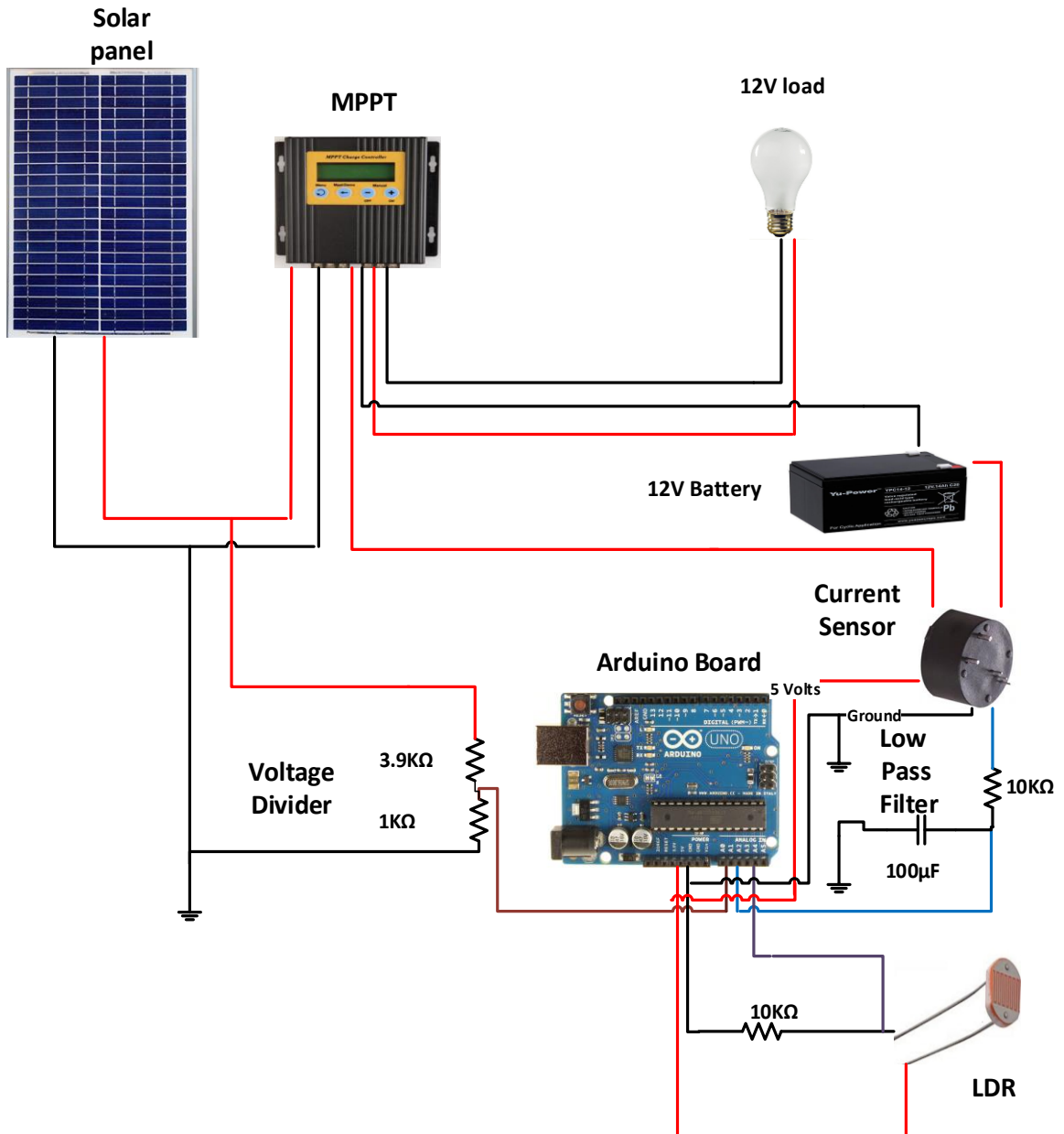


Figure 4-2: System circuit diagram

The Arduino Uno is a microcontroller board based on the ATmega328. It has 14 digital input/output pins (of which 6 can be used as PWM outputs), 6 analog inputs, a 16 MHz ceramic resonator, a USB connection, a power jack, and a reset button. Its supply voltage limit is 6-20 V and it can be powered directly from a 12V PV panel. Two voltage dividers are used to bring input voltages to the microcontroller in measuring range. One for connects the panel output voltage to the analogue input pin of the Arduino and the other is for LDR. Also, output voltage of the current sensor is delivered to the board through a low pass filter in order to read only the low frequency responses. Sensors are connected to the board in company with its Wifi shield powered by the PV panel through adaptor input. Furthermore, a 12V battery is connected to the MPPT output and a 12V light-bulb is used as a load connected to the same node.

4.3 Alert algorithm

The designed system was closely observed and tested during the winter months of 2014. Data was collected in a variety of atmospheric conditions and types of snow collected on the panels. During the experiment it was noted that five centimeters of snow on panels could be a distinguishable feature affecting the PVs performance and this is used as a check point in the algorithm.

Figure 4-3 depicts the average reading of each sensor (in the digital unit) within three months observation categorized based on atmospheric conditions. Voltage, Current and LDR are readings from sensors and voltage drop, that is the difference of voltage amount at present and at the moment before, is calculated by the microcontroller. Moreover, as the hour angle of a point on the Earth's surface is the angle through which the earth would turn

to bring the meridian of the point directly under the sun, two hours time interval from noon to 2pm is considered in this chart to exclude the effect of the hour angle ($120/2=60$ data points for each day).

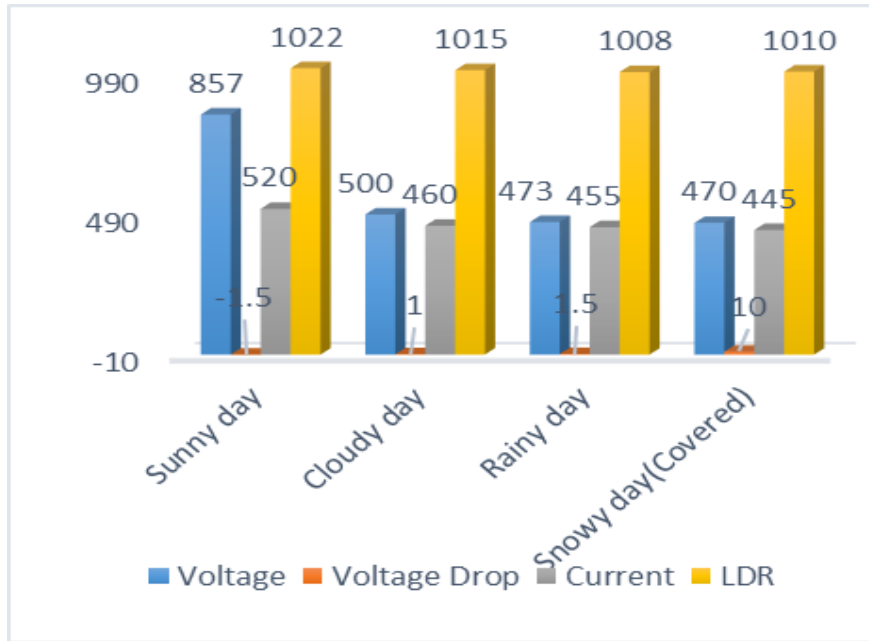


Figure 4-3: Average of sensors readings during three months (12pm-2pm)

It can be seen that current and voltage readings in rainy and snowy days are quite similar. On the other hand, the LDR reading which represents solar irradiance on snowy days is more than on rainy days. Although several similarities were found between a rainy day and a snowy day during the observations based on sensors readings, it was found that thick overcast of clouds can be categorized and differentiated from snow by the value of the panel voltage drop, i.e. the difference in the current voltage reading from the previous voltage reading. Seeking the moments that enough snow has accumulated, as demonstrated in Figure 4-4, the algorithm not only checks that all the sensors to be in certain scope, but also calculates the voltage drop which is a marker of snow detection.

Two promising scenarios are considered to keep track of snow cover on the solar panels. First, as snow is accumulating on the panel, the algorithm starts computing the number of times that the criterion is reached. Second, the present weather is rainy, cloudy or sunny and snow remains, whether from the day before or simply because the panel was not cleared after the first tweet. The common property in both scenarios is a voltage drop due to snow accumulation; however, in the first case there would be a smaller drop compared to the latter.

A short time scale is not required as we are not interested in logging and saving many data points on an SD card. On the other hand, the aforementioned second scenario becomes complex, as on a cloudy evening current sensor readings and a voltage drop could have several similarities with snowy weather. In order to solve the problem, time step was decreased and tuned to two minutes. This provided enough data to make decision and store on a small SD card. Based on three months of observation, two minutes time scale was determined most suitable to apprehend the ratio of voltage drop to detect snow build up. The flowchart shown in Figure 4-4 essentially depicts the snow detection method.

The first step assigns previous voltage and counters including i , j and k to zero. Here “ j ” represents the first and “ k ” represents the second scenario. It sets i , j and k to zero at the end of the day. Subsequently, Arduino monitors voltage, current and LDR and record them on the SD card and then the total counter number increases by one. In the second step, the microcontroller inspects voltage, LDR and current sensor to estimate the recorded numbers based on the defined scope (the defined range for voltage, current and LDR determined based on observations), which is necessary but not sufficient to indicate snow accumulation. When the calculated voltage drop is in the range it adds one to the number

of times the criterion is reached (low stands for between three and ten and high for greater than ten defined in the criteria located after $i++$ and $j++$ in the flowchart above).

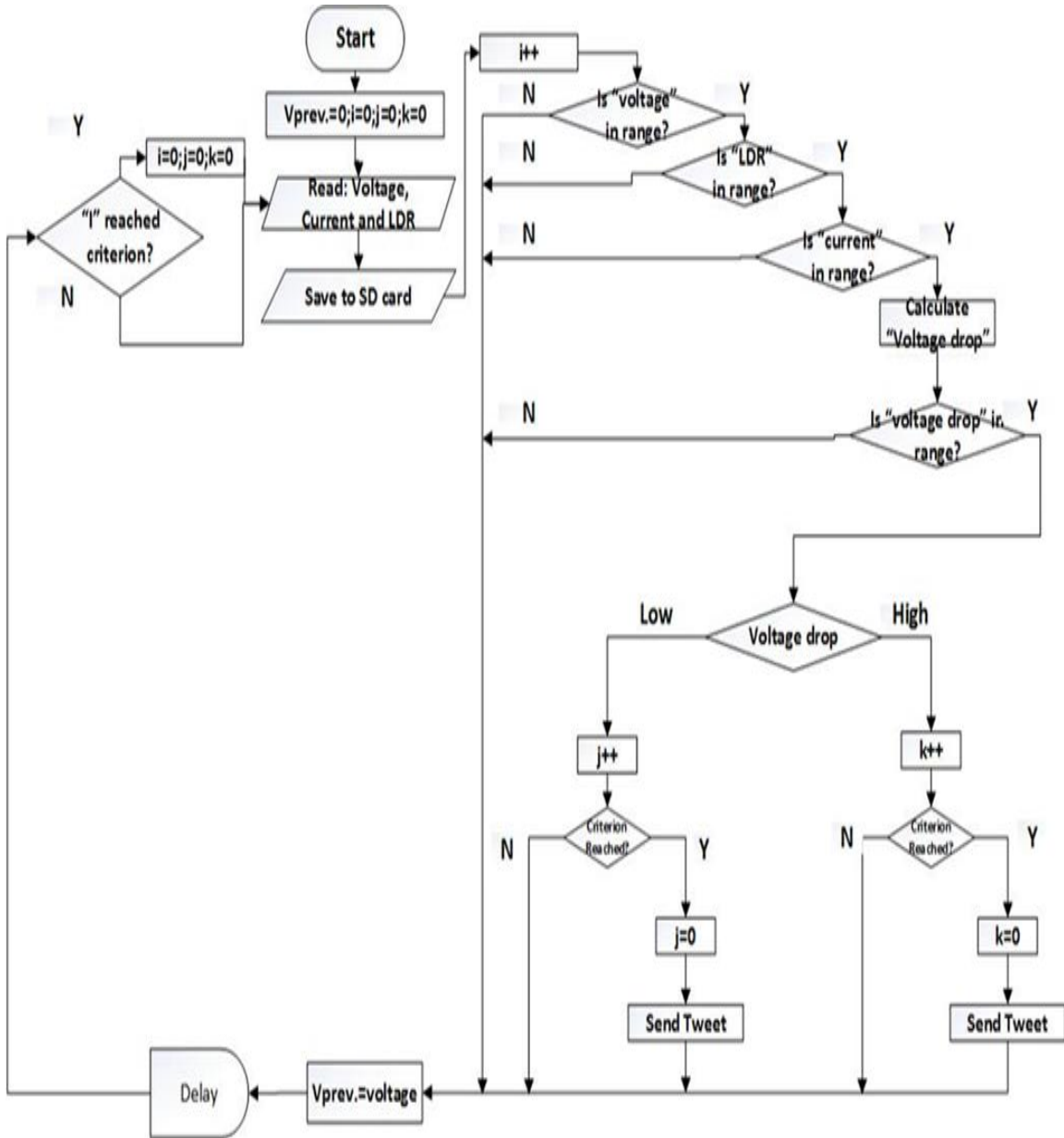


Figure 4-4: Algorithm for snow detection

If “j” or “k” satisfies the condition (considered as $j==6$ or $k==2$), the counter will be set equal to zero and sends a tweet, and both indicate snow build up equally. These threshold values were set, tuned and validated during the experiment. Then, either after tweeting or when any of the conditions are not met, the current voltage will be set equal to the previous voltage along with a delay in order to calculate voltage drop. Finally, microcontroller assesses the number of times the whole process is accomplished and after one day it resets all the counters. If we consider the time between sunrise and sunset equal to approximately 15 hours, we would have $i=450$ since the criterion for “i” is $15*60/2$.

4.4 Arduino code

In the Arduino code, after assigning the input and output pins and defining variables, connection to the Internet follows. The Arduino shield will not connect to networks using WPA2 Enterprise encryption so a WPA network was used [45]. The next step is logging onto Twitter. Twitter Library is a library for Arduino to tweet on Twitter via the Arduino Ethernet Shield [46]. In order to make the library work for the wifi shield some modifications need to be made to the twitter.cpp and twitter.h files in the Arduino’s library. The twitter library works by connecting Arduino to a specific website which in turn will connect to the twitter server. This workaround is because the twitter authentication is a bit code heavy which is difficult to implement on the Arduino. Instead, this code heavy part is implemented on the website and microcontroller instructs the website to tweet [47]. Other than the main loop, two loops are defined as void loops. One is for sending the tweets and the other for writing sensor values on an SD card. The code also checks the criteria and calls the tweeter loop. The implemented method, as described above, is tracking the inputs

from the sensors and calculating voltage drop. If the condition is met, it starts counting based on the two probable scenarios described above. After the counter reaches a specific number contingent upon snow mass, a tweet will be sent and thereupon both counters will be reset. Moreover, a delay of two minutes in the loop using delay commands in the program was found to be the necessary and sufficient condition. This code is available in Appendix. B.

4.5 Experimental Results

The designed system was tested during the winter of 2014 at the Faculty of Engineering and Applied Science, Memorial University of Newfoundland. During this time many data and time stamped pictures of the panel's status was collected and the algorithm was fine tuned. Figure 4-5 depicts the system setup in the lab indicating the MPPT value when the load is on. The multi-meter shows the panels' output voltage which indicates a node voltage other than the parallel node of battery and load. All data points are also stored on an SD card inserted on the Arduino Wifi shield (also available on the author's twitter account).



Figure 4-5: System setup



Figure 4-6: Clean panels



Figure 4-7: Snow on panels

Figure 4-6 shows clear panels while in Figure 4-7 accumulation of snow on the panels is displayed, pointing out the various feasible working conditions. Figure 4-8 and Figure 4-9 exhibit tweeted messages to the author's twitter account according to the state perceived in Figure 4-7 provided with time and date stamp as a reference.



Figure 4-8: Tweeted message



Figure 4-9: Twitter messages

4.6 Conclusion

The designed system is precisely capable of detecting more than five centimeters of snow accumulation as this amount significantly affected the PVs' performance. The novel

algorithm of snow detection and a low cost system as described above has been developed and validated. This chapter presented details of the system setup and the program written for the Arduino. A low cost and low power alert system for PV panels is essential since proper assessment of snow related losses can help improve system performance and maintenance, leading to more energy in climates experiencing snowfall.

For future work, a mathematical formulation relating climate data to voltage and current sensors readings for solar panels should be investigated. Moreover, methods to mitigate snowfall losses such as developing the idea of shedding the snow by means of increasing the slope of the module should be studied thoroughly as this could be the most economical way of removing snow accumulation on solar panels.

5. Connection of large-scale wind power to the isolated grid of Newfoundland

5.1 Introduction

Small-scale renewable systems, discussed in chapter three, generate power (in KW range) to provide electricity for small load, such as a cabin or a house. To generate power on a large scale to meet the power demand of Newfoundland (in MW range) wind farms are one of the best options to develop a sustainable future for this region, due to the following reasons: (1) Newfoundland has an outstanding wind resource. (2) Wind power is a clean and cost-effective source of energy which produces no air pollution. (3) In addition to its environmental benefits, it offers valuable economic benefits to small communities through job creation and investment. However, the uncontrollability of its output power presents a forbidding barrier, resulting in high estimates of auxiliary service costs. For instance, to avoid under frequency load shedding on account of loss of multiple wind farms, it is assumed that wind capacity must be backed up with conventional power generation units. These barriers impose some integration costs relative to system characteristics and wind penetration level due to the fact that aggregate production and consumption must be balanced continuously and fluctuations in load must be matched by fluctuations of controlled generators [48]. Although it is not necessary to compensate for each individual fluctuation, the aggregate control area load and generation need to be balanced. This clearly indicates the importance of wind farms' aggregated power estimation to clarify aforementioned barriers. It is theorized that large scale geographic diversity of wind farms

results in smoothing of overall output power [48]. This results in much smaller up and down ramp rates for an aggregated output power, from geographically dispersed small size wind farms than from a very large single wind farm and reduces the impact of unpredictability of wind resources significantly [49].

5.2 Study Parameters

5.2.1 Load Forecast

The 2010 “NLH Island Demand & Energy Requirements 2018 to 2067” load forecast was utilized as the basis for both peak and light load models. The extreme light load is based on approximately 26% of Newfoundland Power (NP) and NLH rural peak loading while the industrial customers loading was estimated at 78% of forecasted peak account for loading coincidences. The NLH annual average system generation load shape for years 2008- 2011 is illustrated in Figure 5-1 [50]. This load shape depicts load factor and hours of a year and was used to estimate extreme light load NLH system generation. The load factor is the average load divided by the peak load in a specified time period

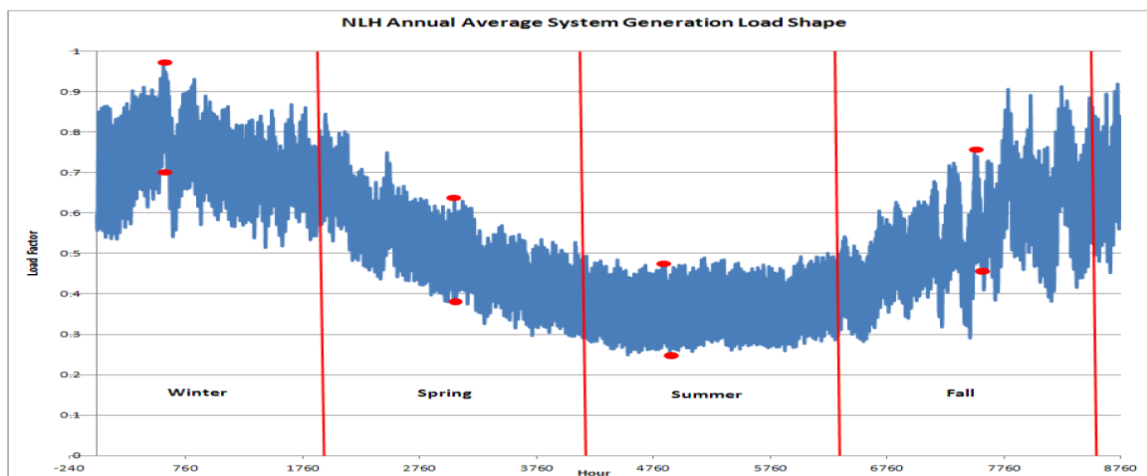


Figure 5-1: 2008-2011 NLH annual average system generation load shape [50]

5.2.2 Wind plants

Distributed wind generation plants is assumed to consist of 9 * 3MW Doubly Fed Induction Generators (DFIG). Twenty wind farms were modeled across the island with the maximum output of each wind turbine farm at 25MW with VAR capability of +/- 13.5 MVARs per plant. Table 5-1 shows a list of twenty distributed wind generating plants on the Newfoundland island grid for the base year 2020 [50].

No.	Plant	Region	Bus #	Point of Interconnection (POI)	
				Location	Bus #
1	Doyles WG1	Western	1001	Doyles 66kV	201
2	Doyles WG2	Western	1002	Doyles 66kV	201
3	Stephenville WG1	Western	1003	Stephenville 66kV	204
4	Stephenville WG2	Western	1004	Stephenville 66kV	204
5	Massey Drive WG1	Western	1005	Massey Drive 66kV	115
6	Peter's Barren WG1	GNP	1006	Peter's Barren 66kV	121
7	Bear Cove WG1	GNP	1007	Bear Cove 138kV	134
8	Buchans WG1	Central	1008	Buchans 66kV	151
9	Springdale WG1	Central	1009	Springdale 138kV	113
10	Cobb's Pond WG1	Central	1010	Cobb's Pond 66kV	316
11	St. Lawrence WG1	Burin Peninsula	1011	St. Lawrence 66kV	372
12	St. Lawrence WG2	Burin Peninsula	1012	St. Lawrence 66kV	372
13	Sunnyside WG1	Western Avalon	1013	Sunnyside 138kV	223
14	Sunnyside WG2	Western Avalon	1014	Sunnyside 138kV	223
15	Fermeuse WG1	Eastern Avalon	1015	Goulds 66kV	457
16	Bay Bulls WG1	Eastern Avalon	1016	Goulds 66kV	457
17	Goulds WG1	Eastern Avalon	1017	Goulds 66kV	457
18	Kelligrews WG1	Eastern Avalon	1018	Kelligrews 66kV	348
19	Bay Roberts WG1	Eastern Avalon	1019	Bay Roberts 66kV	309
20	Heart's Content WG1	Eastern Avalon	1020	Heart's Content 66kV	501

Table 5-1: List of distributed wind plants for the base year 2020 [50]

For dynamic modeling of a doubly fed induction generator, Matlab/ Simulink wind turbine models are used. These models are comprised of four individual models as follows: generator, converter, turbine, and control parameters. Figure 5-2 depicts the characteristic

of a modeled wind turbine in Matlab [51]. In this figure, the turbine output power and turbine speed are in per unit (that is an expression of system quantities as fractions of a defined base unit quantity) of nominal mechanical power and generator synchronous speed, respectively.

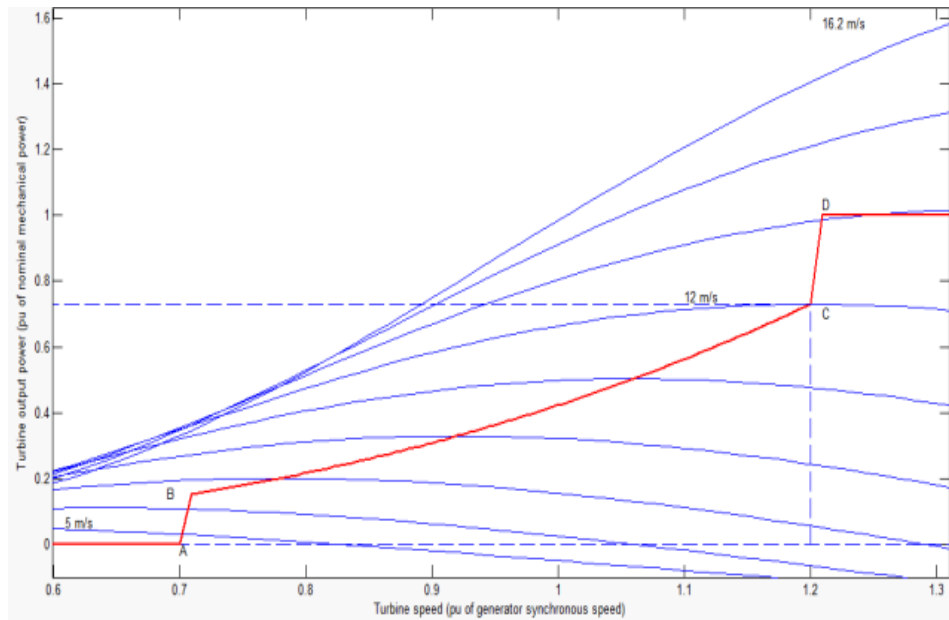


Figure 5-2: Wind turbine power characteristics [51]

5.3 Power system planning and operating criteria

Connection of large wind turbines to grid influences grid stability. Uncertainty about the effect of increased penetration of wind energy on the dynamic behavior of power systems has led to serious concern, resulting in revising and increasing wind turbines' grid connection requirements. An overview of the national grid requirements in several countries shows that the main attention is drawn to fault ride-through (i.e. requirements imposed to avoid significant loss of wind turbine production in the event of faults) and

power control capability (i.e. regulating active and reactive power and performing frequency and voltage control on grid) [52].

The following system planning and operation criteria were used as basis for this study [50].

5.3.1 Voltage Criteria

Under normal conditions, the transmission system is operated so that the voltage is maintained between 95% and 105% of nominal. During contingency events the transmission system voltage is permitted to vary between 90% and 110% of nominal prior to operator intervention. Following an event, operators will take steps (i.e. Re-dispatch generation, switch equipment in or out of service, curtail load or protection) to return the transmission system voltage to 95% to 105% of normal operating range.

5.3.2 Stability Criteria

The frequency of a power system can be considered a measure of the balance or imbalance between production and consumption in the power system. With nominal frequency, production and consumption including losses in transmission and distribution are in balance. If the frequency is below nominal, the consumption of electric energy is higher than production and if it is above nominal the consumption is lower than production [49].

Adding non-dispatchable generation units to the island may result in fewer NLH's dispatchable generation resources being on line leading to fewer generators left to control system frequency. Therefore, frequency excursions become magnified for the same change in load [50]. A theoretical point can be reached where the slightest increase in load will cause the system to become unstable. Frequency protection settings used in these analyses are as follows:

Over Frequency Setting: 61.2 Hz for 0.2 seconds

Under Frequency Setting: 56.4 Hz for 0.2 seconds.

5.4 Study assumptions

The following assumptions were used in the analyses:

- Extreme light load corresponds to worst case scenario and is estimated as 490MW in 2020. This corresponds to an estimated NLH island generation of 511MW.
- Forecasted peak loading is estimated to be 1539MW in 2020. This corresponds to an estimated NLH island generation of 1587MW.
- Wind generators provide VAR support.
- Wind generation is assumed widely.

5.5 NLH's PSS/E model

For load flow study, NL Hydro used distributed wind generating plants consisting of nine 3MW doubly fed induction generators, similar to those of the existing Fermeuse and St. Lawrence wind farms. For dynamic modeling, the PSS/E Generic Wind model “Type 3” of doubly-fed induction generator was used. Figure 5-3-(a) depicts for 2020 an extreme light load base case 500MW wind integration (81% wind penetration). This wind generation is used as the wind capacity of Newfoundland for simulation purposes in this study. Also, this figure indicates each voltage level in the transmission grid of Newfoundland, which operates at voltages from 69 kilovolts (kV) to 230 kV, with different colours as follows [53]:

- 230 kV lines in pink (length: 1,608 kms)

of Matlab/Simulink [51]. A 1kV-12.5kV and a 12.5kV-69kV transformer transmit power to the grid from each 25MW wind turbine and each 100MW wind farm respectively. In the end, all five 100MW wind farms are connected to a 230kV line representing the rest of the grid, through 69kV-138kV and then 138kV-230kV transformers. Each wind turbine has a control system measuring voltage and current and disconnects the turbine in case of instability. The optimum turbine speed producing maximum mechanical energy for a given wind speed is proportional to the wind speed. For wind speeds lower than 10 m/s the rotor is running at a sub synchronous speed. At higher wind speeds, it is running at a hyper synchronous speed. The turbine mechanical power as a function of turbine speed is for wind speeds ranging from 5 m/s to 20 m/s. The Simulink model is run in phasors mode and all blocks are chosen to be compatible with this mode of operation so that transient stability studies can be conducted. Also, all the details of system components and their mathematical equations will be explained in 5.9.5.

Figure 5-4-(a) to (d) details the dynamic model system configuration and Figure 5-5 depicts the protection algorithm implemented in the simulink based Matlab example [51].

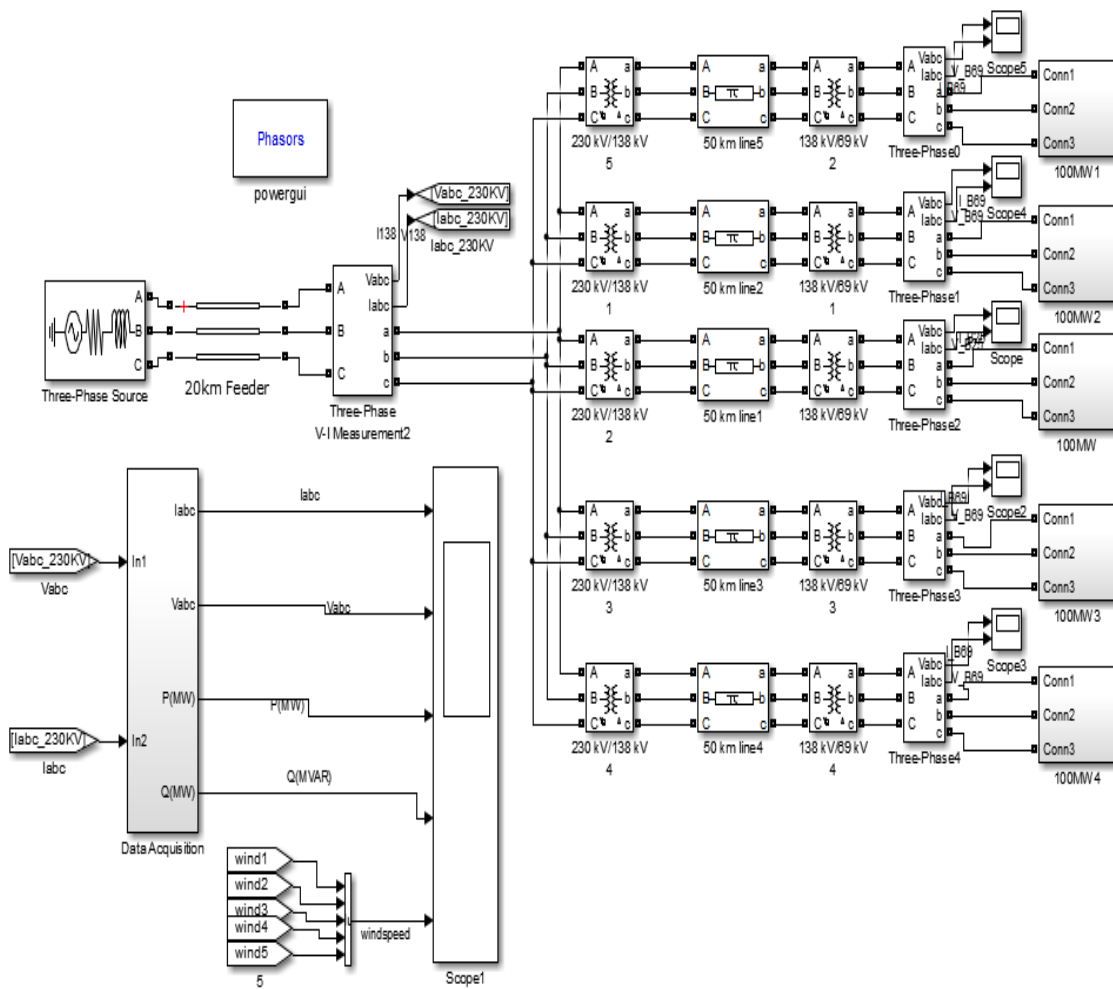


Figure 5-4-(a): Five 100 MW capacity of wind turbines in Newfoundland

Figure 5-4-(a) shows the described system model of five 100MW wind farms connected to utility grid.

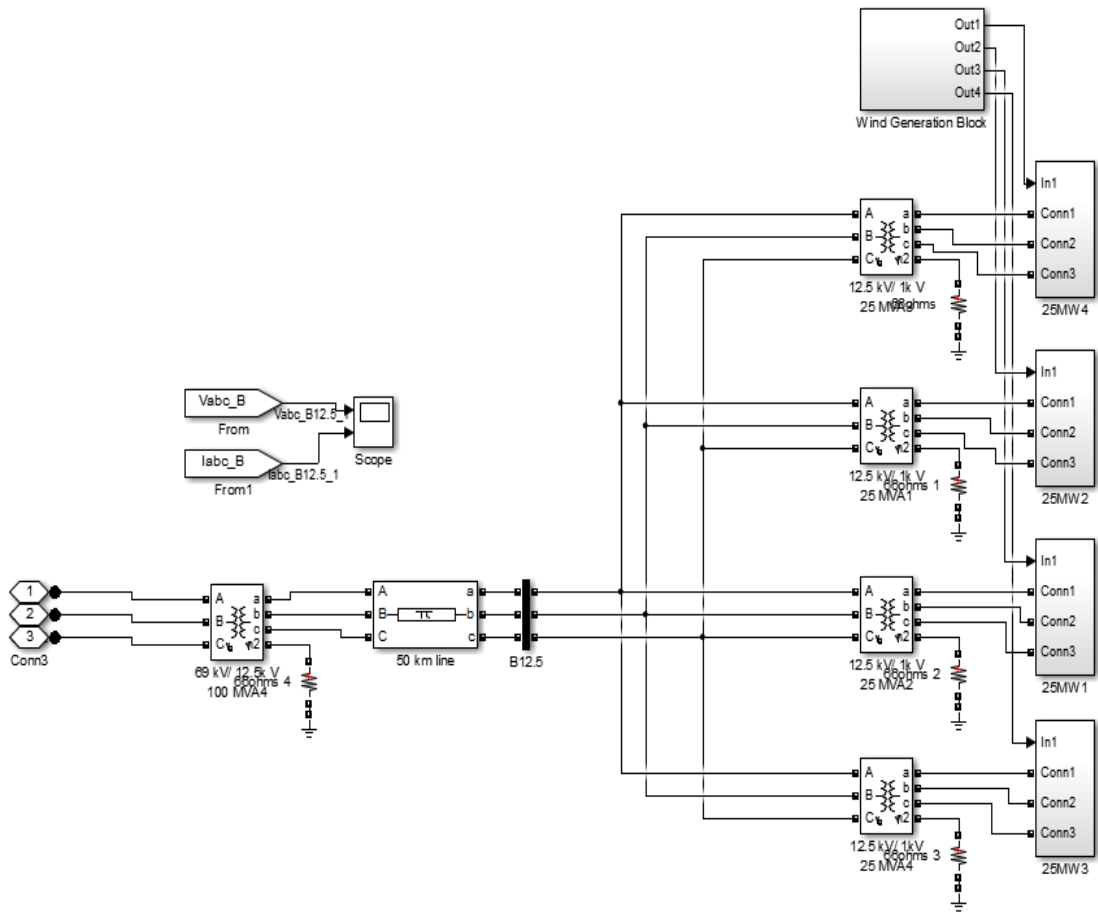


Figure 5-4-(b): Each 100 MW capacity is made of four 25 MW wind farms

Figure 5-4-(b) shows a 100MW wind farm components. A wind generation block generates wind data for each 25MW wind farm. Produced power is injected to the grid through transformers and transmission lines as indicated below.

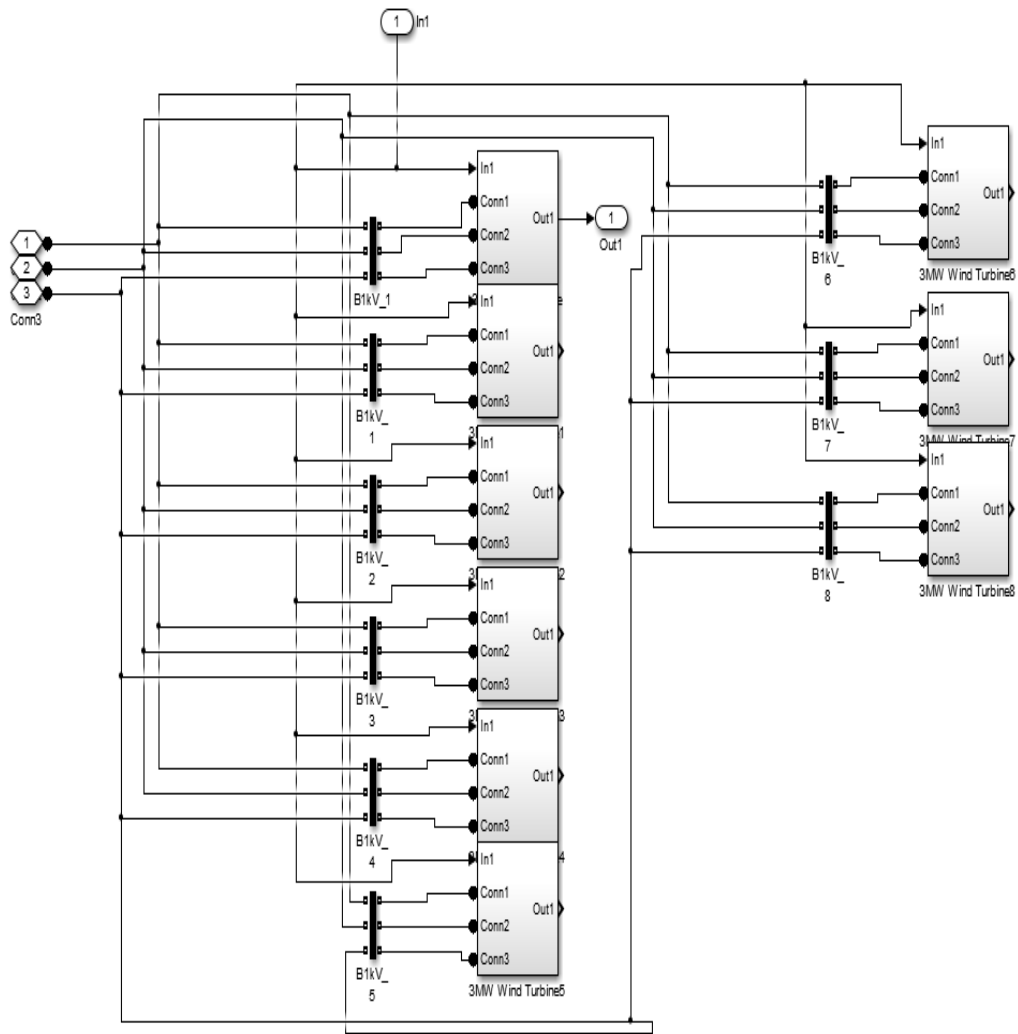


Figure 5-4-(d): Inside a 25MW wind farm

Figure 5-3-(a) to (d): Simulink model

Protection system block (Figure 5-4-(a) and (b)) includes Instantaneous AC over current, AC over current (positive sequence), AC current balance, AC under voltage (positive sequence), AC voltage unbalance (negative sequence), DC over voltage, rotor under and

over speed. However, here we have not used DC protection. Table 5-3 indicates protection block parameters.

Fundamental frequency	60
Instantaneous AC overcurrent (p.u)	10
Maximum AC current (p.u)	0.4
AC under/over voltage (p.u)	0.75/1.1
Maximum voltage unbalance (p.u)	0.05
Under/over speed (p.u)	0.3/1.5

Table 5-3: Protection system parameters

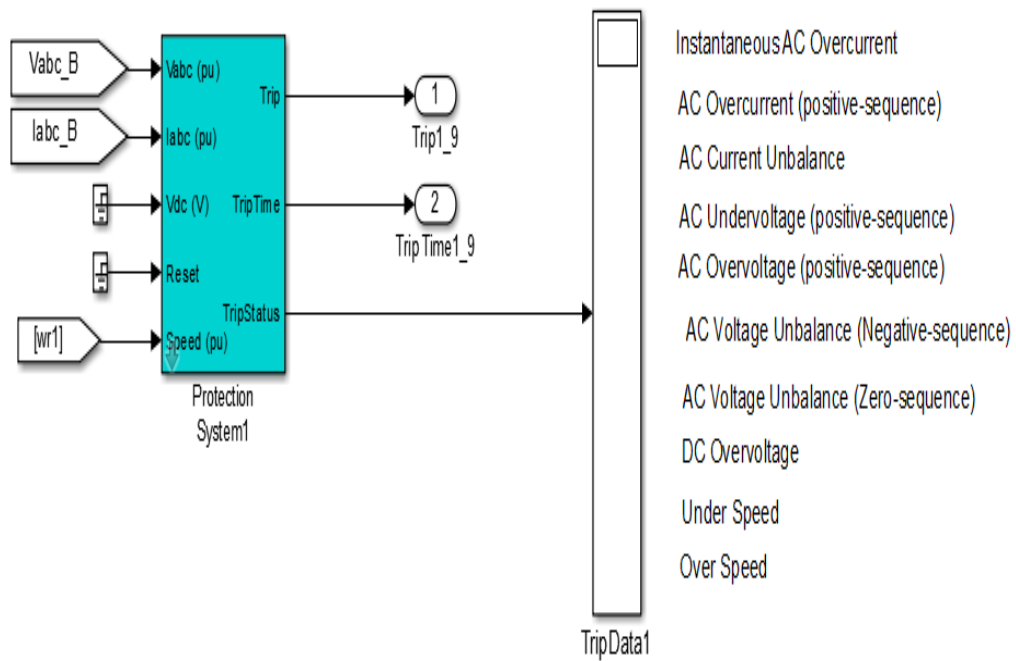


Figure 5-4-(a): Wind turbine protection

Figure 5-4-(b) shows protection system block components. This block checks all the criteria mentioned above. A logical OR operator and a logical AND operator are used to identify trip condition of the system. In the end, a Bistable block is used, which implements a SR Flip-Flop given either to set (S), with regard to the result of logical AND, or reset (R) input, with regard to second logical AND.

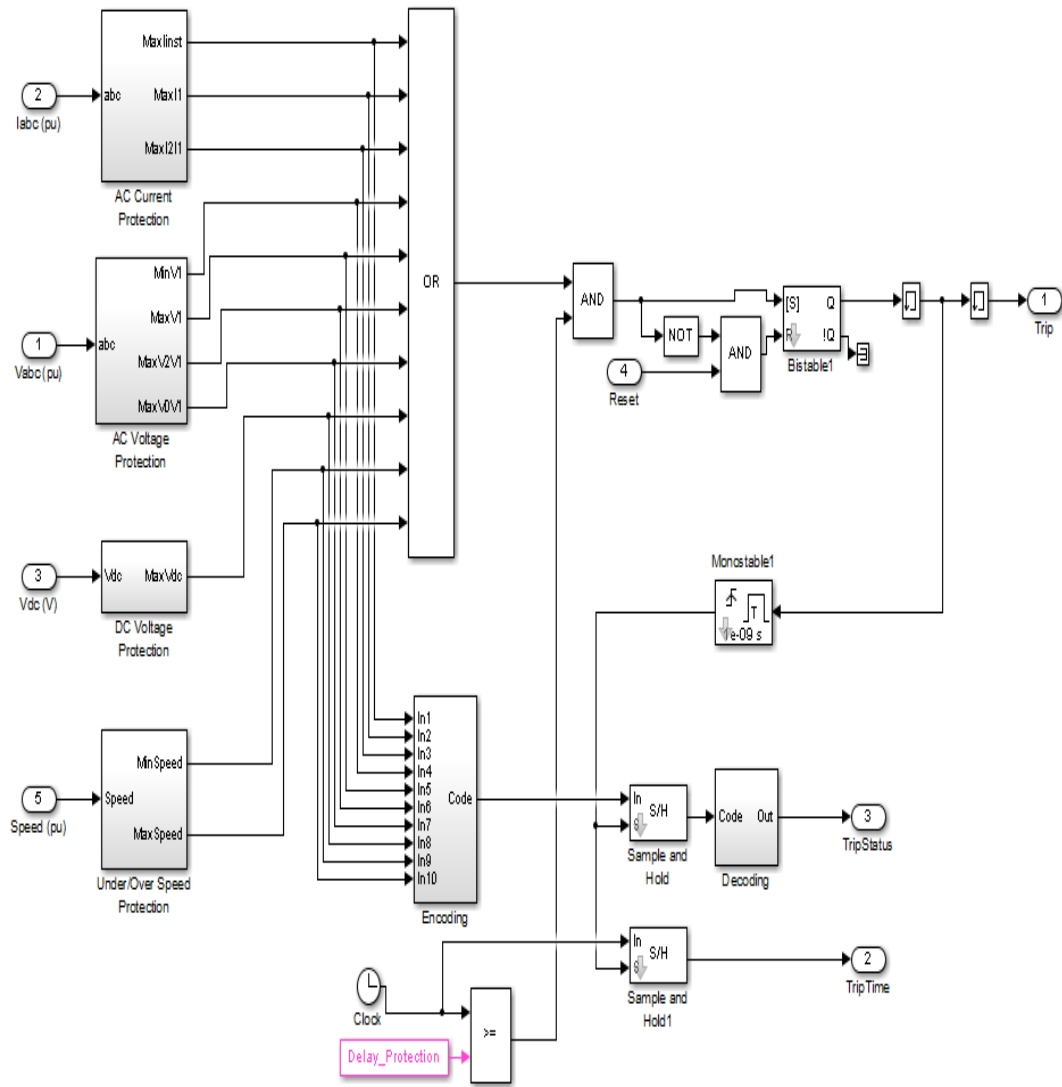


Figure 5-4-(b): Protection system block

Figure 5-4-(a) and (b): Protection algorithm

5.7 Simulation and Analysis

The determination of maximum wind penetration levels to the isolated island system of Newfoundland & Labrador was made by both voltage regulation (steady state) and transient stability of various wind generation dispatch levels. A maximum wind generation of 500

MW was chosen as it represented approximately 100% of NLH generation for the 2020 Extreme Light Load case.

5.7.1 Voltage regulation results

For maximum wind penetration of 500 MW, steady state voltage and current load flow values show there are no voltage concerns with distributed generation throughout the island as the wind generation sources are capable of contributing to voltage support.

With 500MW of wind dispatched in the extreme light load case, existing Non-Utility Generators (NUGs) have been turned off; this in reality is non dispatchable generation that Newfoundland & Labrador Hydro would utilize before non dispatchable wind generation. Based on NLH's report, there are approximately 125MW of NUGs available excluding 50 MW of wind generation. Therefore, the practical steady state limit of non dispatchable wind generation under extreme light loading would be 375MW.

5.7.2 Transient stability

Transient stability is performed at plants operating between cut-in and rated wind speed, probably causing fluctuations in response. The reason is, as shown in Figure 5-2, wind plants working below rated wind speeds may cause fluctuations in the grid.

The analyses are conducted for 10 seconds due to the fact that running this simulation file is not possible for longer periods of time due to the huge amount of calculations to be executed.

In this simulation file, base power is set to be 500KVA and so power, currents and voltages are calculated per unit. Figure 5-6 depicts the response to constant 12m/s wind speed. This

indicates that after passing the transient time (three seconds), no oscillation is observed in the current or voltage.

The next permissible scenario is that each wind farm has a different wind speed, along with a small-magnitude white noise to simulate reality. As a result, very small fluctuations might be observed in Figure 5-7. The first three seconds of the simulation shows quite large oscillations due to the fact that the system is passing through its transient phase and that most of wind variations are in this period. Moreover, there are 180, 3MW wind turbines in the system and the summation of all those small fluctuations results in sizeable oscillations. If this wind capacity were to be installed in one region, wind speed variations would produce huge oscillations in the grid, which proves the theory of the practical impact of diversified wind farms on grid stability, resulting in a more solid grid.

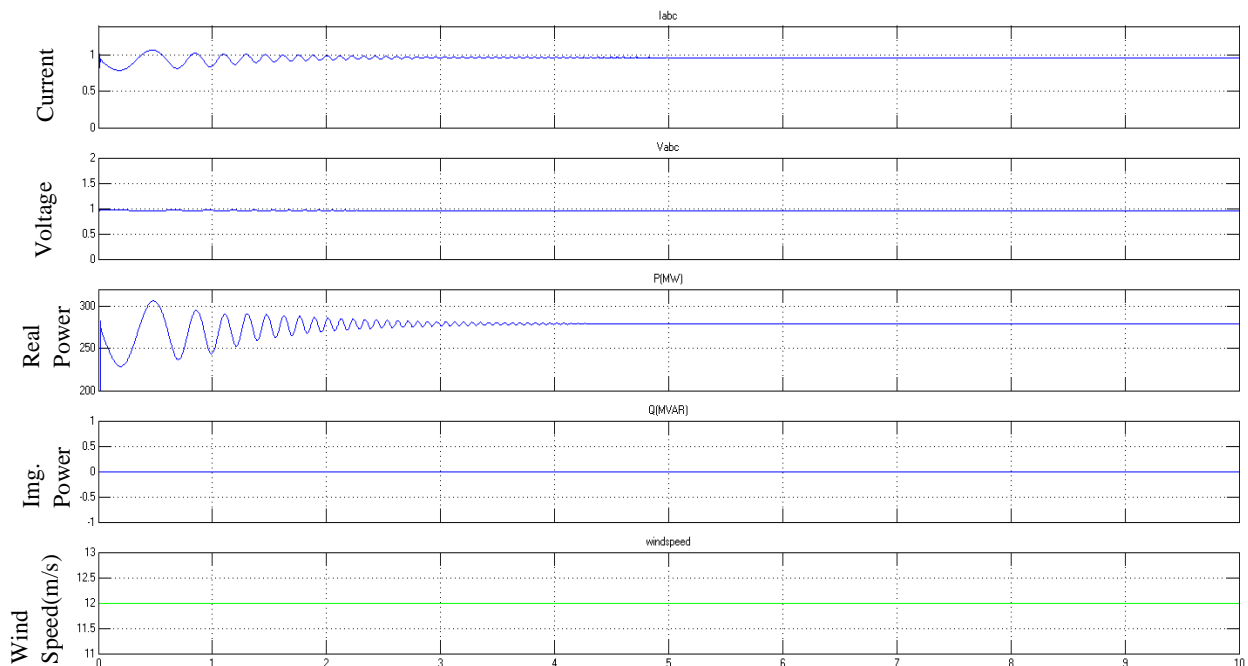


Figure 5-5: Current, voltage, P and Q scopes at constant wind speed

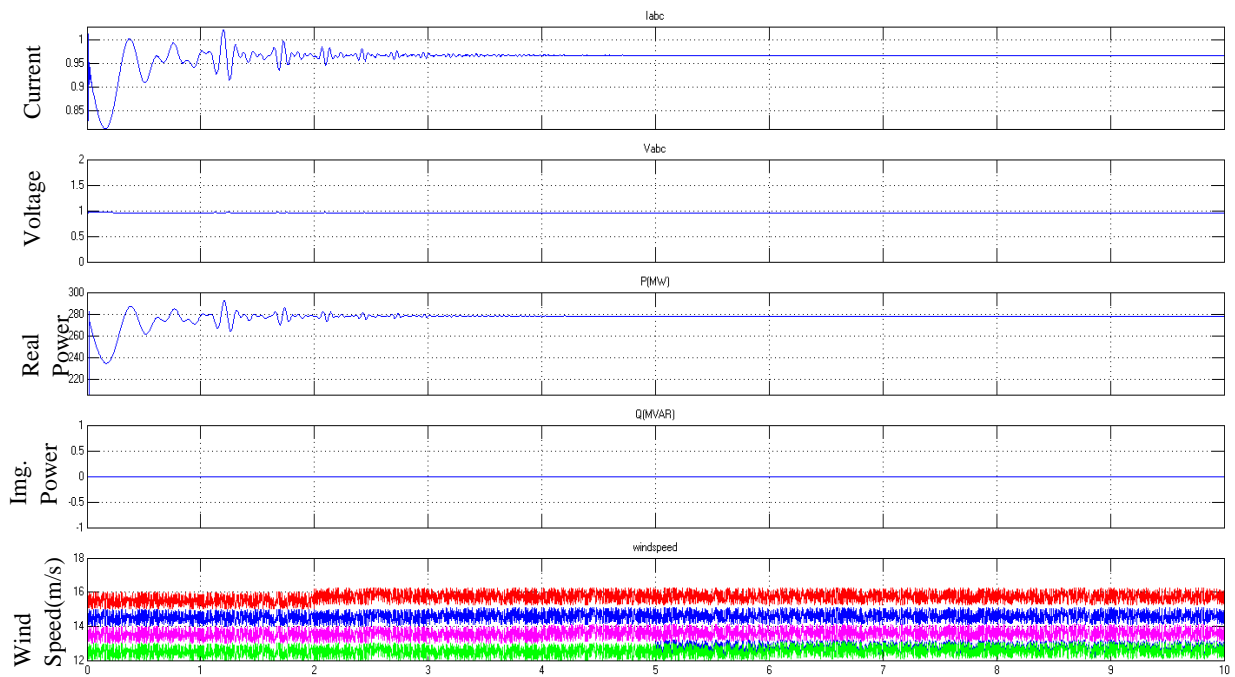


Figure 5-6: Current, voltage, P and Q scope at variable wind speed

5.8 Conclusion

Newfoundland Hydro’s load flow analysis of the base case year 2020 indicate that there are no steady state restrictions up to and including 500MW of wind power generation for the isolated island option. 500MW was the maximum steady state wind generation dispatch analyzed due to the fact that NLH generation at extreme light load conditions approaches this value. The practical steady state limit during extreme light load conditions would be limited to 375MW due to other NUG generation dispatches of approximately 125MW.

Comparing Figure 5-6 and 5-7 it is obvious that wind speed variation has a small effect on current and power output. The effect of diversified wind farms on the stability of the grid is indicated as it reduces the impact of the diurnal and synoptic peak significantly because changing weather patterns do not affect all wind turbines at the same time. Moreover,

dynamic simulation results highlight the importance of voltage and frequency fluctuations in wind farms which can be reduced using a high speed flywheel energy storage system and dispatch of fast response generation such as the use of gas turbines during periods of predicted high winds and high wind penetration.

5.9 Case study: The impact of Fermeuse wind farm on the Newfoundland grid

5.9.1 Introduction

The demand for more power along with interest in clean technologies has driven researchers to develop distributed power generation units using renewable energy sources, which can offer some benefits including fewer emissions [54], [55]. Delivering power to 300 off-grid communities in Canada from a central power station causes a significant amount of loss in transmission lines. In Newfoundland, the power loss in the transmission system is about 9% [56]. Therefore, the formation of small renewable energy plants around rural areas can significantly reduce these losses.

Here, a dynamic model of a 27 MW wind farm located in the rural area of Fermeuse, Newfoundland, Canada is presented. The wind farm dynamic system model is simulated in Matlab/ Simulink with the objective of investigating the effect of wind speed variations on grid voltage and frequency, system voltage and frequency fluctuations when the wind farm trips and reconnects to the grid. This research aims to study the impact of the 27MW Fermeuse wind farm (location 46°58'42"N 52°57'18"W), with 84 GWh annual average energy, on the Newfoundland grid through dynamic simulations. The system consists of nine 3MW doubly fed induction generator (DFIG) based wind turbines, which feed AC power to the isolated utility grid of Newfoundland.

5.9.2 Location of the wind farm

Fermeuse is a small rural community located on the southern shore of the Avalon Peninsula on the island of Newfoundland in the province of Newfoundland and Labrador, Canada.

Figure 5-8 shows a bird's eye view of a part of the wind farm extracted from Bing maps.

Figure 5-9 shows the wind farm connection and switch gears as viewed from the road.



Figure 5-7: Bird-eye view of a part of the wind farm



Figure 5-8: View of the wind farm from its transformer station

5.9.3 Power system planning and operating criteria

Connection of a wind farm to the grid impacts grid stability. There is some concern regarding the increased penetration of wind energy into the power system and about its influence on the dynamic behavior of the power system [55]. The wind generation technology of the Doubly Fed Induction Generator (DFIG), similar to the Vestas V90 used in St. Lawrence NL, and Fermeuse, NL, can provide voltage support on the island when dispatch is widely distributed (i.e. wind farms are geographically dispersed). The voltage and stability criteria of the system are the same as described in section 5.3.1 and 5.3.2.

5.9.4 Single line diagram of the system

Nine wind turbines at the Fermeuse wind farm are shown in a block diagram (Figure 5-10). Each wind turbine at the wind farm is a 3 MW variable-speed doubly-fed induction generator based Vestas-V90. Each wind turbine generator is connected to the grid through a transformer, TW, and a short transmission line. The transmission line (TL3) of the wind farm is connected to bus 4, which is eventually connected to bus 2 using a power transformer, T1. Data for the system buses is provided in Table 5-4.

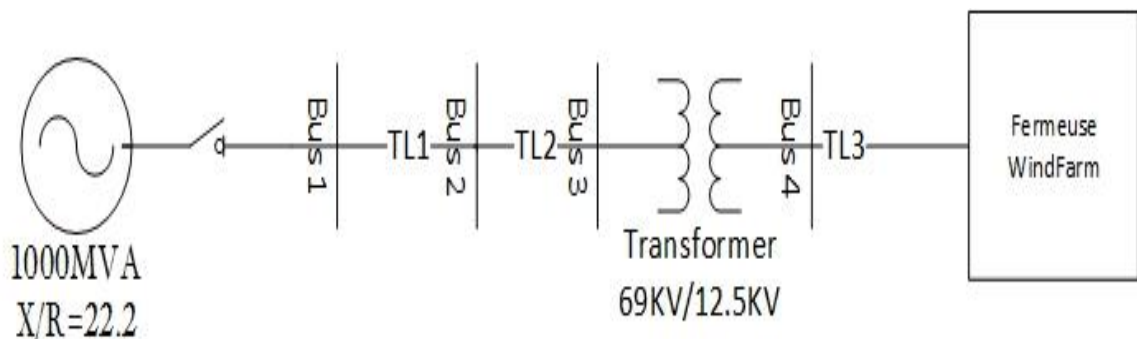


Figure 5-9: Fermeuse wind farm grid connection single line diagram

BUS	P [MW]	Q [MVAR]	V [kV]
1	ΔP	ΔQ	69
2	ΔP	ΔQ	69
3	0	0	69
4	27	12	12.5

Table 5-4: Fermeuse wind farm buses

Moreover, voltage, impedance and apparent power for transmission lines and transformers shown above are provided in Table 5-5.

Component	V [kV]	Z [Ω]	S [MVA]
TL1	69	0.002+j0.0032	40
TL2	69	0.0416+j0.0663	40
TL3	12.5	0.0374+j0.3741	40
T1	69/12.5	0.05+j0.5	40
TW	12.5/1	0.006+j0.0625	5

Table 5-5: Fermeuse wind farm transmission lines and transformers data

5.9.5 System Components

5.9.5.1 Wind power generation system

The developed Fermeuse wind farm model consists of 9 dynamic models of variable-speed, doubly-fed induction generator based wind energy conversion systems (WECS). Each variable speed, doubly-fed induction generator block contains the model of a variable pitch wind turbine rotor and a wound rotor asynchronous generator presented in [57]. The rotor winding is connected to the grid using a back-to-back pulse width modulated (PWM) voltage source converter. Stator, on the other hand, is directly connected to the grid. The Vestas-90 WECS control is utilized with the topology shown below. The decouple control technique is incorporated to control the converters on the rotor side [58].

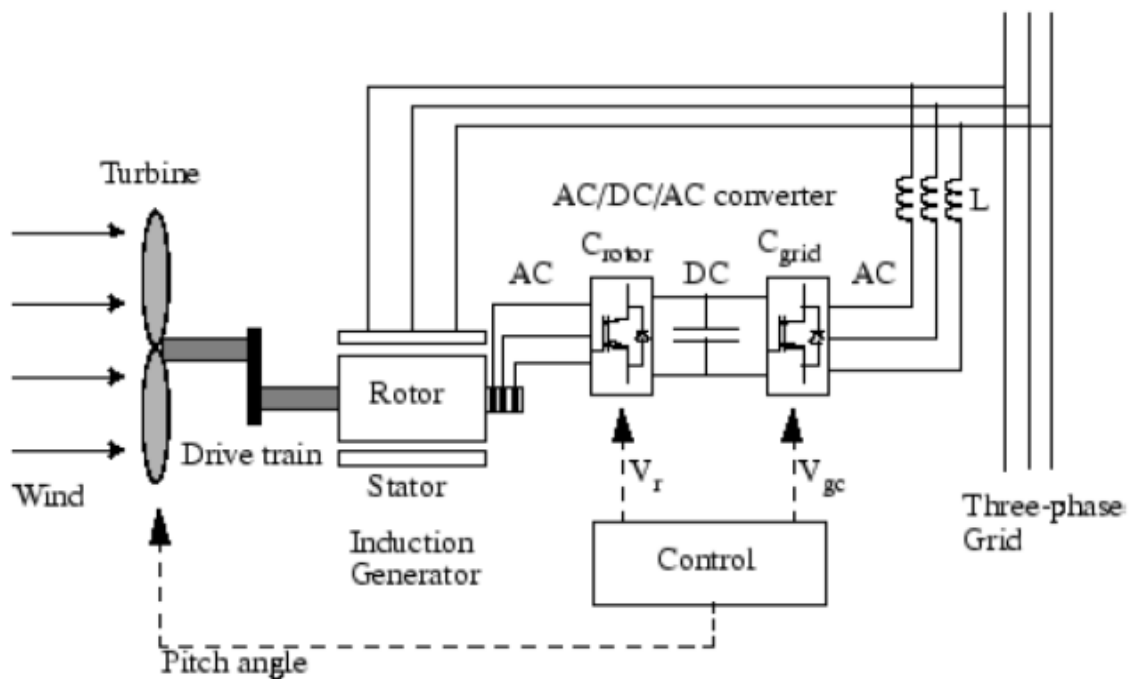


Figure 5-10: Control of a variable speed DFIG generator based wind energy conversion

5.9.5.2 Wind Turbine

In steady state, the mathematical power developed by the wind turbine, P_m , can be expressed with the help of Betz's elementary momentum theory :

$$P_m = C_p(\lambda, \beta) \frac{\rho A}{2} v^3 \quad (23)$$

$$C_p(\lambda, \beta) = C_1 \left(\frac{C_2}{\lambda_i} - C_3 \beta - C_4 \right) e^{\frac{-C_5}{\lambda_i}} + C_6 \lambda \quad (24)$$

$$\frac{1}{\lambda_i} = \frac{1}{\lambda + C_7 \beta} \frac{C_8}{\beta^3 + 1} \quad (25)$$

$$\lambda = \frac{R\omega}{v} \quad (26)$$

Mechanical torque, T_m , is the ratio of mechanical power to turbine speed.

$$T_m = \frac{P_m}{\omega} \quad (27)$$

where $C_p(\lambda, \beta)$, A , v , and β are power coefficient, sweep area, wind speed, and pitch angle respectively.

5.9.5.3 Two-mass model of drivetrain

Florin Iov, et al (2004) [59] indicated that in a two mass model of drivetrain the moment of inertia for the shafts and the gearbox wheels is small, compared to the moment of inertia of the wind turbine rotor and generator, and can simply be neglected. Therefore, in the resultant model only the gearbox ratio has influence on the equivalent system.

The equivalent diagram of gearbox is shown in Figure 5-12 [59] .

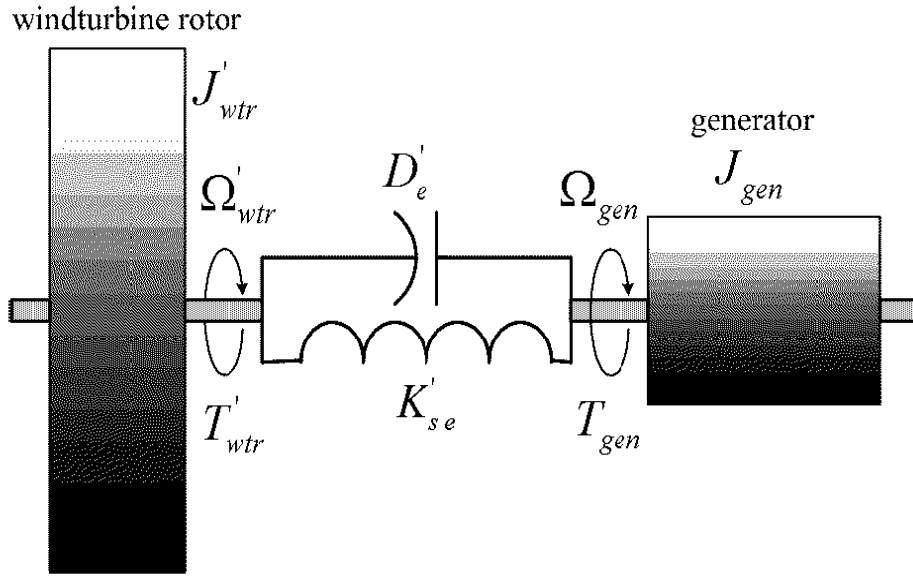


Figure 5-11: Equivalent diagram of the wind turbine drive train

The dynamic equations of the drive-train written on the generator side are as follows [59]:

$$T'_{wtr} = J'_{wtr} \frac{d\Omega'_{wtr}}{dt} + D'_e (\Omega'_{wtr} - \Omega_{gen}) + K'_{se} (\theta'_{wtr} - \theta_{gen}) \quad (28)$$

$$\frac{d\theta'_{wtr}}{dt} = \Omega'_{wtr} \quad (29)$$

$$-T'_{gen} = J_{gen} \frac{d\Omega_{gen}}{dt} + D'_e (\Omega_{gen} - \Omega'_{wtr}) + K'_{se} (\theta_{gen} - \theta'_{wtr}) \quad (30)$$

$$\frac{d\theta_{gen}}{dt} = \Omega_{gen} \quad (31)$$

The equivalent stiffness, K'_{se} , is given by:

$$\frac{1}{K'_{se}} = \frac{1}{K_{wtr}} + \frac{1}{K_{gen}} \quad (32)$$

And the equivalent moment of inertia for the rotor is:

$$J'_{wtr} = \frac{1}{K^2_{gear}} \cdot J_{wtr} \quad (33)$$

Implemented blocks in Matlab/ Simulink representing drivetrain are available in Appendix. C.

5.9.5.4 Generator

A DFIG machine has two sets of three-phase windings, one on rotor and one on stator. The voltage equation for each phase can be written as follows:

$$v(t) = ri(t) + \frac{d\lambda(t)}{dt} \quad (34)$$

Flux terms can be written as functions of current:

$$\lambda = \sum L_k i_k \quad (35)$$

The summation in (35) includes together six windings currents. Krause et al. (2013) [58] indicates that each summation has four types of winding flux terms: Stator-Stator terms, Rotor-Rotor terms, Rotor-Stator terms, and Stator-Rotor terms. Stator-Stator and Rotor-Rotor terms relate a stator winding flux to a stator winding flux and a rotor winding flux to a rotor winding flux respectively. These terms are constant as the position of any pair of stator (or rotor) windings does not change and these inductances are not a function of rotor position. However, in Rotor-Stator (or Stator-Rotor) terms, the inductance will be a function of rotor position determined by rotor angle (θ). In order to find voltages from (34), differentiation of fluxes is inevitable. This results in expression of flux as follows:

$$\frac{d\lambda}{dt} = \frac{dL}{dt} i + \frac{di}{dt} L \quad (36)$$

The differentiation with respect to L , $\frac{dL}{dt}$, will result in time-varying coefficients on the current which makes our set of state equations difficult to solve [58].

In 1929, Robert H. Park proposed a mathematical transformation called abc-to-dq0 transform [60]. This transformation converts the three AC quantities into three quantities, as shown in (37), namely:

- (1) Direct or d-axis component
- (2) Quadrature or q-axis component
- (3) Zero or the 0-axis component

$$\begin{bmatrix} x_d \\ x_q \\ x_0 \end{bmatrix} = T \begin{bmatrix} x_a(t) \\ x_b(t) \\ x_c(t) \end{bmatrix} \quad (37)$$

Using this method, the problem of Stator-Rotor and Rotor-Stator mutual inductances will be solved. In this transformation, it is assumed that the q-axis is 90° ahead of the d-axis in the direction of rotation. This transform is mathematically stated as follows:

$$\begin{bmatrix} i_d \\ i_q \end{bmatrix} = \frac{2}{3} \begin{bmatrix} \cos\theta & \cos(\theta - \frac{2\pi}{3}) & \cos(\theta + \frac{2\pi}{3}) \\ -\sin\theta & -\sin(\theta - \frac{2\pi}{3}) & -\sin(\theta + \frac{2\pi}{3}) \end{bmatrix} \begin{bmatrix} i_a \\ i_b \\ i_c \end{bmatrix} \quad (38)$$

Equation (38) indicates a zero-sequence free equation ($i_0 = 0$), assuming balanced conditions in the system.

According to Krause's model, voltage equations in the arbitrary frame are as follows [58].

$$v_{qds} = R_s i_{qds} + \omega \lambda_{dqs} + p \lambda_{qds} \quad (39)$$

$$v'_{qdr} = R'_r i'_{qdr} + (\omega - \omega_r) \lambda'_{dqr} + p \lambda'_{qdr} \quad (40)$$

where

$$(\lambda_{dqs})^T = [\lambda_{ds} - \lambda_{qs}] \quad (41)$$

$$(\lambda'_{dqr})^T = [\lambda'_{dr} - \lambda'_{qr}] \quad (42)$$

Therefore, voltage equations in expanded form are as follows:

$$v_{qs} = R_s i_{qs} + \omega \lambda_{ds} + p \lambda_{qs} \quad (43)$$

$$v_{ds} = R_s i_{ds} - \omega \lambda_{qs} + p \lambda_{ds} \quad (44)$$

$$v'_{qr} = R'_r i'_{qr} + (\omega - \omega_r) \lambda'_{dr} + p \lambda'_{qr} \quad (45)$$

$$v'_{dr} = R'_r i'_{dr} - (\omega - \omega_r) \lambda'_{qr} + p \lambda'_{dr} \quad (46)$$

Flux linkage equations can also be expanded as follows:

$$\lambda_{qs} = L_{ls} i_{qs} + L_m (i_{qs} + i'_{qr}) \quad (47)$$

$$\lambda_{ds} = L_{ls} i_{ds} + L_m (i_{ds} + i'_{dr}) \quad (48)$$

$$\lambda'_{qr} = L'_{lr} i'_{qr} + L_m (i_{qs} + i'_{qr}) \quad (49)$$

$$\lambda'_{dr} = L'_{lr} i'_{dr} + L_m (i_{ds} + i'_{dr}) \quad (50)$$

Flux linkage equations in terms of reactance are as follows:

$$\varphi_{qs} = X_{ls} i_{qs} + X_m (i_{qs} + i'_{qr}) \quad (51)$$

$$\varphi_{ds} = X_{ls} i_{ds} + X_m (i_{ds} + i'_{dr}) \quad (52)$$

$$\varphi'_{qr} = X'_{lr} i'_{qr} + X_m (i_{qs} + i'_{qr}) \quad (53)$$

$$\varphi'_{dr} = X'_{lr} i'_{dr} + X_m (i_{ds} + i'_{dr}) \quad (54)$$

The dynamic equivalent (d-q) circuit of a doubly-fed induction machine in a synchronously rotating reference frame is represented in Figure 5-13 [61]. The output voltages for the

doubly-fed induction generator is implemented using d – q-axis transformation in the synchronously rotating reference frame [57].

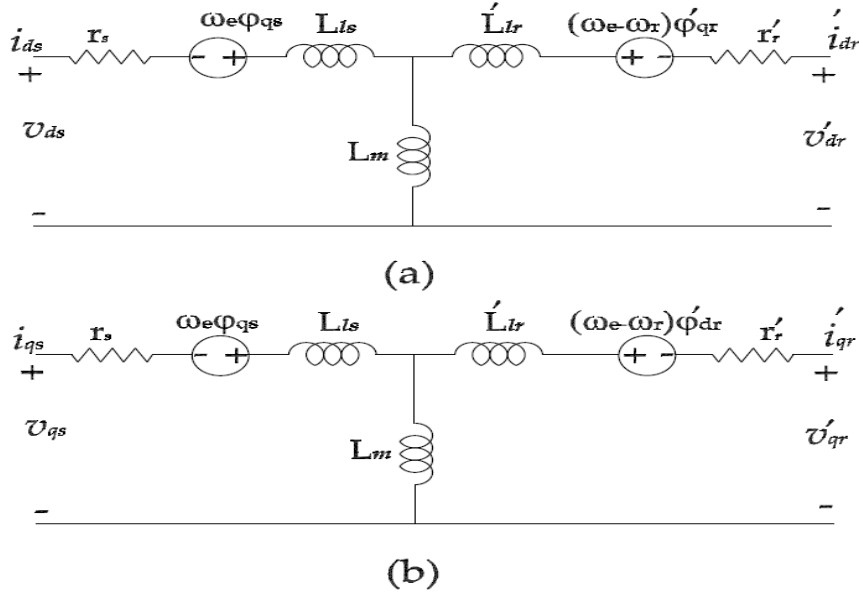


Figure 5-12: Equivalent circuit representation of an induction machine in synchronously rotating reference frame: (a) d-axis; (b) q-axis

Implemented blocks representing the generators are available in Appendix. C.

5.9.5.5 Converter

As Figure 5-11 indicates, the control system of the DFIG converters are divided into two parts of: (1) a rotor- side converter control and (2) a grid- side converter control. The average model of a wind turbine is utilized to remove fluctuations in both the current and the output power of the wind farm, which are the result of switching in the converter [57].

An AC-DC-AC pulse width modulation (PWM) converter is modeled by voltage sources. In the voltage-sources converters, forced-commutated power electronic devices (IGBTs) synthesize an AC voltage from a DC voltage source. Slip rings connect the rotor windings

to the grid. These rotor windings are supplied at a variable frequency through the converter. However, stator windings are connected directly to the grid.

Miller, Nicholas W. et al. (2003) have used the below model to describe the electrical control used in the referenced model of the DFIG wind turbine [62]. Figure 5-14 represents a simplified equivalent of the supervisory VAR controller for the entire wind farm. It details an excitation control model that imposes active and reactive powers distributed to the system, based on inputs from the turbine (P_{ord}) and from the supervisory VAR controller (Q_{ord}).

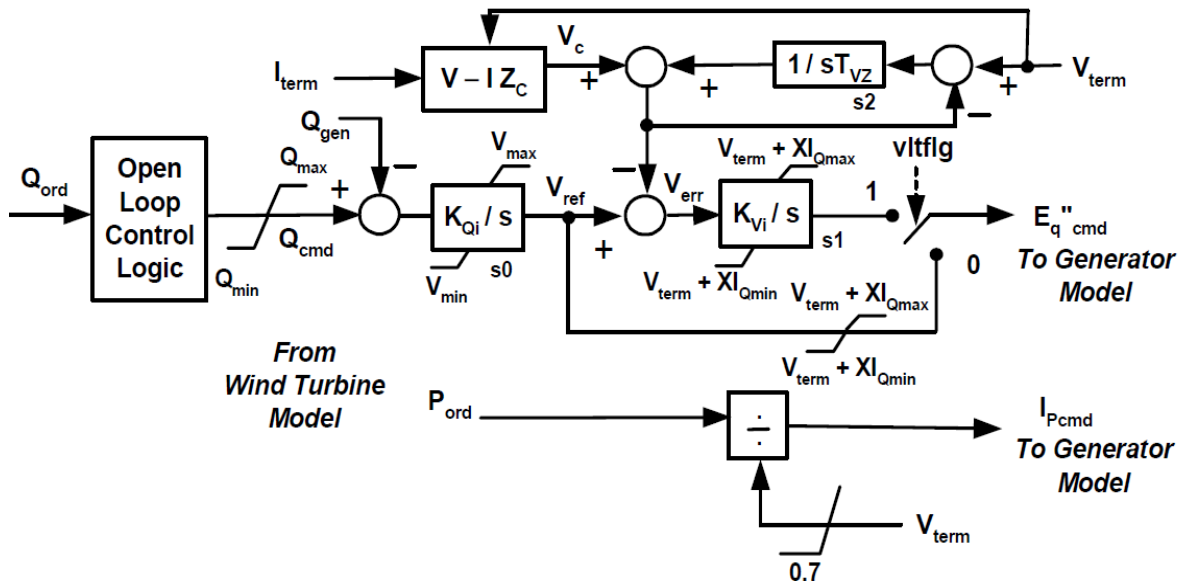


Figure 5-13: Electrical control model of wind turbine [62]

5.9.6 Simulink system model

The Simulink model is a mathematical interpretation of the explained single line diagram of the system (Figure 5-10). This includes a model of a wind turbine, transformers, a Pi model of transmission lines, a utility grid and some measurement blocks. These blocks are

connected to build the model of the Fermeuse wind farm system. Details of the developed model are shown in Figure 5-15 (a), (b).

Figure 5-15 (a) indicates wind farm connection to the grid. First, the level of voltage is adjusted, 12.5kV to 69kV, using a 40MVA transformer, and then connected to the utility grid through a transmission line. Each wind turbine is set to receive different wind speeds to represent the real situation. Moreover, injected current and voltage from the wind farm delivered by TL1 to the grid are measured, using three phase V-I measurement blocks, and the output power of the wind farm is calculated, in the data acquisition block, through ten seconds of running the simulation. In the end, the phase angle of utility voltage is measured using a phase locked loop (PLL) closed-loop control system in a d-q synchronous frame. PLL tracks the phase and frequency of a three-phase sinusoidal signal through using an internal frequency oscillator. The control system adjusts the internal oscillator frequency to keep the phases, difference at zero.

Figure 5-15- (b) shows Fermeuse wind farm detailed model including nine 3MW wind turbines, transformers, and transmission line.

More details of the system design are described in Appendix. C.

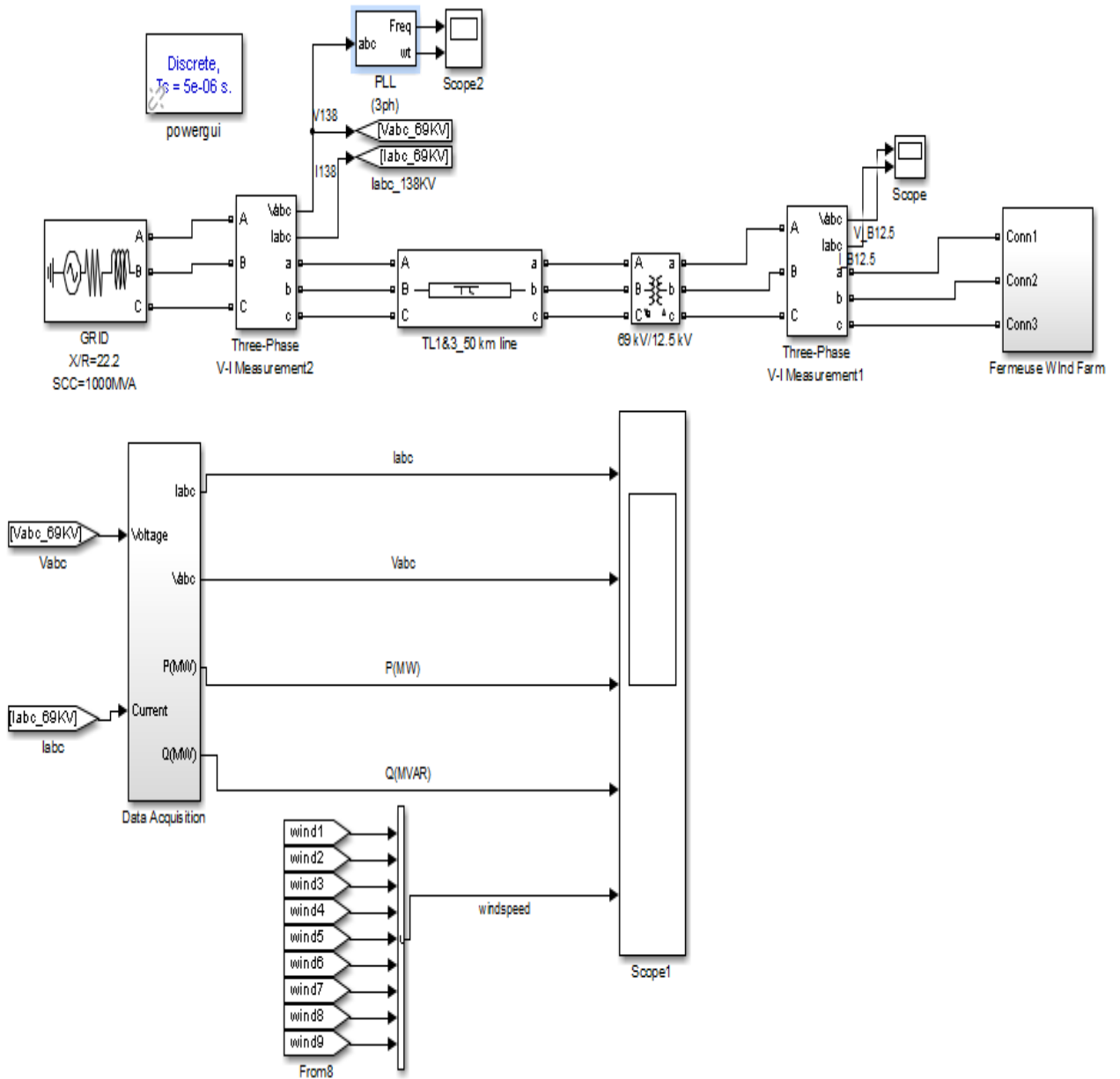


Figure 5-15-(a): General view of wind farm

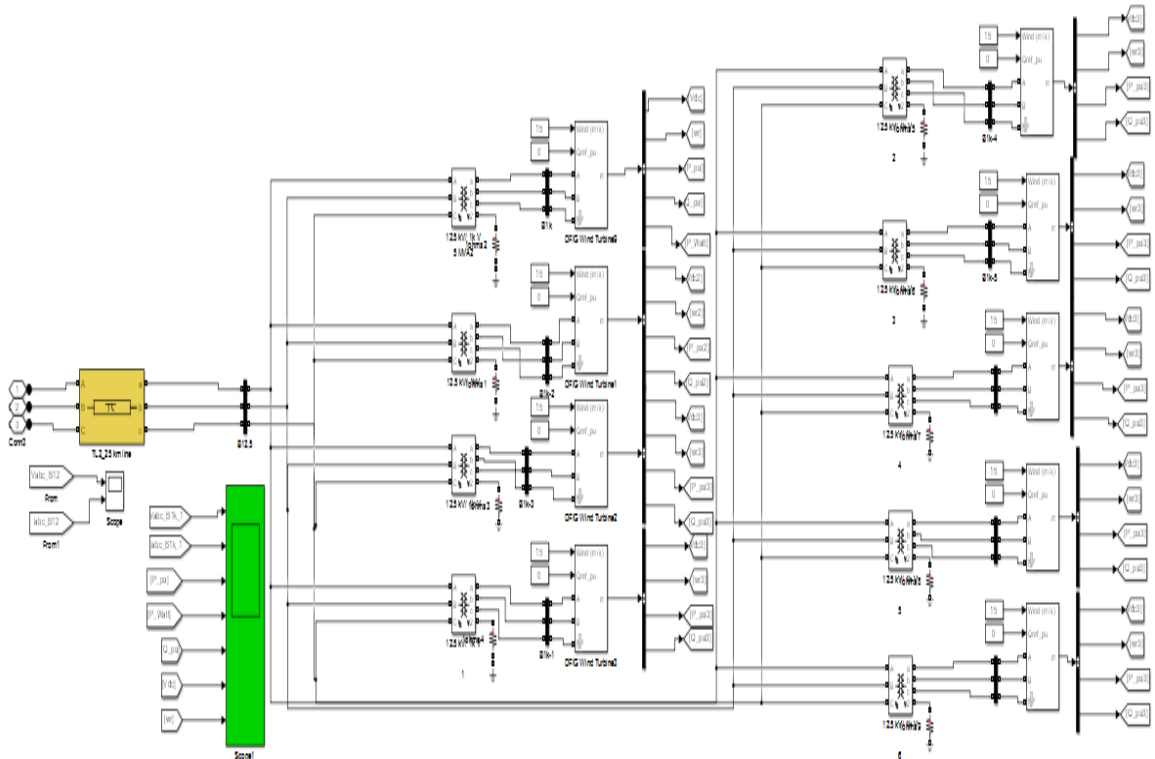


Figure 5-15-(b): Fermeuse wind farm detailed model

Figure 5-14: Simulink model of wind farm

In order to accurately model wind turbines, data in Table 5-6 and Table 5-7 were used based on manufacturer provided [63].

Table 5-6: Wind turbine specifications

Rated power	3 MW
Rotor diameter	90 m
Nominal speed	16.1 rpm
Rotor speed range	9.9-18.4 rpm
Number of blades	3
Blade length	44 m
Gearbox ratio	1:109
Cut-in wind speed	4 m/s
Cut-out wind speed	25 m/s

Table 5-7: Induction generator parameters

Type	DFIG
Nominal power	3 MW
Voltage	1000V
Rated speed	1758 rpm
Number of poles	4
Total inertia constant	3.02s
Friction coefficient	0.01
r_s, r'_r	2.35m Ω , 1.67m Ω
L_{ls}, L'_{lr}	0.151H, 0.1379H
L_m	2.47H

5.9.7 Simulation Results

Three different scenarios are considered: (1) at variable wind speeds, (2) at constant wind speed, and (3) when the wind farm trips due to a fault and then reconnects to the grid. Current, voltage, and frequency reported in this paper are measured by the three-phase V-I measurement block upon connection to the utility grid. Since wind farms have many mechanical and electrical components, a few small fluctuations in current and frequency can be observed in the first 2 seconds of all the simulation results.

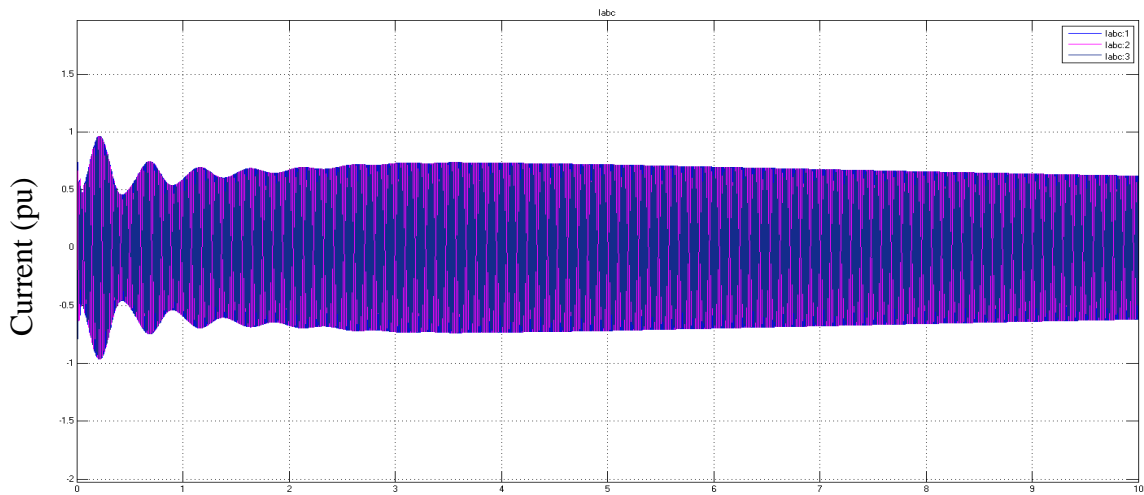


Figure 5-16- (a): Current

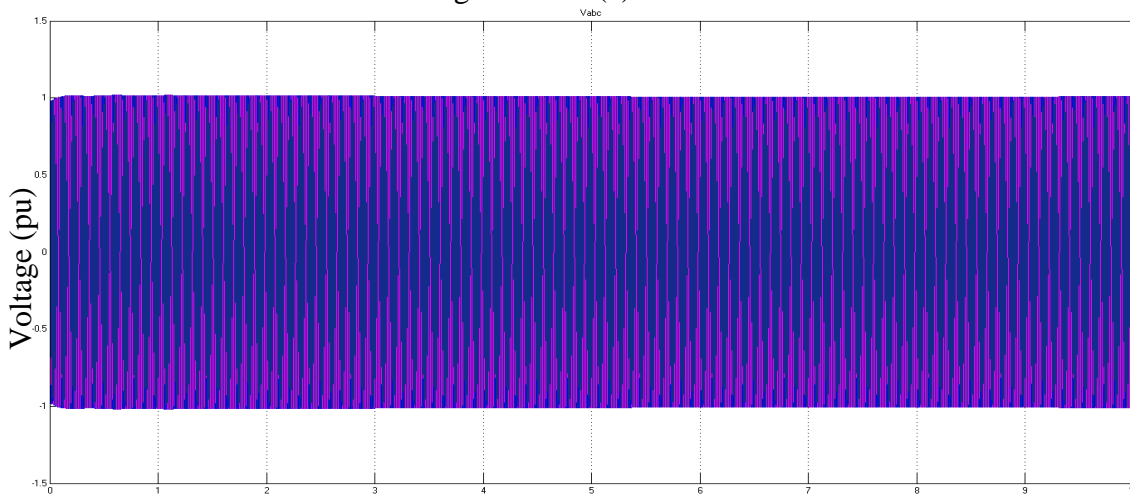


Figure 5-16-(b): Voltage

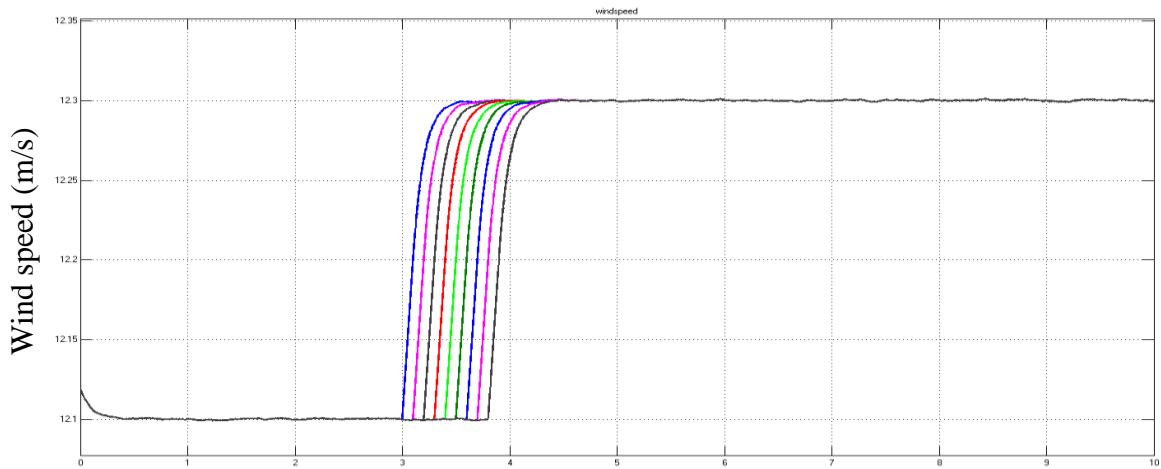


Figure 5-16-(c): Wind speed variations from 12.1 m/s to 12.3 m/s

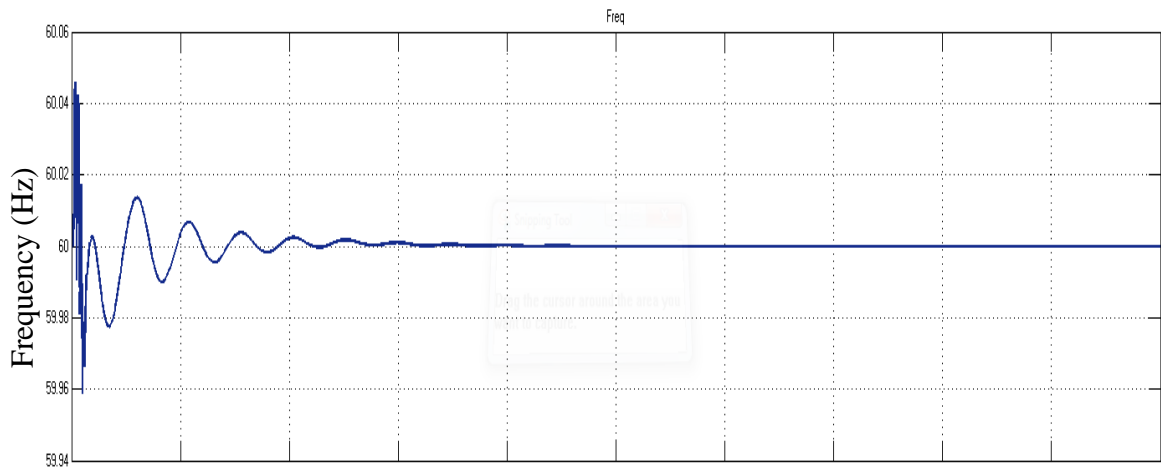


Figure 5-16-(d): System frequency

Figure 5-15- (a) to (d): Simulink model results for variable wind speeds

Figure 5-16-(a) to (d) shows the initial system transient and the effect of wind speed variation on the output power and system frequency.

In Figure 5-16-(a), the current is less than 1pu since generators are not working at their full power. Figure 5-16-(d) shows that there is no significant change in the system frequency after a wind speed variation of 0.2m/s in 1second.

Secondly, the simulation results of the system with a constant wind speed of 15 m/s are as follows:

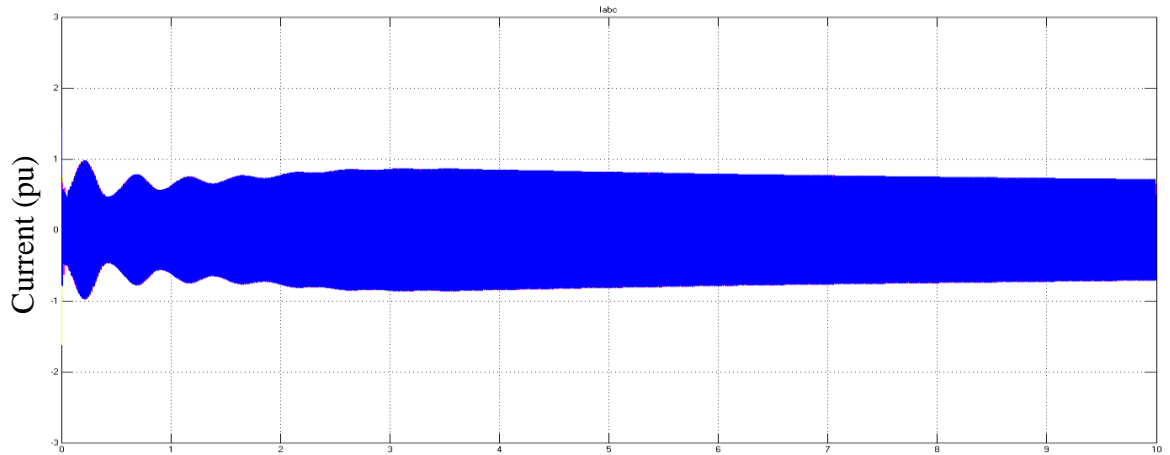


Figure 5-17- (a): Current

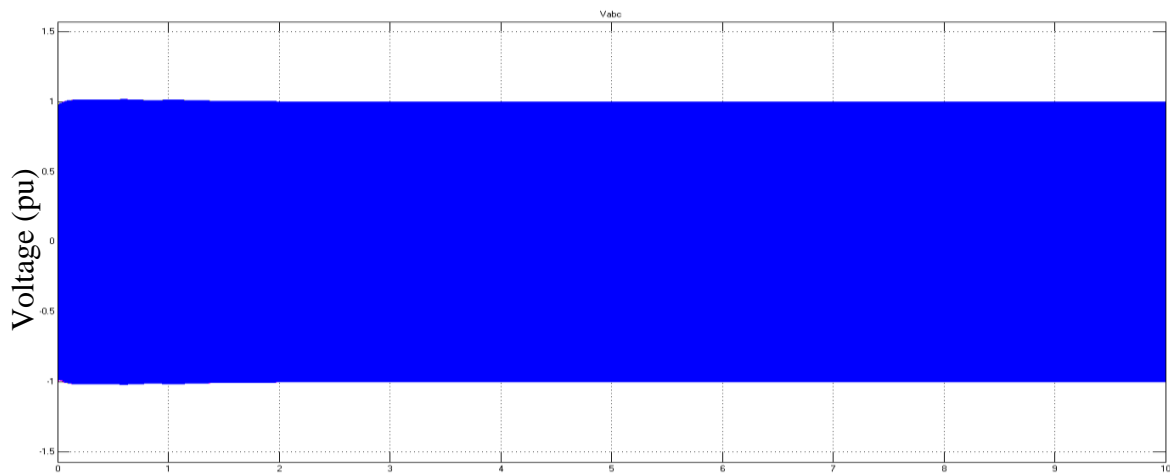


Figure 5-17- (b): Voltage

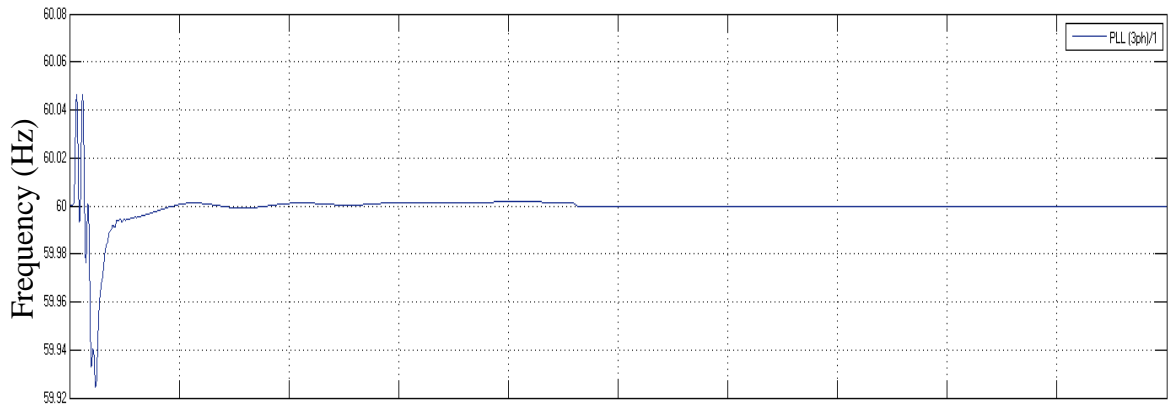


Figure 5-17- (c): Frequency

Figure 5-16-(a) to (c): Simulink model results for constant wind speed

Figure 5-17 shows the initial system simulation transient and power variation. The current is less than 1PU while the wind speed is above the rated speed because of the loss regarding to the transmission lines.

Comparing frequency and current in these two scenarios, it is clear that variable wind speeds cause very small fluctuations in the frequency and the current injected into the grid, meaning the grid is quite stiff.

Thirdly, simulation results in case of a fault happening on transmission line 3, TL3 shown in Figure 5-18, at $t=5s$ are shown the wind farm trips and then reconnects to the grid at $t=15$. The simulation, this time, is run for 60 seconds. Figure 5-18 indicates measured and calculated values at the receiving end of the line (at 69kV bus).

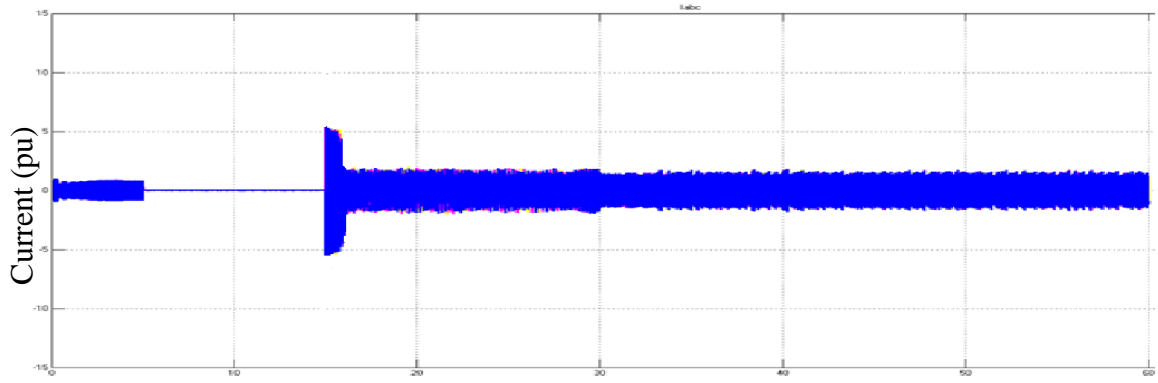


Figure 5-18-(a): Current

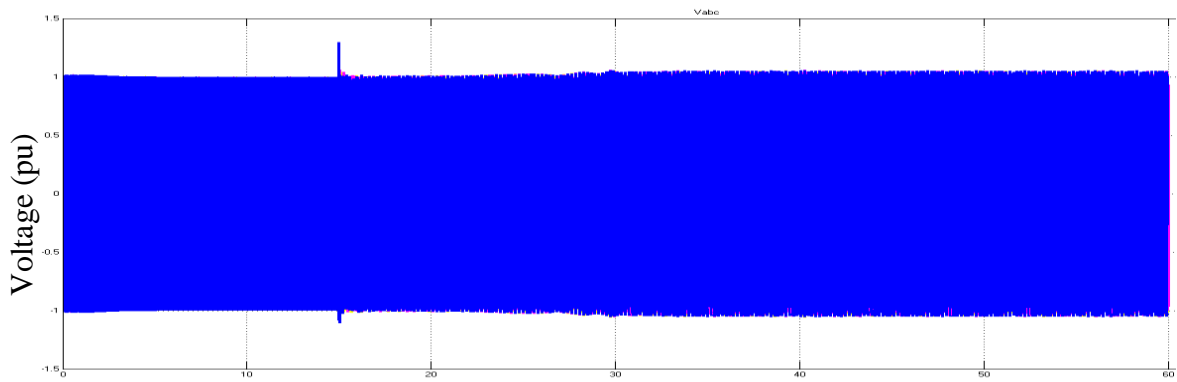


Figure 5-18-(b): Voltage

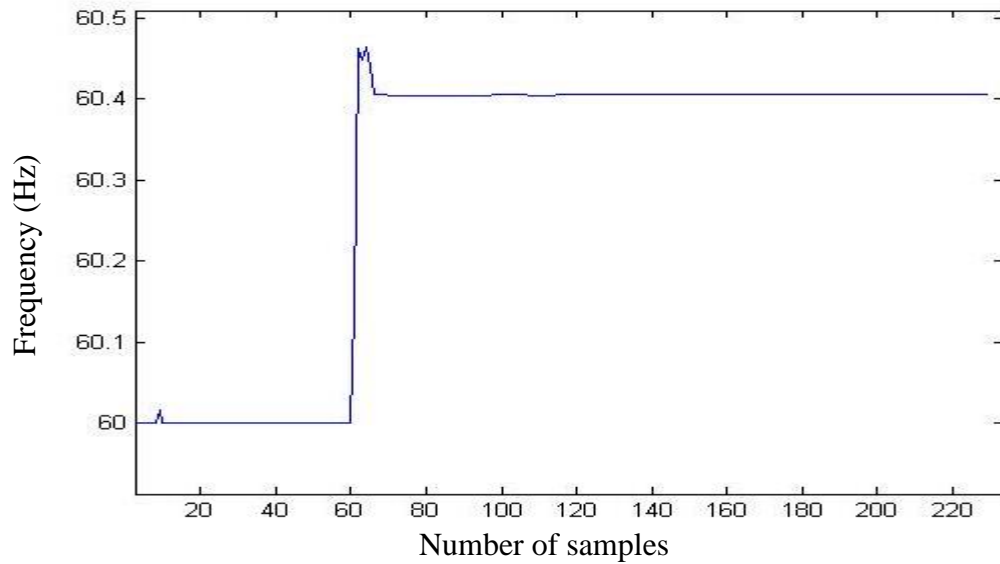


Figure 5-18-(c): Frequency

Figure 5-17-(a) to (c): Simulink results when fault occurs

From Figure 5-18-(a) to (c) it is obvious that reconnection of the wind farm to the grid causes fluctuations in current, and so in power, voltage, and frequency. In Figure 5-18-(a), since the instantaneous overcurrent is less than 10 per unit, the wind farm operates without any issue. Moreover, a resting trend can be seen in this figure and 15 seconds after the reconnection, current variation of less than 2% is perceived. Voltage variation of less than 5% is also observed in Figure 5-18-(b). These indicate that the system maintains synchronism. In Figure 5-18-(c), to eliminate fluctuations generated by PID regulator inside the PLL block and also harmonics coming from the converters Matlab commands (findpeaks command of Matlab) were used, which detected 230 peaks in the frequency response,. Sixtieth sample in the above figure is equivalent to reconnection time ($t=15$). Moreover, this plot indicates that system trip and reconnection will result in frequency variations of 0.4 Hz. Frequency increase after reconnection is due to adding power generation to utility while load is constant.

The Low Voltage Ride Through, LVRT, capability of the wind turbines enables them to ride through the fault condition since this much variation in frequency and voltage is normally allowed in the grid and usually dies out in few seconds.

5.9.8 Conclusion

A Simulink model of the 27 MW wind farm, including 9 DFIG wind turbines with the power of 3MW, transformers, transmission lines, utility grid, and measurement blocks, located in Fermeuse, NL, Canada is presented in this paper. Contingency analyses are conducted and the results are reported. System simulation is done for three cases namely constant and variable wind speeds and when a fault occurs. Simulation results show

expected variation in the system voltage and frequency. This chapter concludes that the developed model is able to represent the dynamics of the Fermeuse wind farm and how the farm can affect the power system.

6. Conclusion

6.1 Introduction

Decreases in the cost of renewable energy generators such as solar panels and wind turbines, increasing demand for renewable energy sources to provide a sustainable future, and worldwide regulations to reduce greenhouse gas emissions have made renewable energy sources (RES) the strongest candidate to substitute for oil/gas power plants. Newfoundland and Labrador's wealth of natural resources has established the province as a global energy and resource-based powerhouse which magnifies the importance of study of renewable energy setups for this region.

6.2 Concluding summary

This thesis described models and analyses of the stand-alone and grid-connected renewable energy systems for Newfoundland in order to meet current and future electricity needs with environmentally friendly, stable, competitively priced power. Moreover, it addressed snow as an obstacle to the optimal use of solar panels in small-scale systems for this region and described an algorithm for snow detection and sending alerts to address this issue. This thesis details potential design improvements as follows:

(1) For small-scale renewable energy systems, a unique methodology for optimally sizing the combination of wind turbine, solar panel, and a battery bank in a Wind-PV Hybrid system was introduced. This method allows 2% lack of power supply in a year, resulting in a 30% reduction of the initial cost of the system. Two off-grid systems were detailed, modeled and implemented in Matlab code and the sizing results of both systems were then

compared to the acquired results of the Homer software. Some minor differences were observed in the sizing results due to the fact that the HOMER software uses some unknown methods to account for interest rate, replacement, and maintenance costs.

(2) To generate the maximum energy from photovoltaic systems, a snow detection system was designed, built, and then tested for three months during the winter of 2014 in the engineering building at Memorial University of Newfoundland using solar panels, a battery, a load, a microcontroller, a voltage and a current sensor, and a light dependent resistor. This system was validated to be capable of precisely identifying more than 5 cm of snow accumulation on solar panels and sending alerts, resulting in a more efficient performance of solar panels.

(3) In order to analyze the connection of large-scale wind power to the isolated grid of Newfoundland, simulation of 500MW of wind capacity was conducted with the purpose of probing stability and reliability of the grid using Matlab/ Simulink. Due to the fact that simulation could take a few days to run, as there were many static and dynamic parts in the system, simulation was conducted in phasor simulation type. Moreover, the impact of the Fermeuse wind farm on the isolated grid of Newfoundland was explored for three permissible scenarios. Results indicate that variable wind speeds cause very small fluctuations in the frequency and the current injected into the grid, meaning the grid is quite stiff. Also, system trip and reconnection will result in a frequency variation of 0.35 Hz, where harmonics coming from the converters were removed using Matlab commands, and a voltage variation of less than 5%.

6.3 Recommendations for improvement

Future work can be done to study renewable energy systems for Newfoundland. For the hybrid wind-PV-battery system the following recommendations are suggested:

- Different types of long term and short term storage systems can be used with the proposed hybrid system.
- Instead of using dump load to dissipate excess energy, other methods could be evaluated to make use of this energy.

To improve snow detection performance the following actions are recommended:

- Use of a pyranometer instead of a light dependent resistor (LDR) could increase the accuracy of the snow detection system.
- It is required to investigate a mathematical formulation relating climate data to voltage and current sensors readings for solar panels.
- Methods to mitigate snowfall losses such as developing the idea of shedding the snow by means of increasing the slope of the module should be studied thoroughly as this could be the most economical manner of removing snow accumulation on solar panels.

For grid connected wind farms the following recommendations are suggested:

- Study of harmonics generated by the power electronics of variable speed wind turbines is recommended.
- To reduce transmission lines losses, HVDC systems can be used to transmit power.

- Soft starters can be used to integrate induction generator wind turbines with the power grid, resulting in less fluctuation during switching. However, for doubly-fed induction generator wind turbines a better control algorithm can solve this issue.
- A fault makes the converter of the DFIG disconnect from rotor. Use of a static synchronous compensator (STATCOM) unit, a shunt connected reactive compensation equipment which is capable of generating and/or absorbing reactive power, the output of which can be varied so as to maintain control of specific parameters of the electric power system enables supporting reactive power to the grid. Therefore, grid voltage can be recovered faster.

References

- [1] Yang, Hongxing, Wei Zhou, Lin Lu, and Zhaohong Fang. "Optimal sizing method for stand-alone hybrid solar–wind system with LPSP technology by using genetic algorithm," *Solar energy*, no. 82(4), pp. 354–367, 2008.
- [2] Chen, Zhe. "Issues of connecting wind farms into power systems," in *IEEE/PES Transmission and Distribution Conference and Exhibition*, Dalian, China, 2005.
- [3] Ribeiro, E. F. F., AJ Marques Cardoso, and C. Boccaletti. "Uninterruptible energy production in standalone power systems for telecommunication," *International conference on renewable energies and power quality*, Valencia, 2009.
- [4] Chong, W. T., M. S. Naghavi, S. C. Poh, T. M. I. Mahlia, and K. C. Pan, "Techno-economic analysis of a wind–solar hybrid renewable energy system with rainwater collection feature for urban high-rise application," *Applied Energy*, vol. 88, no. 11, p. 4067–4077, 2011.
- [5] Asrari, Arash, Abolfazl Ghasemi, and Mohammad Hossein Javidi. "Economic evaluation of hybrid," *Renewable and Sustainable Energy Reviews*, vol. 16, pp. 3123-3130, 2012.
- [6] Kabalci, Ersan. "Design and analysis of a hybrid renewable energy plant with solar and wind power," *Energy Conversion and Management*, vol. 72, pp. 51-59, 2013.
- [7] Zhou, Wei, Chengzhi Lou, Zhongshi Li, Lin Lu, and Hongxing Yang. "Current status of research on optimum sizing of stand-alone hybrid solar-wind power generation systems," *Applied energy*, vol. 87, pp. 380-389, 2010.
- [8] Diaf, Said, Gilles Notton, M. Belhamel, M. Haddadi, and Alain Louche. "Design and techno-economical optimization for hybrid PV/wind system under various," *Applr Energy*, vol. 85, no. 10, pp. 968-987, 2008.
- [9] Yang, H. X., L. Lu, and J. Burnett. "Weather data and probability analysis of hybrid photovoltaic–wind power generation systems in Hong Kong," *Renew Energy*, vol. 28, no. 11, pp. 1813-1824, 2003.
- [10] Luna-Rubio, R., M. Trejo-Perea, D. Vargas-Vázquez, and G. J. Ríos-Moreno "Optimal sizing of renewable hybrids energy systems: A review of methodologies," *Solar Energy*, vol. 86, pp. 1077-1088, 2012.

- [11] Escobar, Beatriz, José Hernández, Romeli Barbosa, and Ysmael Verde-Gómez. "Analytical model as a tool for the sizing of a hydrogen production system based on renewable energy: The Mexican Caribbean as a case of study," *International Journal of Hydrogen Energy*, vol. 38, pp. 12562-12569, 2013.
- [12] Sinha, Sunanda, and S. S. Chandel. "Review of software tools for hybrid renewable energy systems," *Renewable and sustainable energy reviews*, vol. 32, pp. 192-205, 2014.
- [13] L. L. Bucciarelli, "Estimating loss-of-power probabilities of stand-alone photovoltaic solar energy systems," *Solar Energy* 32, no. 2, pp. 205-209, 1984.
- [14] Erdinc, O., and M. Uzunoglu. "Optimum design of hybrid renewable energy systems: Overview of different approaches," *Renewable and Sustainable Energy Reviews*, vol. 16, pp. 1412-1425, 2012.
- [15] Ahmed Said Al Busaidi, Hussein A Kazem and Mohammad Farooq Khan. "A review of optimum sizing techniques for off-grid hybrid PV-wind renewable energy systems," *International journal of students research in technology & management*, vol. 2, no. 3, pp. 93-102, 2014.
- [16] Mellit, A., Soteris A. Kalogirou, L. Hontoria, and S. Shaari. "Artificial intelligence techniques for sizing photovoltaic systems," *Renew Sustain Energy Rev*, vol. 13, no. 2, pp. 406-419, 2009.
- [17] Collette, Yann, and Patrick Siarry. "Multiobjective optimization: principles and case studies," Berlin: Springer, 2004.
- [18] Y. Rashidi, M. Moallem, S. Vojdani. "Wireless ZIGBEE system for performance monitoring of photovoltaic panels," in *Photovoltaic Specialists Conference (PVSC)*, Seattle, WA, 2011.
- [19] Andrews, Rob W., Andrew Pollard, and Joshua M. Pearce. "The effects of snowfall on solar photovoltaic performance," *Solar Energy*, vol. 92, pp. 84-97, 2013.
- [20] R. W. Andrews and J. M. Pearce, "Prediction of energy effects on photovoltaic systems due to snowfall events," *Photovoltaic Specialists Conference (PVSC)*, pp. 3386-3391, 2012.
- [21] G. S. B. Becker, W. Weber, C. Vodermayr, M. Zehner and G. Kummerle, "An approach to the impact of snow on the yield of grid-connected PV systems," *Proc. European PVSEC*, 2006.

- [22] Wirth, Georg, Marion Schroedter-Homscheidt, Mike Zehner, and Gerd Becker. "Satellite-based snow identification and its impact on monitoring photovoltaic systems," *Solar Energy*, vol. 84, pp. 215-226, 2010.
- [23] CANWEA, "Powering Canada's future".
- [24] Chen, Zhe. "Issues of connecting wind farms into power systems," in *IEEE/PES transmission and distribution*, Dalian, China, 2005.
- [25] E. v. o. T. R. T. 3.2.6, "Wind turbines connected to grids with voltage below 100 kV –Technical regulations for the properties and the control of wind turbines," 2004.
- [26] C. T.T., "Voltage stability investigation of grid connected wind farm," in *Proceedings of world academy of science*, 2008.
- [27] I. 61400-21, "Power quality requirements for wind whines," 2001.
- [28] D. C. r. 1.-E. (. edition), "Connection of wind turbines to low and medium voltage networks," 1998.
- [29] [Online]. Available: <http://efxkits.com/blog/working-of-solar-wind-hybrid-system/>.
- [30] © Hill Country Wind Power, L.P., 2015. [Online]. Available: <http://www.hillcountrywindpower.com/wind-basics.php>.
- [31] [Online]. Available: http://www.power-sonic.com/images/powersonic/technical/1277751263_20100627-TechManual-Lo.pdf.
- [32] "Photovoltaic systems : A buyer's guide," [Online]. Available: <http://www.energyalternatives.ca/PDF/Photovoltaic%20Systems%20-%20A%20buyers%20Guide.pdf>.
- [33] [Online]. Available: <http://www.mainerural.org/wp-content/uploads/2013/01/Wind-Turbine-Buyers-Guide-2011.pdf>.
- [34] [Online]. Available: http://www.urbanwind.net/pdf/CATALOGUE_V2.pdf.
- [35] K. Raiambal and C. Chellamuthu, "Modeling and simulation of grid connected wind electric generating system.," in *TENCON'02. Proceedings. 2002 IEEE Region 10 Conference on Computers, Communications, Control and Power Engineering. Vol. 3.*, 2002.

- [36] Zhou, Wei, Hongxing Yang, and Zhaohong Fang. "A novel model for photovoltaic array performance prediction," *Applied Energy* 84 (12), pp. 1187-1198, 2007.
- [37] Messenger, Roger A., and Jerry Ventre. "Photovoltaic systems engineering," CRC press, 2004.
- [38] Stevens, John W., and Garth P. Corey. "A Study of Lead-Acid Battery Efficiency Near Top-of-Charge and the Impact on PV System Design," in *Photovoltaic Specialists Conference; Conference Record of the Twenty Fifth IEEE. IEEE, 1996.*, 1996.
- [39] Xu, Daming, Longyun Kang, Liuchen Chang, and Binggang Cao., "Optimal sizing of standalone hybrid wind/PV power systems using genetic algorithms," *Canadian Conference IEEE*, pp. 1722-1725, 2005.
- [40] "Homer Energy," [Online]. Available: <http://www.homerenergy.com/software.html>.
- [41] Becker, Gerd, Bruno Schiebelsberger, Walter Weber, Christian Vodermayr, Mike Zehner, and Gerald Kummerle. "An approach to the impact of snow on the yield of grid connected PV systems," in *Proc. European PVSEC*, 2006.
- [42] Powers, Loren, Jeff Newmiller, and Tim Townsend. "Measuring and modeling the effect of snow on photovoltaic system performance," in *Photovoltaic Specialists Conference (PVSC), 35th IEEE*, 2010.
- [43] Brench, Bronwyn L. "Snow-covering effects on the power output of solar photovoltaic arrays," in *NASA STI/Recon Technical Report*, 1979.
- [44] Townsend, Tim, and Loren Powers. "Photovoltaics and snow: An update from two winters of measurements in the sierra," in *Photovoltaic Specialists Conference (PVSC), 2011 37th IEEE*, 2011.
- [45] "<http://playground.arduino.cc/Code/TwitterLibrary>," [Online].
- [46] "Arduino tweet. [Online]. Available: <http://arduino-tweet.appspot.com/>," [Online].
- [47] "Arduino search results. [Online]. Available: <http://www.instructables.com/howto/arduino/>," [Online].
- [48] Parsons, Brian, Michael Milligan, Bob Zavadil, Daniel Brooks, Brendan Kirby, Ken Dragoon, and Jim Caldwell. "Grid impacts of wind power: A summary of recent studies in the united states" NREL/ CP-500-34318".

- [49] Ackermann, Thomas, ed "Wind Power in Power Systems," John Wiley and sons,Ltd., Publication.
- [50] [Online]. Available: <http://www.powerinourhands.ca>.
- [51] [Online]. Available:
<http://www.mathworks.com/help/phymod/sps/examples/wind-farm-dfig-phasor-model.html>.
- [52] Iov, Florin, Anca Daniela Hansen, Poul Ejnar Sørensen, and Nicolaos Antonio Cutululis. "Mapping of grid faults and grid codes," Reso report, 2007.
- [53] "Newfoundland and Labrador hydro," [Online]. Available:
<http://hydroblog.nalcorenergy.com/electricity-101-a-primer-on-our-electrical-grid/>.
- [54] Blaabjerg, Frede, Remus Teodorescu, Marco Liserre, and Adrian V. Timbus. "Overview of control and grid synchronization for distributed power generation systems," *Industrial Electronics, IEEE Transactions*, vol. 53.5, pp. 1398-1409, 2006.
- [55] Abbey, C., F. Katiraei, C. Brothers, L. Dignard-Bailey, and G. Joos. "Integration of Distributed Generation and Wind Energy in Canada," in *Invited paper IEEE Power Engineering Society General Meeting PES'06 Proceedings, Montreal, CA*, June, 2006.
- [56] Expert estimates, based on transmission losses published in Energy Statistics Handbook, A joint publication of Statistics Canada and Natural Resources Canada.
- [57] [Online]. Available:
<http://www.mathworks.com/help/phymod/sps/examples/wind-farm-dfig-average-model.html>.
- [58] Krause, Paul C., Oleg Wasynczuk, Scott D. Sudhoff, and Steven Pekarek." Analysis of electric machinery and drive systems," John Wiley & Sons, 2013.
- [59] F. Iov, A. D. Hansen, P. Sorensen and F. Blaabjerg, "Wind turbine blockset in matlab/simulink," *Aalborg University*, 2004.
- [60] R. H. Park, "Two-reaction theory of synchronous machines generalized method of analysis-part I," *American Institute of Electrical Engineers, Transactions of the 48.3* , pp. 716-727, 1929.

- [61] Krause, Paul C., Oleg Wasynczuk, Scott D. Sudhoff, and Steven Pekarek., "Analysis of Electric Machinery and Drive Systems," vol. 2nd edition, John Wiley & Sons, 2013.
- [62] Miller, Nicholas W., William W. Price, and Juan J. Sanchez-Gasca "Dynamic modeling of GE 1.5 and 3.6 wind turbine-generators," GE-Power systems energy consulting (2003).
- [63] "Vestas," [Online]. Available:
http://www.vestas.com/Files/Filer/EN/Brochures/ProductbrochureV90_3_0_UK

Appendices

A.1. Annual energy output of wind turbines

The below code explains a method to calculate annual energy output of the wind turbine specified in table 4.

```
power=[0 0 4 10 20 34 51 76 110 144 192 248 293 300 300 300];  
  
load winddatafor12m.txt;  
  
hr=hist(winddatafor12m,16);  
  
energy=power.*hr;  
  
annualenergyoutput=sum(energy)
```

A.2. Matlab code:

```
clc  
clear all  
close all  
load ACload.txt  
load DCload.txt  
load Wind.txt  
load Solar.txt  
load tempwind.txt  
Npv=4;  
Nwt=1;  
Nbat=5;% #of strings ( 2bat at each string)  
tilt=45;  
TArray=tempwind(:,2)';  
IrradArray=Solar(:,1)';  
WindArray=Wind(:,1)';  
LArray=(ACload(:,1)+DCload(:,1))';  
[NLPS,GenerateArray,EwtArray,EpvArray,KtArray] =  
LPS(Nwt,Nbat,Npv,tilt,TArray,IrradArray,LArray,WindArray);  
%% initialization  
  
mincost=20000;  
opt=[0,0,0,0];  
N batt=0;% total number of bats  
NLPSnew=[];
```

```

optnew=[];

for Nbat=5:7 % # of strings; 2bats per string
    for Nwt=1:4
        for Npv=4:7
            for tilt=45:50
                if LPS(Nwt, Nbat, Npv, tilt, TArray,
IrradArray, LArray, WindArray)== 200%Desirable NLPSP
                    NLPSPnew=[NLPSPnew,NLPSP];
                    c=cost(Npv, Nwt, Nbat);
                    if c<mincost
                        if NLPSP<= min(NLPSPnew)
                            mincost=c;
                            Nbatt=2*Nbat;
                            opt=[Nbatt,Nwt,Npv,tilt];
                            optnew=[optnew,opt];
                        end
                    end
                end
            end
        end
    end
end

disp(opt)
disp(mincost)
disp(NLPSP)
PVArray=sum(EpvArray)
WindTurbine=sum(EwtArray)
TotalPower=sum(GenerateArray)

.....
function [NLPSP,GenerateArray,EwtArray,EpvArray,KtArray] =
LPS(Nwt,Nbat,Npv,tilt,TArray,IrradArray,LArray,WindArray)

    EBatMax = 13.872*Nbat;% each 1156Ah, 6V; 2bats per
string ==> 1156*12=13.872 Kwh
    EBatMin = 0.5*EBatMax;
    Ebat     = EBatMax;

    %save data as matrices
    EwtArray=[];
    EpvArray=[];
    EbatArray=[];

```

```

GenerateArray=[];
NLPS = 0;
KtArray=[];
B0Array=[];
for i=1:8760
    T    = TArray(i);
    Gz   = IrradArray(i);
    L    = LArray(i);
    Wind = WindArray(i);

    [B0, delta, w0, ws] = daily_beam(i,tilt);
    B0Array=[B0Array,B0];
    [Epv,Kt] = out_PV(Gz, Npv, T, B0, tilt, delta, w0,
ws);

    KtArray=[KtArray,Kt];
    EpvArray=[EpvArray,Epv];
    Ewt = out_wt(Wind, Nwt);
    EwtArray=[EwtArray,Ewt];
    Generate = Epv + Ewt;
    [EBatNew, Gbat] = out_bat(Ebat, EBatMin, EBatMax,
Generate, L);
    EbatArray=[EbatArray,EBatNew];
    Ebat = EBatNew;
    Generate = Generate + Gbat;
    GenerateArray=[GenerateArray,Generate];

    Net = L - Generate*0.9;
    if Net > 0
        NLPS = NLPS + 1;
    end
end
end
end
function Ewt= out_wt(wind,Nwt)
    Ewt=Nwt*0.001*0.68*(0.002*(wind)^5-0.0015*(wind)^4-
0.45*(wind)^3+10.73*(wind)^2-52.22*(wind)+74.0291);
end
function [Epv,Kt]=out_PV( Gz,Npv,T,B0,tilt,delta,w0,ws )
    Kt=Gz/B0;
    % OR :
    Dz=Gz*(0.9511*Kt-0.1604*Kt+4.388*(Kt)^2-
16.638*(Kt)^3+12.336*(Kt)^4);
    Dz=Gz*(1-1.13*Kt);
    Bz=Gz-Dz; %Rz=0;
    Bt=Bz*(cosd(47-
tilt)*cosd(delta)*sind(w0)+w0*0.017*sind(47-

```

```

tilt)*sind(delta))/(0.681*cosd(delta)*sind(ws)+ws*0.017*0.73
*sind(delta));
    Dt=Dz*(1+cosd(tilt))/2;
    Gt=Bt+Dt;

    Epv=0.1*(Npv)*(1-0.00297*(T-25))*1*(Gt/1.367);
end

```

```

.....
function [E1, Gbat] = out_bat(E0, Emin, Emax, Generate, L)
% E0: stored energy in bats in previous hour.
% E1: NEW stored energy in bats(after one hour)
% Gbat:energy from bats to the system

    if Generate > L
        E1 = min(Emax, E0*0.998 + (Generate - L/0.9)*0.8);
    else
        E1 = max(Emin, E0*0.998 - (Generate - L/0.9)*0.8);
    end

    Gbat = E0 - E1;

end

```

```

.....
function W = cost(Nwt,Nbat,Npv)
W = 600*Nwt+200*Npv+1300*Nbat*2;
end

%%Cwpb=Cwt*Nwt+Cpv*Npv+Cbat*Nbat

```

A.3. Fitting polynomial

```

>>x=[0,1,2,3,4,5,6,7,8,9,10,11,12,13,14,15,16,17,18,19,20];
>>y=[0,0,0,0.008,0.019,0.036,0.058,0.083,0.121,0.160,0.221,0
.282,0.373,0.478,0.547,0.050,0.053,0.064,0.075,0.079,0.084];
>>[A,S]=polyfit(x,y,6);
>>f=polyval(A,x);
>> plot(x,y,'o',x,f,'-')

```

A.4.Wind turbine function

After inputting wind speed and power data and fitting a second degree polynomial, the function is written as follows:

```
>>x=[0,1,2,3,4,5,6,7,8,9,10,11,12,13,14];
>>y=[0,0,0,0.008,0.019,0.036,0.058,0.083,0.121,0.160,0.221,0
.282,0.373,0.478,0.547];
>> A=polyfit(x,y,2)
A =
    0.0040   -0.0184    0.0165
>>x=[15,16,17,18,19,20];
>>y=[0.050,0.053,0.064,0.075,0.079,0.084];
>>B=polyfit(x,y,2)
B =
   -0.0003    0.0187   -0.1595

function wt_out= example_wt(wind,Nwt)
    if wind<14
        wt_out=-Nwt*(0.004*(wind).^2-0.0184*(wind)+0.0165);
    else
        wt_out=0;
    end
end
```

```
>> gen_wt=example_wt(wind,Nwt);
```

```
>> sum(gen_wt)
```

A.5. Output power

In order to calculate the output power and save it as a matrix we write:

```
Nwt=1;
```

```
load wind_resource.txt
```

```
gen=0;
```

```
GEN=[];
```

```
for i=1:8760
```

```
    wind=wind_resource(i,1);
```

```
    wt_out= example_wt2(wind,Nwt);
```

```
    gen=gen+wt_out;
```

```
    GEN=[GEN,gen];
```

```
end
```

B. Snow detection code on Arduino:

In this appendix the code implemented in Arduino Uno micro controller is presented.

```
#include <SPI.h> #include <WiFi.h>
```

```
#include <Twitter.h>
```

```
#include <SD.h>
```

```
File myFile;
```

```
char ssid[] = "*****";
```

```
char pass[] = "*****";
```

```
Twitter twitter("*****");
```

```
char dataString[150];
```

```
int PV;int PPV;int LDR;int CS;int A;int B;int K;int i=0;int j=0;
```

```
char tweetText[140];
```

```
int status = WL_IDLE_STATUS;
```

```
WiFiServer server(80);
```

```
void setup()
```

```
{
```

```
Serial.begin(9600);

pinMode(10, OUTPUT);

pinMode(0,INPUT);

while ( status != WL_CONNECTED) {

Serial.print("Attempting to connect to SSID: ");

Serial.println(ssid);

status = WiFi.begin(ssid, pass);

if (!SD.begin(4))

{

Serial.println("Card failed, or not present");

return;

}

Serial.println("card initialized.");

delay(9000);

}

}

void tweet(char msg[])
```

```
{  
  
Serial.println("Connecting to Twitter");  
  
if(twitter.post(msg))  
  
{  
  
int status = twitter.wait(&Serial);  
  
if (status==200){  
  
Serial.println("Successful");  
  
} else {  
  
Serial.println("Connection to Twitter failed");  
  
Serial.println("20 Seconds timeout started");  
  
delay(9000);}  
  
}  
  
}  
  
void loop()  
  
{  
  
Serial.println("PPV=");  
  
Serial.println(PPV);  
  
}
```

```
delay(80000);

i++;

String dataString="";

for (int analogPin=0; analogPin<=2; analogPin++)

{

    PV = analogRead(0);

    LDR= analogRead(1);

    CS= analogRead(2);

    int sensor=analogRead(analogPin);

    dataString += String(sensor);

    if (analogPin<=2)

    {dataString += ",";}

    B=Serial.read();

}

File dataFile = SD.open("datalog.txt", FILE_WRITE);

if (dataFile)

{
```

```

dataFile.println(dataString);

dataFile.close();

Serial.println(dataString);

} else {

Serial.println("error opening datalog.txt");}

Serial.println("Vdrop=");

A=PPV-PV;

Serial.println(A);

if (PV<=485 && PV>330 && CS>420 && CS<470 && LDR>1000 &&A>3&&
A<10)

{j ++;}

if (PV<=485 && PV>330 && CS>420 && CS<470 && LDR>=1010 &&A>=10)

{K++;}

if(i==6||K==2)

{

i=0;

K=0;

```

```
    sprintf(tweetText, "Panel needs to be cleaned: PV=%d,LDR=%d,CS=%d,Vdrop=%d." ,
PV,LDR,CS,A);

    tweet(tweetText);

    Serial.println("Panel needs to be cleaned");

    delay(20000);

} else if(PV>0 && LDR>100) {

    sprintf(tweetText, "Working fine: PV=%d,LDR=%d,CS=%d,Vdrop=%d.",
PV,LDR,CS,A);

    tweet(tweetText);

    Serial.println("Working fine");

    delay(20000);

}

if (j>=450)// this is the total counter

    {i=0;

    j=0;

    K=0;}

Serial.print("i = ");
```

```
Serial.println(i);
```

```
Serial.print("j = ");
```

```
Serial.println(j);
```

```
PPV=PV;
```

```
Serial.flush();
```

```
}
```

C. Wind farm simulation blocks

In This appendix, the block diagrams represent the subsystems which are modeled by mathematical equations are presented.

First, to generate a realistic wind model for a wind farm, distance of wind turbines are taken into account. Moreover, a random noise with small amplitude is added to model small wind changes as time goes by.

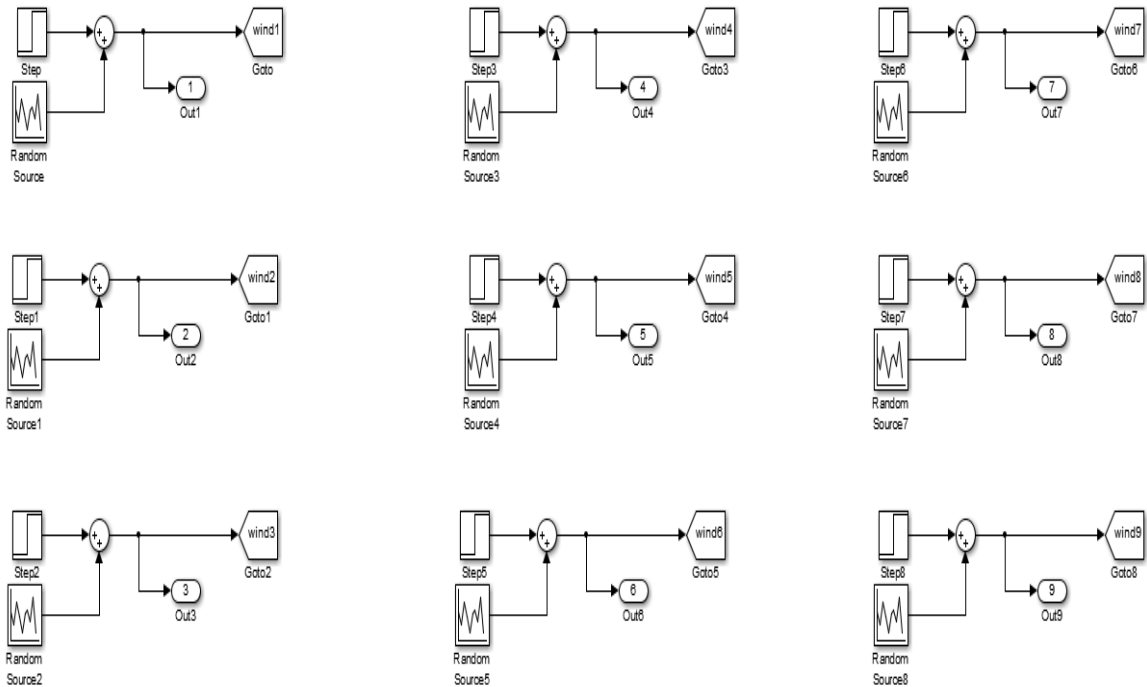


Figure C-1: Wind generation block

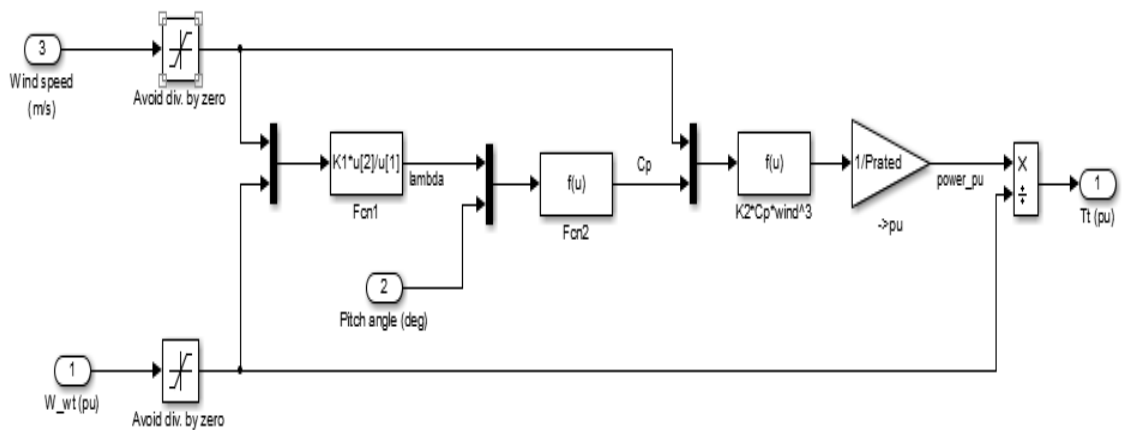


Figure C-2: Wind turbine block

Wind turbine drive train based on a 2-masse model

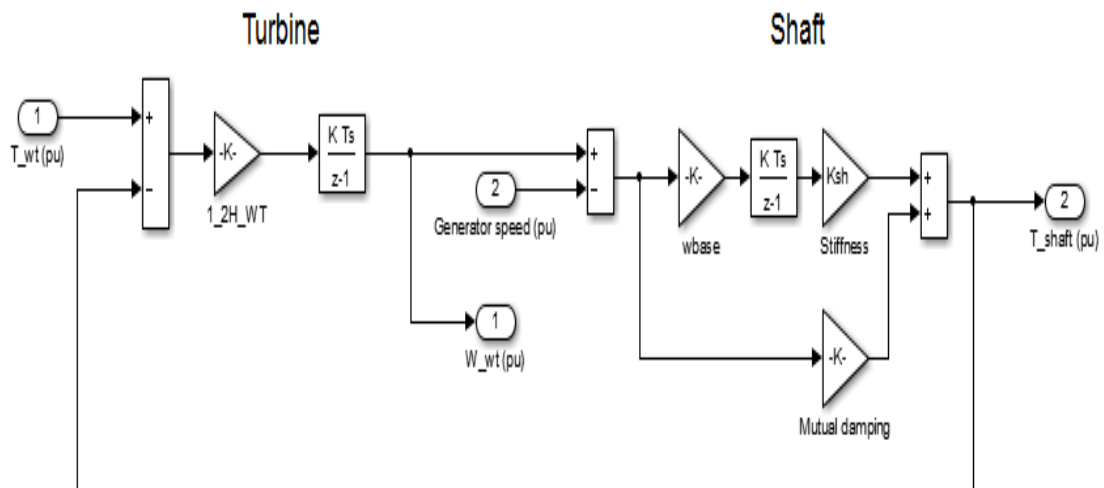


Figure C-3: Drivetrain block

Secondly, turbine model (Figure C-2) and drivetrain model (Figure C-3) are connected together to calculate the developed torque of turbine (Figure C-4).

Turbine and Drive Train

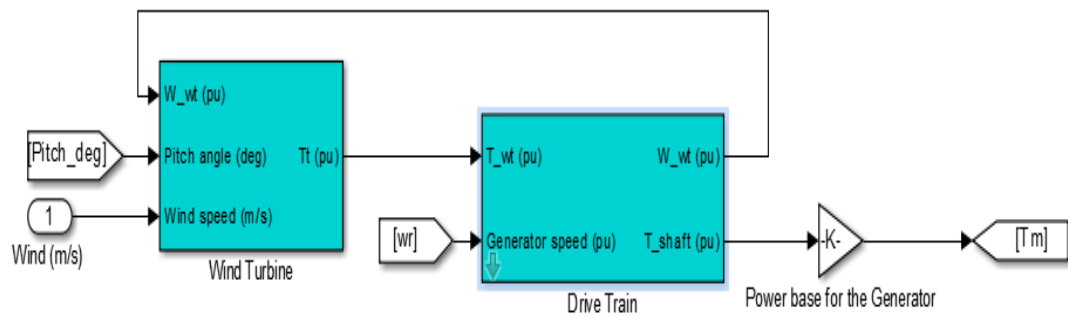


Figure C-4: Wind turbine and drivetrain

Figure C-5 indicates a 27MW DFIG wind turbine. It includes a three phase AC line, a filter, a choke, an asynchronous machine and its control parts.

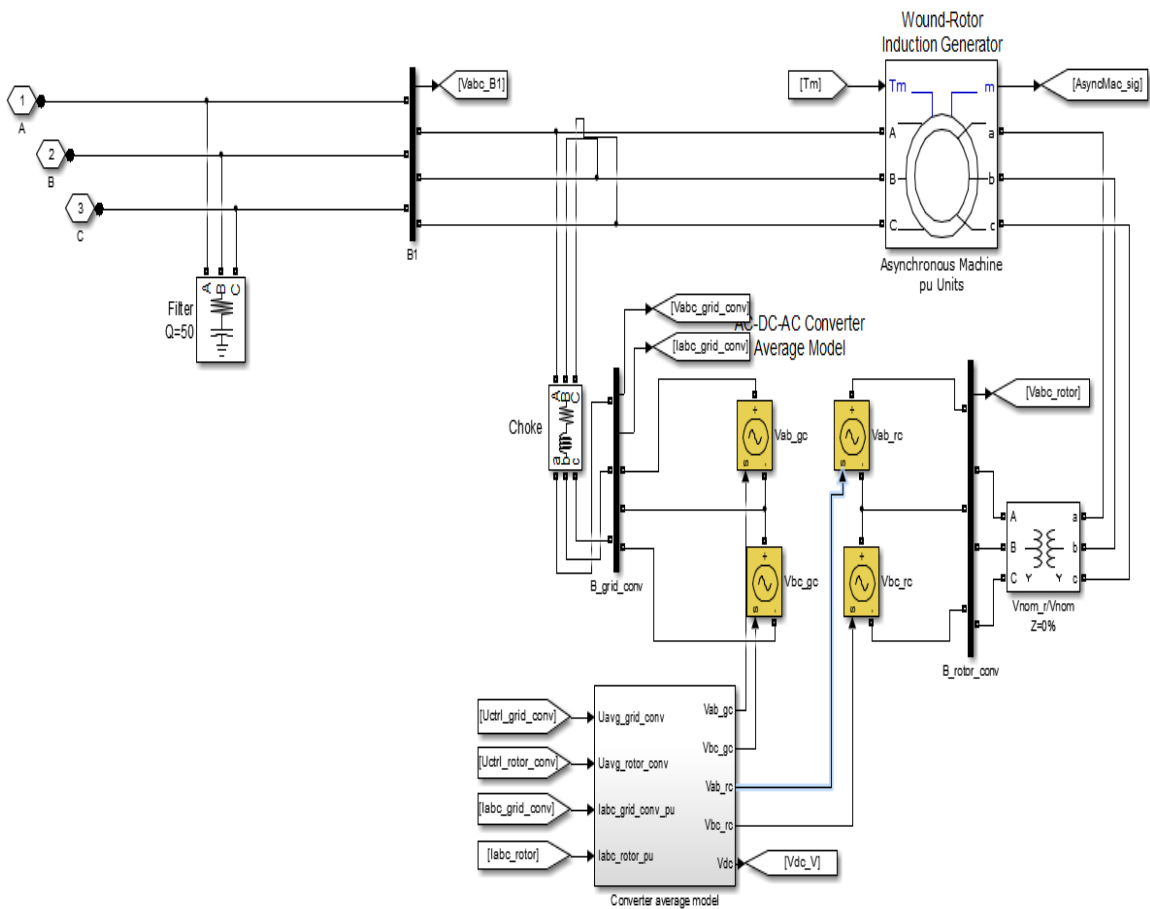


Figure C-5: A 27MW DFIG wind turbine

The Controlled Current Source block (in Figure C-5) converts the Simulink® input signal into an equivalent current source and the generated current is driven by the input signal of the block.

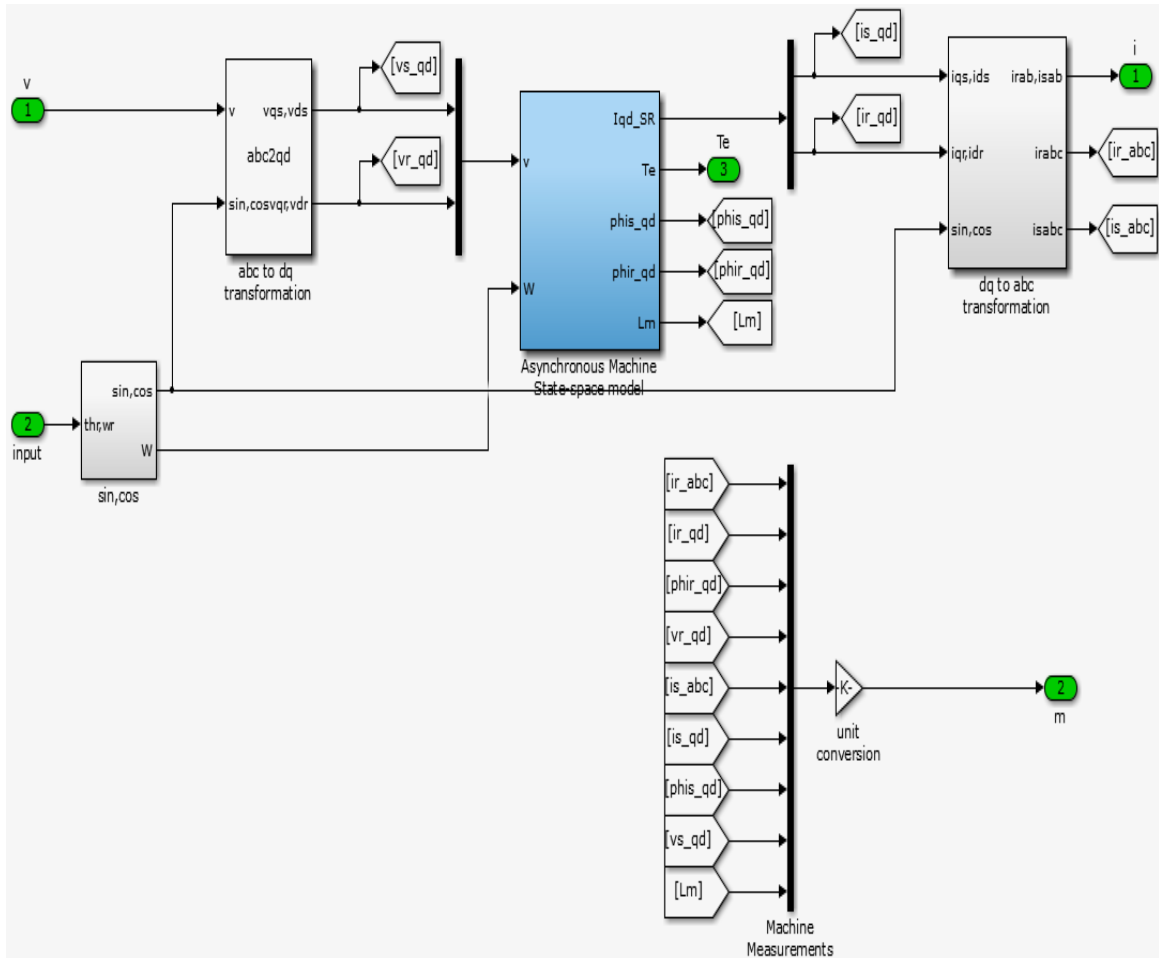


Figure C-6: Electrical model of wound rotor using abc to d-q transformation and state space model of asynchronous machine

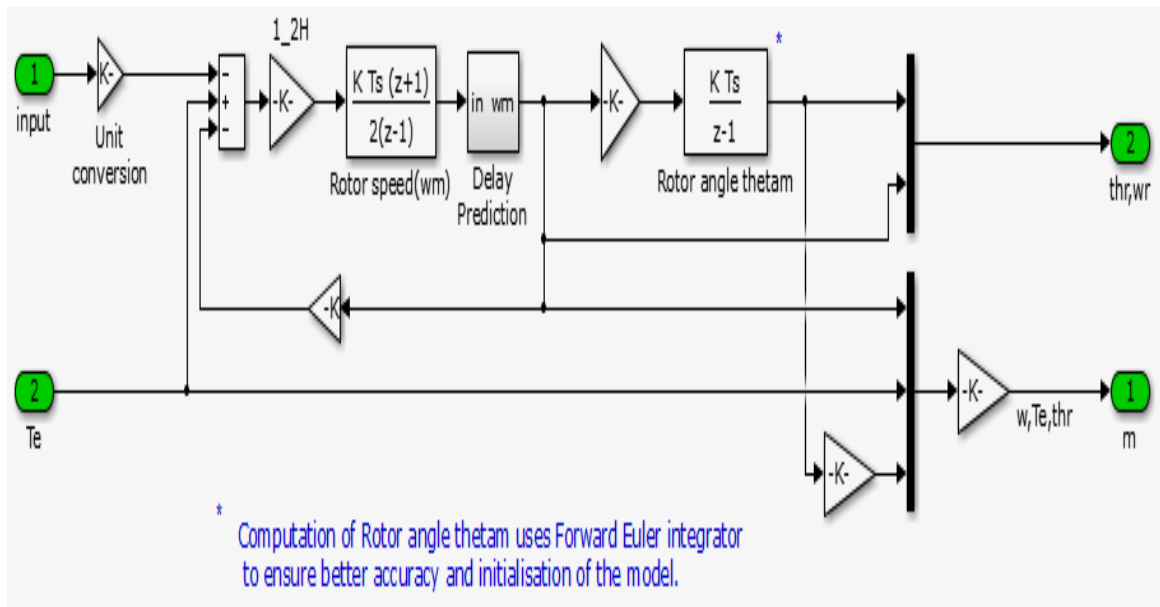


Figure C-7: Mechanical model of machine

Figure C-6 and C-7 indicate electrical and mechanical model of a DFIG machine. As described before, electrical model of machine uses d-q-0 transformation.

The Controlled Current Source block (in Figure C-5) converts the Simulink® input signal into an equivalent current source and the generated current is driven by the input signal of the block. Below figures indicate the method to generate input signals to be used in the controlled current source blocks of the converter average model shown in Figure C-5.

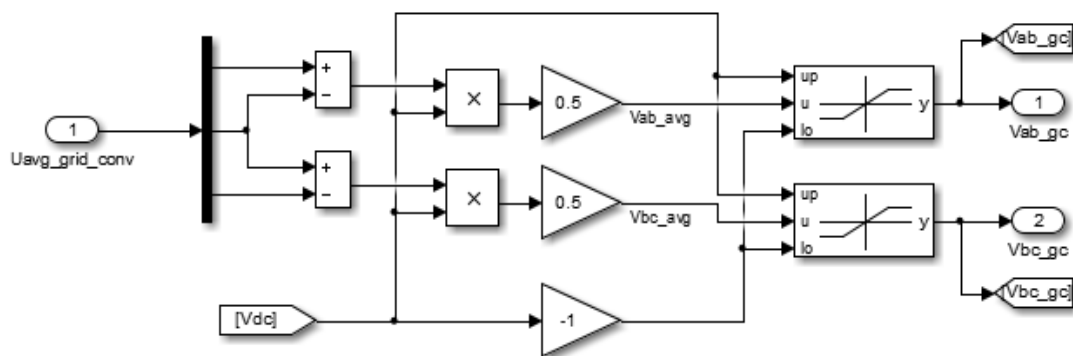


Figure C-8: Calculate Vab-gc

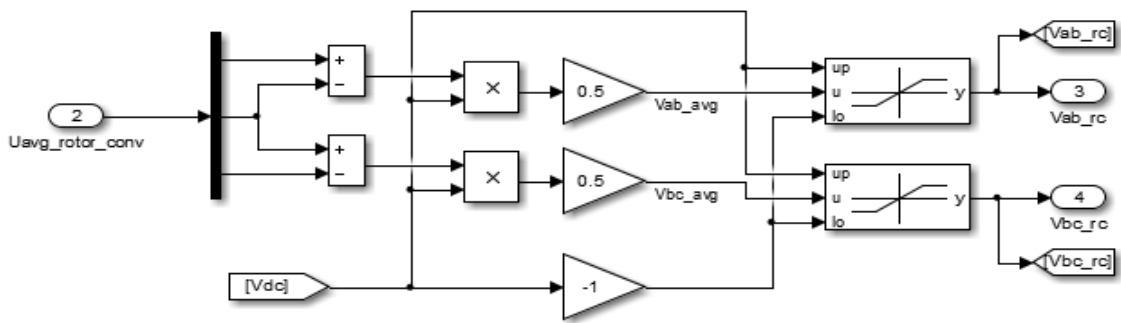
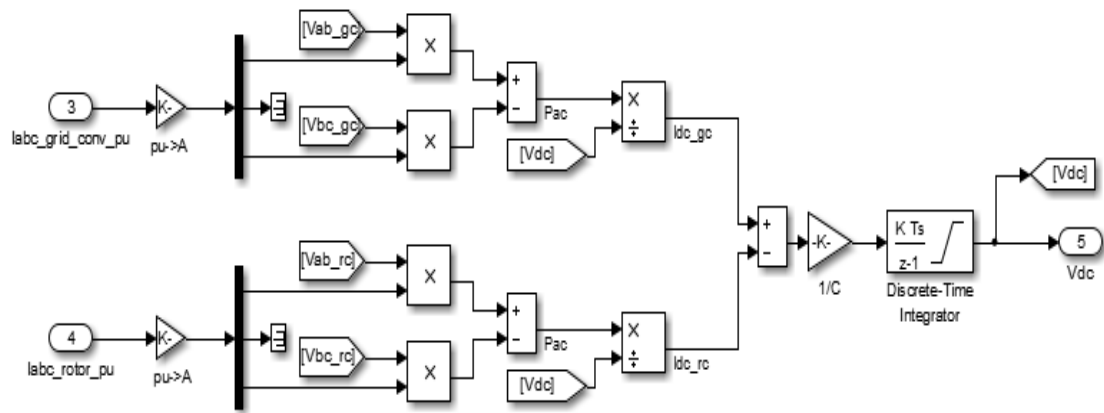


Figure C-9: Calculate Vab-rc



$$Pac = Vab \cdot Ia - Vbc \cdot Ic$$

$$Pdc = Vdc \cdot Idc$$

Figure C-10: Calculate Vdc